AEDC-TR-76-73
AFATL-TR-76-54

cy. 1

STATIC STABILITY AND DRAG EFFECTS OF VARIOUS EXTERNAL STORE CONFIGURATIONS ON THE F-15 AIRCRAFT AT MACH NUMBERS FROM 0.6 TO 1.3

PROPULSION WIND TUNNEL FACILITY
ARNOLD ENGINEERING DEVELOPMENT CENTER
AIR FORCE SYSTEMS COMMAND
ARNOLD AIR FORCE STATION, TENNESSEE 37389

April 1977

Final Report for Period October 14 and 15, 1975

Approved for public release; distribution unlimited

Prepared for

AIR FORCE ARMAMENT LABORATORY (DLJC)
EGLIN AIR FORCE BASE, FLORIDA 32542

NOTICES

When U. S. Government drawings specifications, or other data are used for any purpose other than a definitely related Government procurement operation, the Government thereby incurs no responsibility nor any obligation whatsoever, and the fact that the Government may have formulated, furnished, or in any way supplied the said drawings, specifications, or other data, is not to be regarded by implication or otherwise, or in any manner licensing the holder or any other person or corporation, or conveying any rights or permission to manufacture, use, or sell any patented invention that may in any way be related thereto.

Qualified users may obtain copies of this report from the Defense Documentation Center.

References to named commercial products in this report are not to be considered in any sense as an endorsement of the product by the United States Air Force or the Government.

This report has been reviewed by the Information Office (OI) and is releasable to the National Technical Information Service (NTIS). At NTIS, it will be available to the general public, including foreign nations.

APPROVAL STATEMENT

This technical report has been reviewed and is approved for publication.

FOR THE COMMANDER

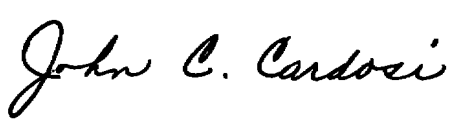

JOHN C. CARDOSI
Lt Colonel, USAF
Chief Air Force Test Director, PWT
Directorate of Test

ALAN L. DEVEREAUX
Colonel, USAF
Director of Test

UNCLASSIFIED

REPORT DOCUMENTATION PAGE		READ INSTRUCTIONS BEFORE COMPLETING FORM
1 REPORT NUMBER AEDC-TR-76-73 AFATL-TR-76-54	2 GOVT ACCESSION NO.	3 RECIPIENT'S CATALOG NUMBER
4 TITLE (and Subtitle) STATIC STABILITY AND DRAG EFFECTS OF VARIOUS EXTERNAL STORE CONFIGURATIONS ON THE F-15 AIRCRAFT AT MACH NUMBERS FROM 0.6 TO 1.3		5 TYPE OF REPORT & PERIOD COVERED Final Report - October 14 and 15, 1975 6 PERFORMING ORG. REPORT NUMBER
7. AUTHOR(s) James M. Whoric - ARO, Inc.		8 CONTRACT OR GRANT NUMBER(s)
9 PERFORMING ORGANIZATION NAME AND ADDRESS Arnold Engineering Development Center (XO) Air Force Systems Command Arnold Air Force Station, Tennessee 37389		10 PROGRAM ELEMENT, PROJECT, TASK AREA & WORK UNIT NUMBERS Program Element 62602F Project 2567, Task 02
11 CONTROLLING OFFICE NAME AND ADDRESS Air Force Armament Laboratory (DLJC) Eglin Air Force Base Florida 32542		12 REPORT DATE April 1977 13. NUMBER OF PAGES 83
14 MONITORING AGENCY NAME & ADDRESS(if different from Controlling Office)		15. SECURITY CLASS. (of this report) UNCLASSIFIED 15a DECLASSIFICATION/DOWNGRADING SCHEDULE N/A

16 DISTRIBUTION STATEMENT (of this Report)

Approved for public release; distribution unlimited.

17 DISTRIBUTION STATEMENT (of the abstract entered in Block 20, if different from Report)

1. Stores -- Stability
2. [illegible] -- Drag

18 SUPPLEMENTARY NOTES

Available in DDC

19 KEY WORDS (Continue on reverse side if necessary and identify by block number)

external stores
static stability
drag effects
external-store effects
transonic flow
aerodynamic characteristics

20 ABSTRACT (Continue on reverse side if necessary and identify by block number)

The results of transonic wind tunnel tests in which the effects of external stores on the aerodynamic characteristics of the F-15 aircraft were determined are presented and discussed. The analysis includes evaluations of the incremental drag rise, the incremental changes in static margin, and the lateral-directional derivatives associated with the various store configurations. Wind tunnel coefficient data for several baseline

DD FORM 1 JAN 73 1473 EDITION OF 1 NOV 65 IS OBSOLETE

UNCLASSIFIED

20. ABSTRACT (Continued)

configurations are also presented. Data are presented for various combinations of the Tactical Electronic Warfare System Pods (TEWS), the AIM-7F, the 600-gal fuel tanks, the GBU-15 (CW), the SUU-30H/B, and the Advance Short Range Missile (ASRM) stores. Data are presented for Mach numbers ranging from 0.6 to 1.3 at angles of attack from -4 to 20 deg at zero-deg sideslip angle, and for sideslip angles from -4 to 10 deg at angles of attack of 0, 10, 15, and 20 deg.

PREFACE

The work reported herein was conducted at the Arnold Engineering Development Center (AEDC), Air Force Systems Command (AFSC), at the request of the Air Force Armament Laboratory (AFATL/DLJC) under Program Element 62602F, Project 2567, Task 02. The AFATL project monitor was Major R. E. VanPutte. The results of these tests were obtained by ARO, Inc., AEDC Division (a Sverdrup Corporation Company), operating contractor for the AEDC, AFSC, Arnold Air Force Station, Tennessee, under ARO Project No. P41C-A3A. The author of this report was James M. Whoric, ARO, Inc. The data analysis was completed on November 13, 1975, and the manuscript (ARO Control No. ARO-PWT-TR-76-14) was submitted for publication on February 9, 1976.

CONTENTS

ILLUSTRATIONS

Figure Page

Figure Page

TABLES

1.0 INTRODUCTION

Wind tunnel tests were conducted to establish a data base on the effects of external stores on the aerodynamic characteristics of the F-15. The tests were conducted in the Aerodynamic Wind Tunnel (4T) of the AEDC Propulsion Wind Tunnel (PWT) facility utilizing 0.05-scale models of the F-15 aircraft, the Tactical Electronic Warfare System (TEWS) pods, the 600-gal fuel tanks, the GBU-15 (CW), the AIM-7F, the SUU-30H/B, and the Advance Short Range Missile (ASRM) stores. Static longitudinal stability and drag data were obtained for all external store configurations at Mach numbers ranging from 0.6 to 1.3. Angle of attack was varied from -4 to 20 deg at a sideslip angle of zero deg. Lateral-directional stability data were obtained for selected configurations over the same Mach number range. For these data, the sideslip angle was varied from -4 to 10 deg at angles of attack of 0, 10, 15, and 20 deg.

2.0 APPARATUS

2.1 TEST FACILITY

The Aerodynamic Wind Tunnel (4T) is a closed-loop, continuous-flow, variable-density tunnel in which the Mach number can be varied from 0.1 to 1.3. Also, nozzle blocks can be installed to give nominal Mach numbers of 1.6 and 2.0. At all Mach numbers, the stagnation pressure can be varied from 300 to 3,700 psfa. The test section is 4 ft square and 12.5 ft long with perforated, variable porosity (0.5- to 10-percent open) walls. It is completely enclosed in a plenum chamber from which the air can be evacuated, allowing part of the tunnel airflow to be removed through the perforated walls of the test section. A more complete description of this test facility can be found in the Test Facilities Handbook.*

The tunnel 4T support system for the models consists of a pitch sector with strut and sting attachment which has a pitch capability of -8 to 28 deg with respect to the tunnel centerline and a roll capability of -180 to 180 deg with respect to the sting centerline.

2.2 TEST ARTICLES

The test articles were 0.05-scale models of the F-15 aircraft, the 600-gal fuel tanks, the Tactical Electronic Warfare System (TEWS) pods, the AIM-7F, the GBU-15 (CW), the SUU-30H/B, the Advance Short Range Missile (ASRM) stores, and associated suspension

*Test Facilities Handbook (Tenth Edition). "Propulsion Wind Tunnel Facility, Vol. 4." Arnold Engineering Development Center, May 1974.

equipment. A photograph of the F-15 configured with the SUU-30H/B stores, the AIM-7F stores, and the centerline 600-gal fuel tank is shown in Fig. 1. Sketches of the F-15 model and wing panel are presented in Figs. 2 and 3. Two flow-through inlet configurations were used during these tests. Sketches showing the basic dimensions of these inlets are presented in Fig. 4. The store suspension equipment used with the various stores is shown in Fig. 5. The TEWS, the 600-gal fuel tanks, and the GBU-15 (CW) stores were all suspended from the F-15 using appropriate pylons (Figs. 5a, b, and c). The ASRM stores were mounted in tandem and required a special pylon adapter (Fig. 5d) for proper suspension, whereas, a MER (Fig. 5e) was used in conjunction with a pylon for the SUU-30H/B store suspension. The AIM-7F stores were fuselage mounted. Details and dimensions of the 0.05-scale models of the various external stores mentioned above are shown in Fig. 6. A configuration identification key is presented in Fig. 7. Shown in that figure along with the aircraft load configuration are store profiles scaled with respect to each other. The configurations are identified numerically for reference in the remainder of this report.

2.3 INSTRUMENTATION

A six-component, internal, strain-gage balance was used to measure the forces and moments on the F-15 model. Two base pressure measurements were made using transducers and orifice tubes which extended just inside of the base of the model.

3.0 TEST DESCRIPTION

3.1 TEST CONDITIONS, PROCEDURES, AND TEST PROGRAM

The models were tested at the following nominal test conditions:

M_∞	p_t, psfa	Re x 10^{-6}, per foot
0.6	1,200	1.94
0.8	↓	2.30
0.9	↓	2.42
1.1	↓	2.53
1.3	↓	2.50

In addition, configurations 101, 201, and 206 were also tested at M_∞ = 0.85, 0.95, 0.975, and 1.2.

The test procedures were conventional in nature, consisting of varying the model angle of attack incrementally at a constant sideslip angle, or varying the model angle of

sideslip at a constant angle of attack while holding the Mach number constant. The model stabilator angle was held constant at zero deg with respect to a model waterline throughout the test.

The test program that was completed is presented in Table 1. As indicated, configuration 218 was not tested because of a fin interference problem. This table provides a key to all the wind tunnel data obtained during these tests.

3.2 DATA REDUCTION AND CORRECTIONS

Wind tunnel force and moment data were reduced to coefficient form in the stability axis system. Base drag was calculated using an average of two base pressure measurements and was used to calculate forebody coefficients. However, all data presented in this report are measured coefficients. Moments were referenced to MS 27.86 (25.65-percent MAC), WL 5.81, and BL 0. Corrections for the components of model weight normally termed static tares were also applied to the data.

The angle of attack was corrected for sting and balance deflections caused by the aerodynamic loads. The model was tested both upright and inverted to provide the data to correct for tunnel-flow angularity and model-balance misalignment. Based on these data, the angle of attack was corrected as indicated by the data presented in Fig. 8.

3.3 DATA UNCERTAINTY

The data uncertainties determined for a confidence level of 95 percent are presented in Table 2. The aerodynamic coefficient uncertainties include the uncertainties of Mach number and dynamic pressure along with the uncertainty contribution associated with the particular balance. Model angle of attack uncertainty has been estimated to be ±0.1 deg and model roll angle ±0.4 deg.

4.0 TEST RESULTS, ANALYSIS, AND DISCUSSION

Presented in the following sections is a discussion of the effect of the inlet configuration and the effect of various store configurations on the static longitudinal stability, drag, and lateral-directional stability derivatives of the F-15 model. Coefficient data as well as incremental data are presented and discussed.

The static margins were evaluated by taking the slope of a least-squares fit of the pitching-moment coefficient versus lift-coefficient curve over the nominal angle-of-attack range from -2 to 6 deg. All static margin characteristics are given from the general moment reference point of 25.65-percent chord and do not consider the actual flight center of gravity, which may be substantially changed by the addition of stores.

Drag coefficients were evaluated at specific lift coefficients from curve fits of the data, from which the drag increments were then calculated. Lateral-directional derivatives were also evaluated from least-squares curve fits of the data over the sideslip-angle range from -4 to 4 deg.

4.1 EFFECT OF THE INLET CONFIGURATION ON THE LONGITUDINAL STABILITY AND DRAG

Since the F-15 inlet configuration varies with aircraft angle of attack, the F-15 model was initially tested with two inlet configurations. One inlet configuration was representative of the low angle-of-attack configuration, and the other was representative of the high angle-of-attack configuration (Fig. 4).

A comparison of the data obtained with the F-15 model configured with these two inlet configurations (Figs. 9 and 10) shows that the static longitudinal stability as determined by the slope of pitching-moment coefficient versus lift coefficient curve was generally independent of inlet configuration for lift coefficients up to about 0.6. However, the high alpha inlet did show a more negative zero-lift pitching-moment coefficient when compared with the low alpha configuraiton. At lift coefficients greater than 0.6, the F-15 with the high alpha inlet configuration was somewhat more stable longitudinally than with the low alpha inlet configuration. The drag was also lower (Fig. 10) with the high alpha inlet than with the low alpha inlet. Based on the results of these data, the decision was made to conduct the remainder of the test with the model configured with the high alpha inlet.

4.2 EFFECT OF EXTERNAL STORE CONFIGURATIONS ON STATIC LONGITUDINAL STABILITY

To assess the effects of the various external store configurations on the static longitudinal stability of the F-15 aircraft, four configurations were selected as baseline configurations. They were configuration 201 (clean, no stores or suspension equipment), configuration 210 (AIM-7F and centerline 600-gal fuel tank), configuration 211 (AIM-7F only), and configuration 215 (centerline 600-gal fuel tank only). The pitching-moment coefficient data for these baseline configurations and the static margins derived from these data are presented in Figs. 11 and 12. The data that will be used in the discussion of the effects of various external stores on the static longitudinal stability will be presented as incremental changes in static margin as various stores are added symmetrically to the armament stations of the F-15 model. When store-alone increments are available (i.e., increments measured without stores present at the other armament station), the incremental data are presented as direct comparison of the static margin change produced when a

particular store is added to the F-15 at a particular armament station alone, to the static margin change produced by that same store at the same armament station when stores were present at the other armament stations. For those stores for which store-alone increment data were not obtained, the incremental data are presented as single curves for the various configurations for comparison. As an additional aid in identifying the data, the numbers of the two configurations for which the increments were calculated are listed in the header information of each plot. For example, in Fig. 13, the data represented by the squares are the incremental changes in static margin which were measured when the TEWS stores were added to the clean aircraft at armament stations 1 and 9. These increments were calculated by taking the difference between the static margin calculated for configurations 202 and 201 at each test Mach number. In Fig. 13a, the data represented by circles are also the incremental changes produced by adding the TEWS stores to the F-15 at stations 1 and 9, but with the F-15 carrying the centerline 600-gal fuel tank. Similarly, in Figs. 13b and c, the circles present the static margin increments produced by the TEWS at stations 1 and 9 with the model configured with different stores at the other stations.

The data obtained for adding stores to the F-15 outboard wing stations (1 and 9) are presented in Fig. 13, to the inboard wing stations (2 and 8) in Figs. 14 through 18, to the fuselage stations (3, 4, 6, and 7) in Fig. 19, and to the fuselage centerline station (5) in Fig. 20. These data show that when external stores were added symmetrically to the F-15 aircraft at any of the armament stations, except the fuselage centerline (station 5), the effect was always destabilizing and essentially independent of Mach number. Static margin changes of from 2- to 3-percent chord were produced by the store configurations suspended on the wing stations with the MER-mounted SUU-30H/B stores producing the largest change (Fig. 17). The AIM-7F stores at the fuselage stations (3, 4, 6, and 7) produced smaller changes in static margin than the stores that were added to the wing armament stations. At the centerline fuselage station (5), the data in Fig. 20 show that the centerline 600-gal fuel tank usually had a stabilizing effect on the F-15 model.

In general, the changes in static margins which were produced by adding specific stores to any armament station on the clean configuration were larger than when the same stores were added to the F-15 with stores present at the other armament stations. This fact is further illustrated by the data presented in Fig. 21. A comparison is shown between the static margin change measured for configurations 206 and 217 and the static margin change that was computed by adding the static margin increments measured when each external store in the configuration was carried alone on the F-15 aircraft. Summing the individual components over-predicted the static margin change actually measured for these two configurations, except at Mach number 1.3. Also noteworthy is the fact that the data in Fig. 21a at Mach numbers 0.95 and 0.975 show that the destabilizing effect of the external stores of configuration 206 decreased until finally a stabilizing effect was noted at Mach number 0.975.

4.3 EFFECTS OF EXTERNAL STORE CONFIGURATIONS ON THE DRAG CHARACTERISTICS

The data which show the effects of the various external store configurations on the drag characteristics of the F-15 are presented in Figs. 22 through 30 as a function of lift coefficient. As with the longitudinal stability data, the wind tunnel coefficient data of the baseline configurations are presented first (Fig. 22), and then the incremental changes in the drag coefficients for the various configurations are presented. The data presentation for the drag effects discussion will follow the same format as for the stability discussion. Incremental changes in drag coefficient caused by adding stores symmetrically to the outboard wing stations (1 and 9) are presented in Fig. 23, to the inboard wing stations (2 and 8) in Figs. 24 through 28, to the fuselage stations (3, 4, 6, and 7) in Fig. 29, and to the centerline fuselage station (5) in Fig. 30.

These data show that the addition of external stores to the F-15 to any armament station always produced an increase in drag at low values of lift coefficients ($0 \leqslant C_L \leqslant 0.6$). This was also generally true at the higher values of lift coefficients, but there were some cases of drag reduction ($\Delta C_D < 0$) noted in the high lift coefficient range (Fig. 23). Moreover, in the high lift coefficient range, larger drag increments were generally noted when stores were added to the F-15 with stores present at the other armament stations than were noted without stores present at the other armament stations. This effect was most pronounced at Mach numbers 1.1 and 1.3.

It is also of interest to determine whether the drag increments for external store configurations consisting of different stores or store configurations at several armament stations can be predicted by adding up the drag increments measured when each store or store configuration of the multiple carriage configuration was carried alone by the F-15 aircraft. A comparison of such a summation of drag increments to the total drag increment measured for configurations 217 and 206 is presented in Fig. 31. These comparisons show that the drag increment predicted for configuration 217 (Fig. 31a) agrees well at low lift coefficients at subsonic Mach numbers, whereas at the high lift coefficients and at the supersonic Mach numbers, the drag increment was generally underpredicted when individual increments were summed. This trend follows the general trend noted above, which was that the presence of stores at other armament stations generally increased the drag increment of a particular store or store configuration. However, the data for configuration 206 in Fig. 31b show that the drag increment predicted by summing individual increments agrees well with the total measured drag increment even at high lift coefficients, except at Mach number 1.3 where the drag increment was somewhat under-predicted. It appears that additional individual store data are needed before any definite conclusions can be made as to the validity of summing the drag increments of

individual stores to predict the total drag increment of an external store configuration of different stores at several armament stations. However, from the data available from these tests, it appears that summing the individual store drag increments did reasonably predict the total drag increment of a multiple carriage configuration at the low values of lift coefficient corresponding to cruise conditions.

4.4 EFFECT OF EXTERNAL STORE CONFIGURATIONS ON THE LATERAL-DIRECTIONAL STABILITY DERIVATIVES

Lateral-directional stability data were obtained for five external store configurations of the model F-15 aircraft. Data were obtained at 0-, 10-, 15-, and 20-deg angle of attack for configurations 201, 203, 206, and 209 and at 20-deg angle of attack for configuration 213. The lateral-directional data for configuration 201, which will be considered the baseline configuration, are presented in Fig. 32, and the lateral-directional derivatives calculated from these data are presented in Fig. 33. The data in Fig. 33 indicate a marked decrease in C_{n_β} with aircraft angle of attack for the clean configuration (201) with directional instability ($C_{n_\beta} < 0$) being noted at α = 20 deg at Mach numbers 1.2 and 1.3. The data in this figure also show that, as the aircraft angle of attack was increased, an improvement in effective dihedral was experienced as indicated by the negative shift in C_{ℓ_β}. Adding external stores to configuration 201 had the effect of shifting C_{n_β} negatively at the subsonic Mach numbers for all configurations tested, as can be seen from the data in Fig. 34. These data also show that the addition of external stores in general improved the dihedral effect of the F-15, producing more negative values of C_{ℓ_β}. However, the TEWS and the SUU-30H/B stores for some conditions (Figs. 34b, c, and d) reduced the effective dihedral of the F-15.

5.0 SUMMARY OF RESULTS

Transonic Wind tunnel tests were conducted to determine the effect of external carriage of various configurations of stores on the aerodynamic characteristics of the F-15 aircraft. The tests were conducted with 0.05-scale models of the F-15 and external stores. The results of the analysis of the data from these tests in which the model moment reference point was constant at 25.65 percent of the mean aerodynamic chord are summarized as follows:

1. When compared with the low alpha inlet configuration, the high alpha inlet configuration showed a more negative zero lift pitching-moment coefficient, did not significantly change the static longitudinal stability, and exhibited slightly lower drag.

2. With the exception of the SUU-30H/B configuration (206) at Mach numbers 0.95 and 0.975, the effect of adding external stores to the F-15 model at armament stations 1 and 9, and 2 and 8 was always destabilizing with respect to static longitudinal stability and essentially independent of Mach number. In general, the stores produced a 2- to 3-percent chord change in static margin for the stores and store configurations tested.

3. Adding the 600-gal fuel tank to the F-15 model at armament station 5 generally produced a slight increase in static longitudinal stability.

4. Changes in static margins which were produced by adding external stores to the F-15 model at any armament station were generally always smaller when external stores were present at the other armament stations than without stores present at the other armament stations.

5. Summing the drag increments measured when individual stores were added to the F-15 model without other stores present reasonably predicted the total drag increment measured for multiple carriage store configurations at the low values of lift coefficients corresponding to cruise conditions. However, except at Mach number 1.3, summing the individual static margin increments overpredicted the total static margin increment, by as much as 50 percent in some cases.

6. Increasing the angle of attack reduced the static directional stability derivative for the clean configuration. However, the effective dihedral of the clean configuration was essentially constant for angles of attack up to 10 deg. Above 10-deg angle of attack, the the effective dihedral increased with increasing angle of attack.

7. At the subsonic Mach numbers, adding external stores to the clean configuration reduced the static directional stability derivative at each angle of attack for all configurations tested.

8. In general, the effective dihedral of the F-15 model was improved at each angle of attack when external stores were added to the clean configuration. Some degradation of effective dihedral was noted at some conditions when the F-15 model was carrying the Tactical Electronic Warfare Systems pods or the SUU-30H/B stores.

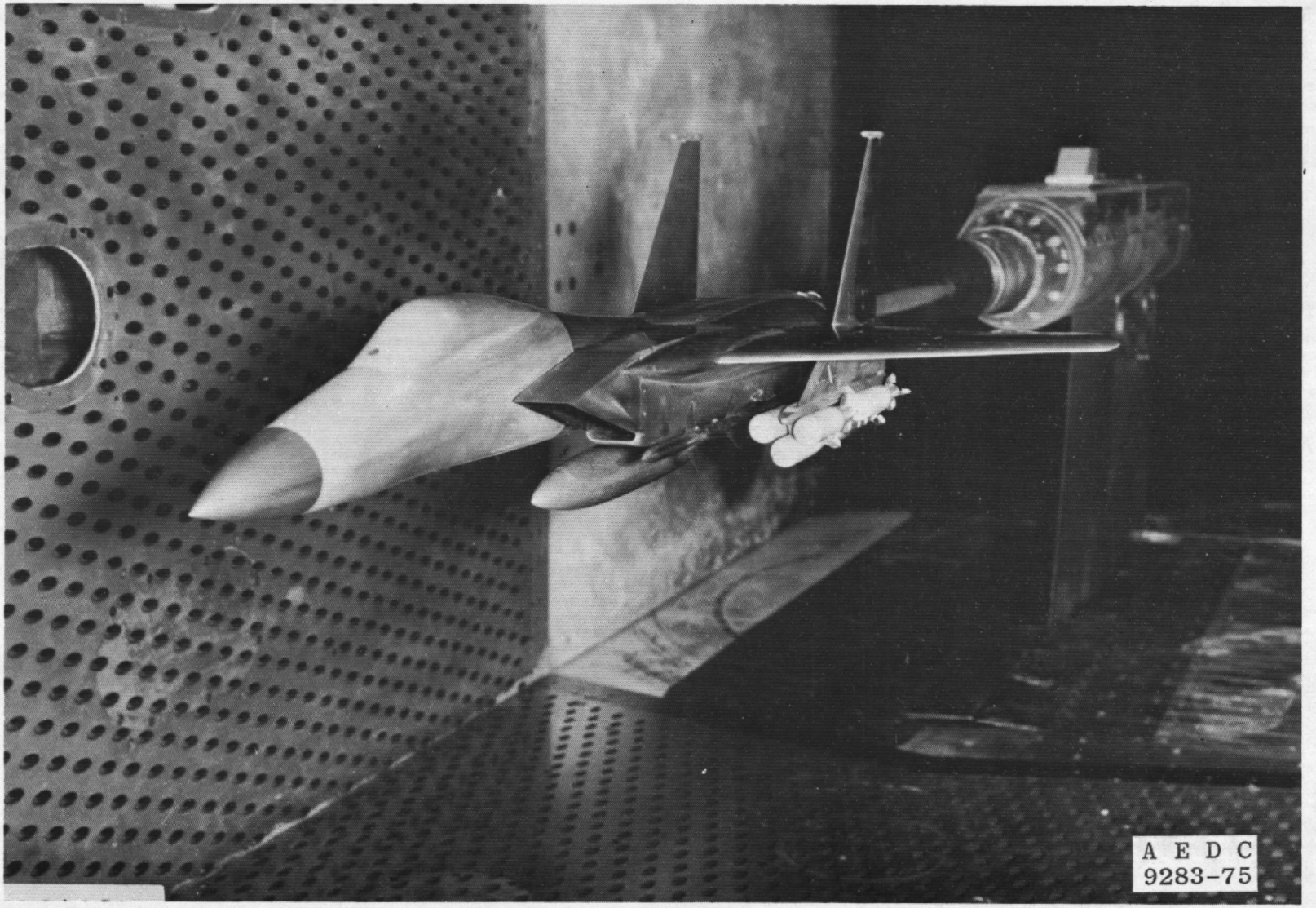

Figure 1. Tunnel installation of configuration 209.

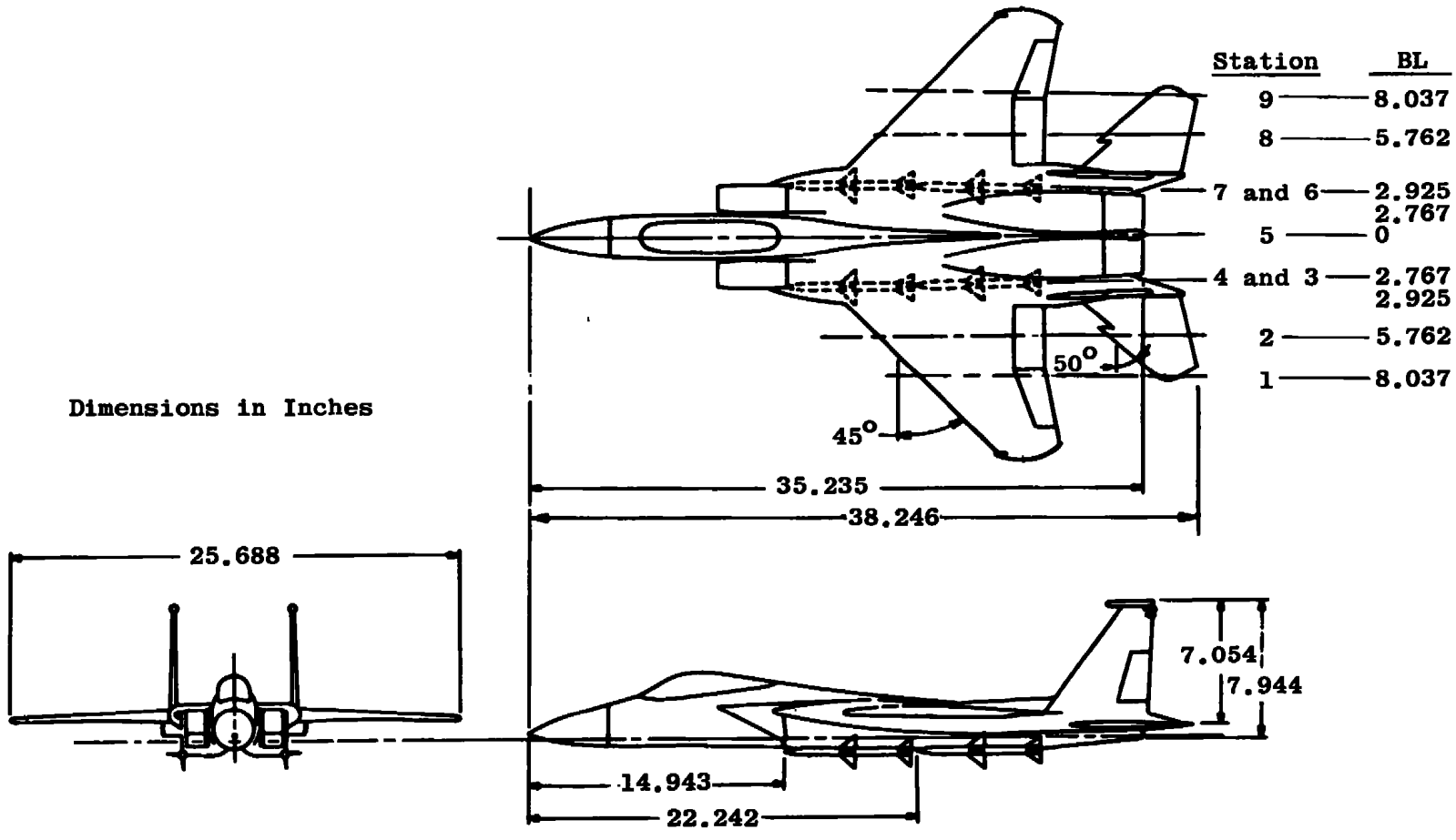

Figure 2. 0.05-scale F-15 model.

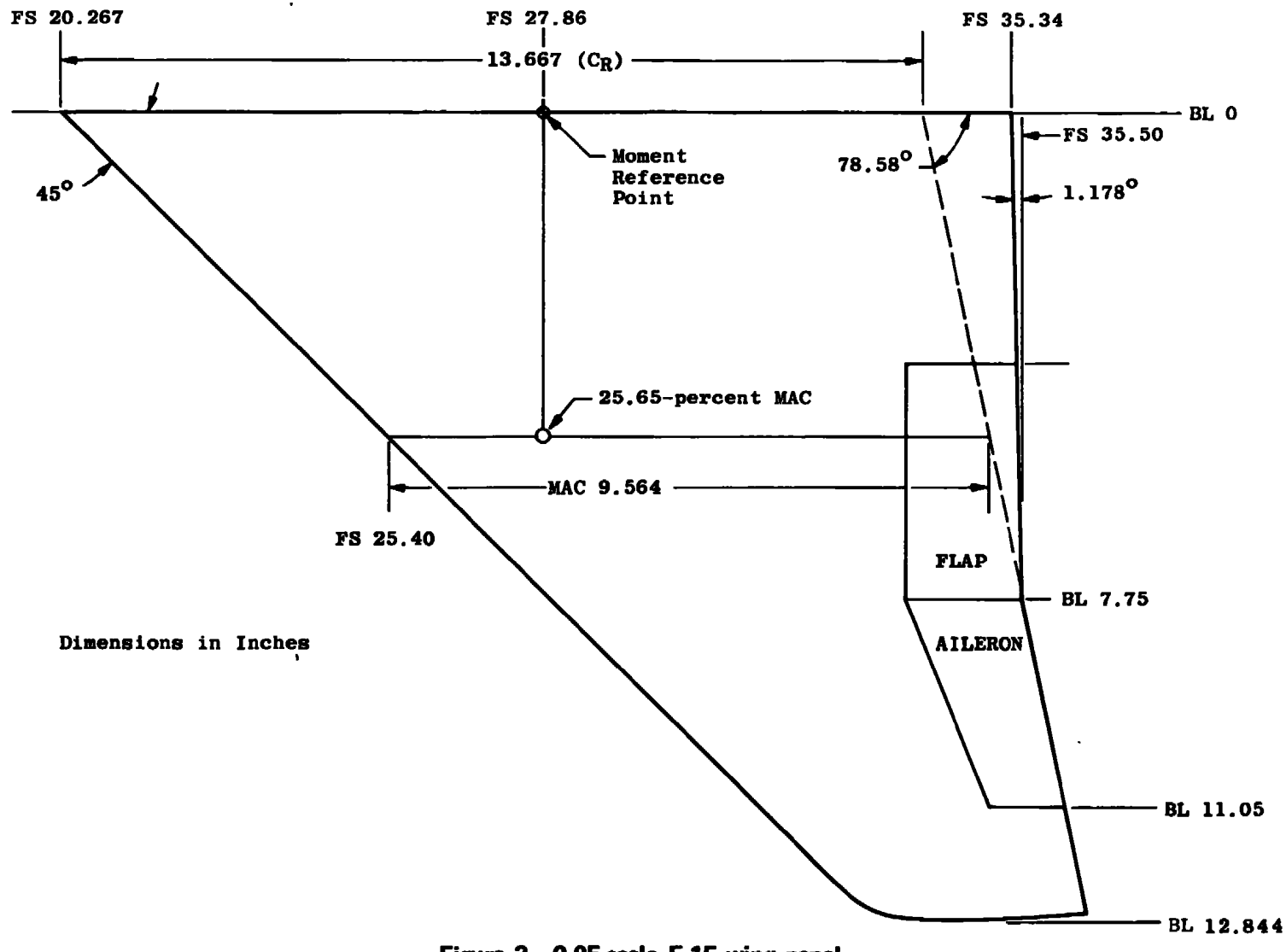

Figure 3. 0.05-scale F-15 wing panel.

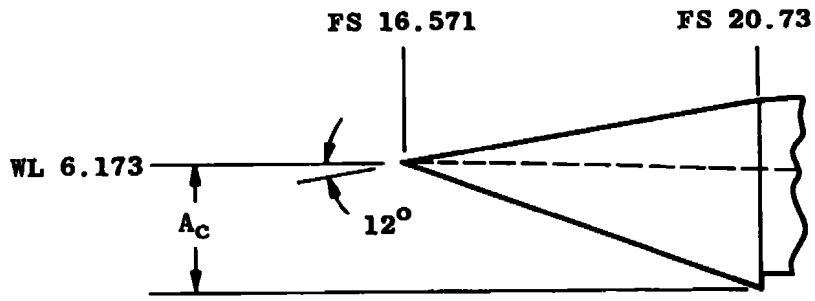

Capture Area, A_C = 0.0119 ft^2/Inlet
Throat Area, A_T = 0.0108 ft^2/Inlet

a. High-alpha inlet, configuration 201

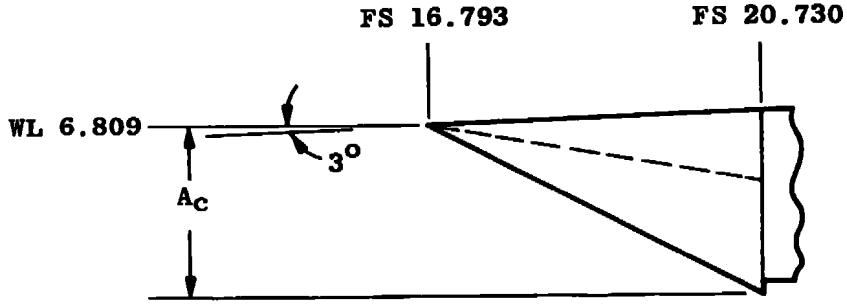

Capture Area, A_C = 0.0184 ft^2/Inlet
Throat Area, A_T = 0.0.275 ft^2/Inlet

Stations in Inches

b. Low-alpha inlet, configuration 101

Figure 4. Inlet configurations.

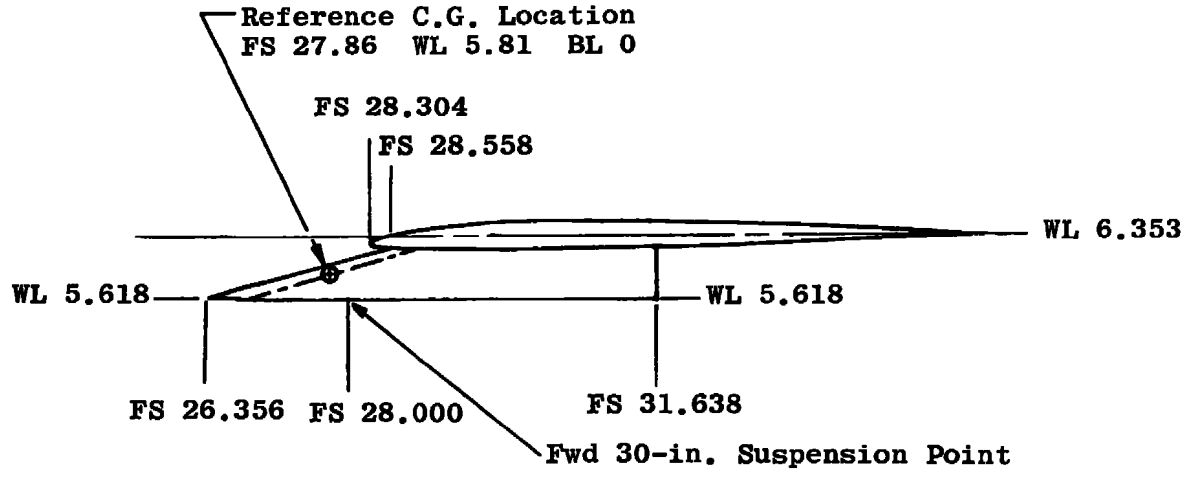

Dimensions in Inches

a. F-15, 0.05-scale outboard pylon model

Figure 5. F-15 external store suspension equipment.

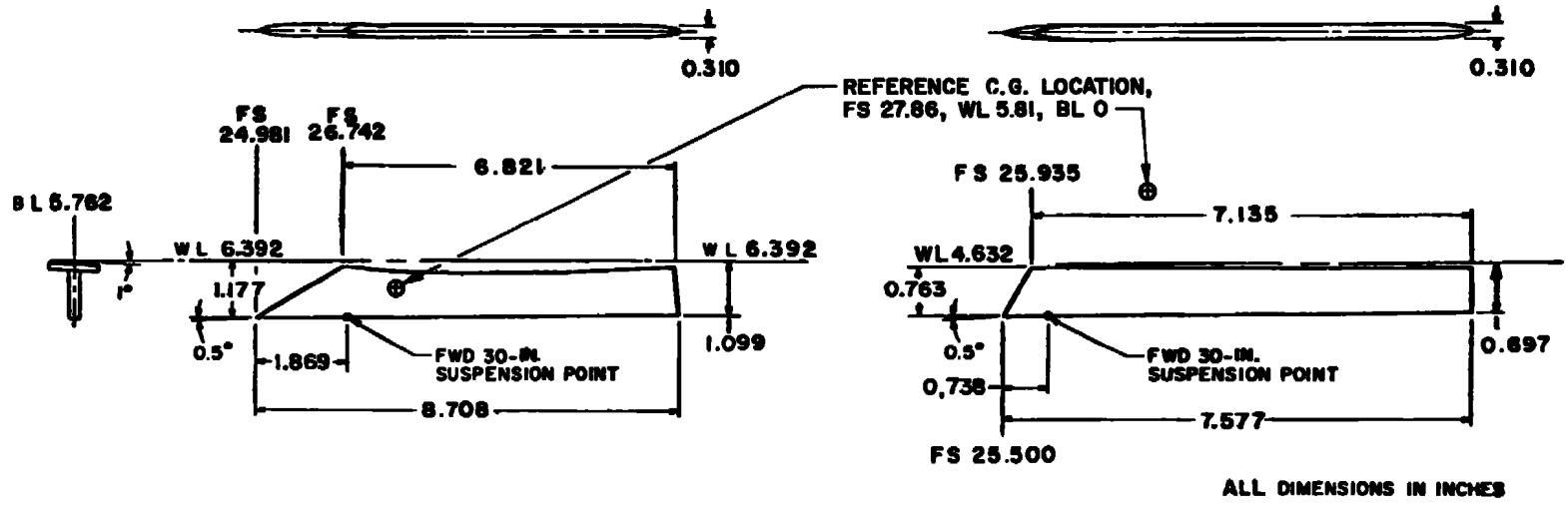

b. Inboard wing pylon

c. Centerline pylon

Figure 5. Continued.

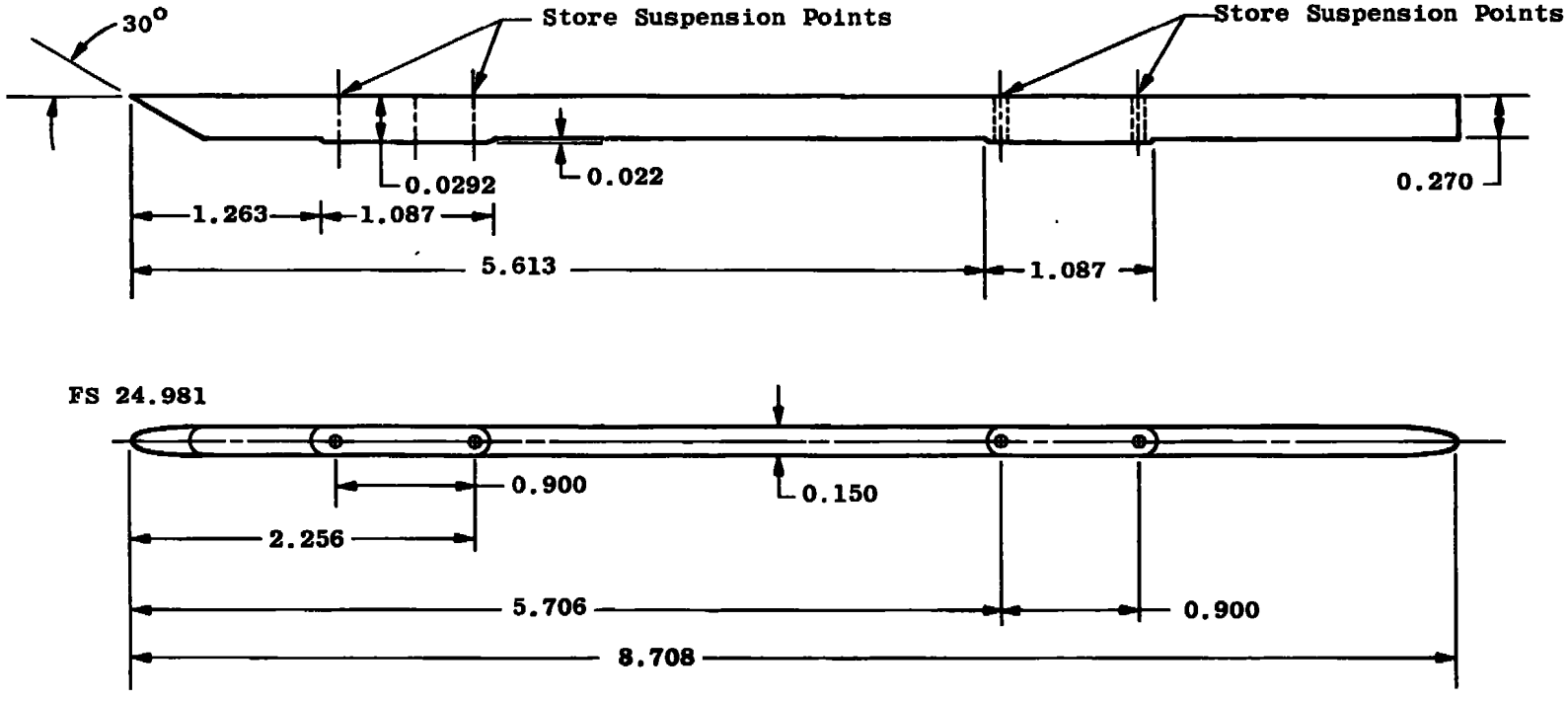

Dimensions in Inches

d. ASRM pylon adaptor
Figure 5. Continued.

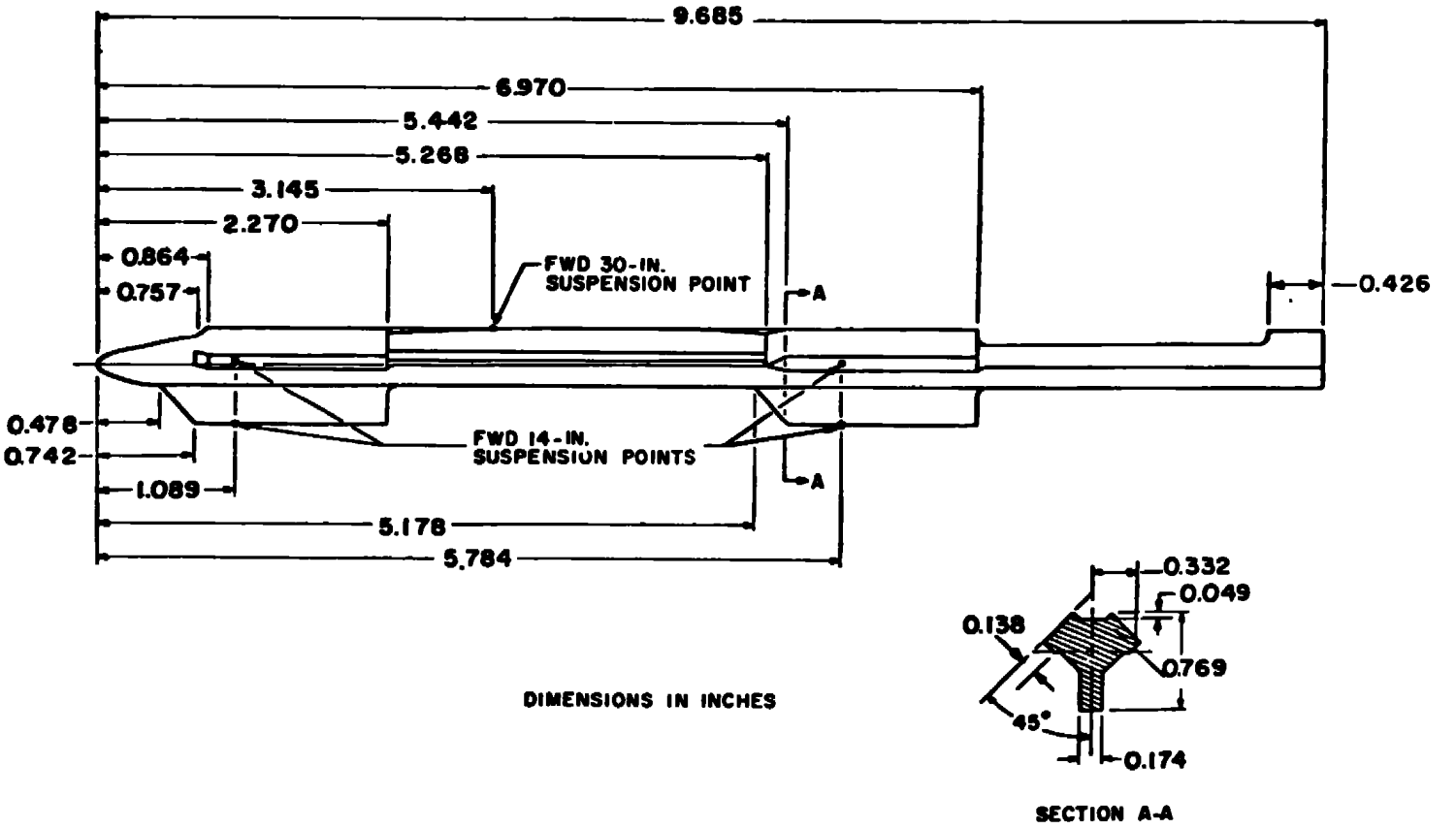

e. Multiple ejector rack, type 200 (MER-200)
Figure 5. Concluded.

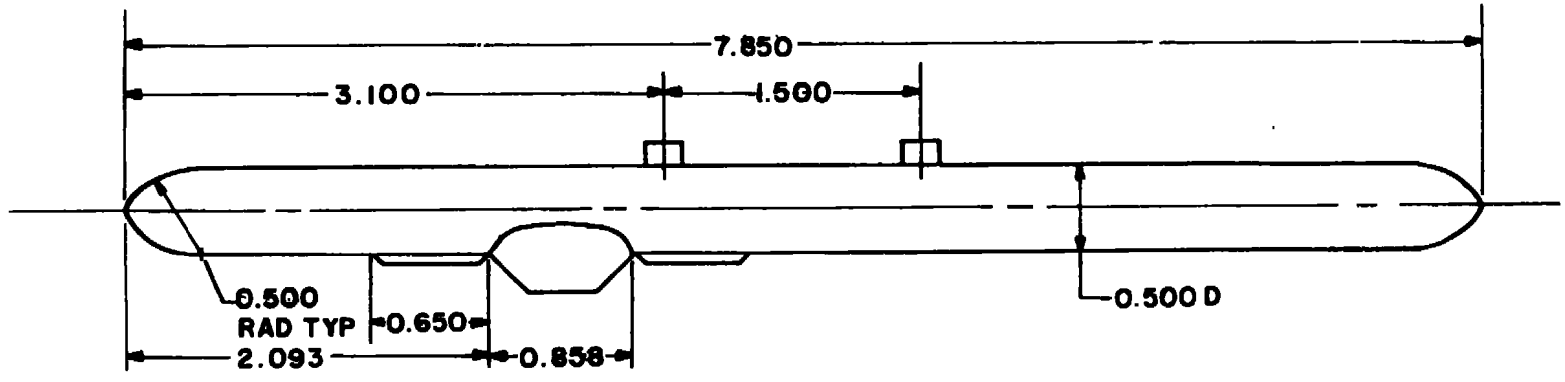

FS 26.356

DIMENSIONS IN INCHES

a. TEWS

Figure 6. 0.05-scale external stores.

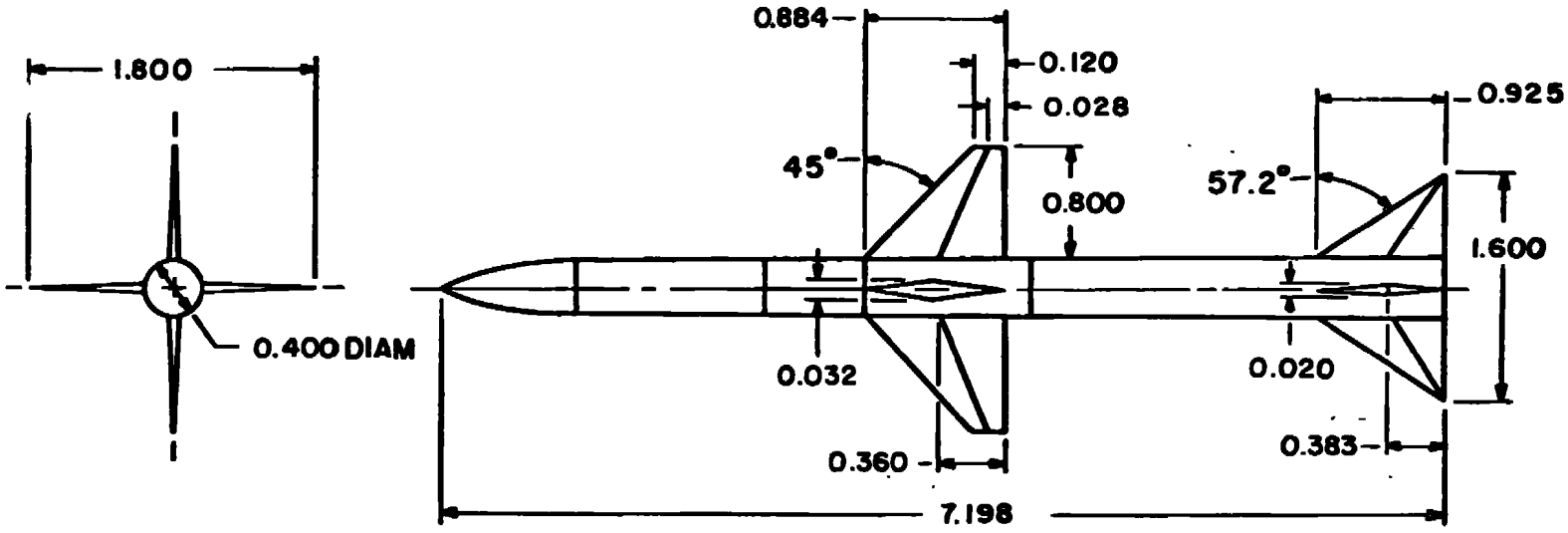

DIMENSIONS IN INCHES

b. AIM-7F

Figure 6. Continued.

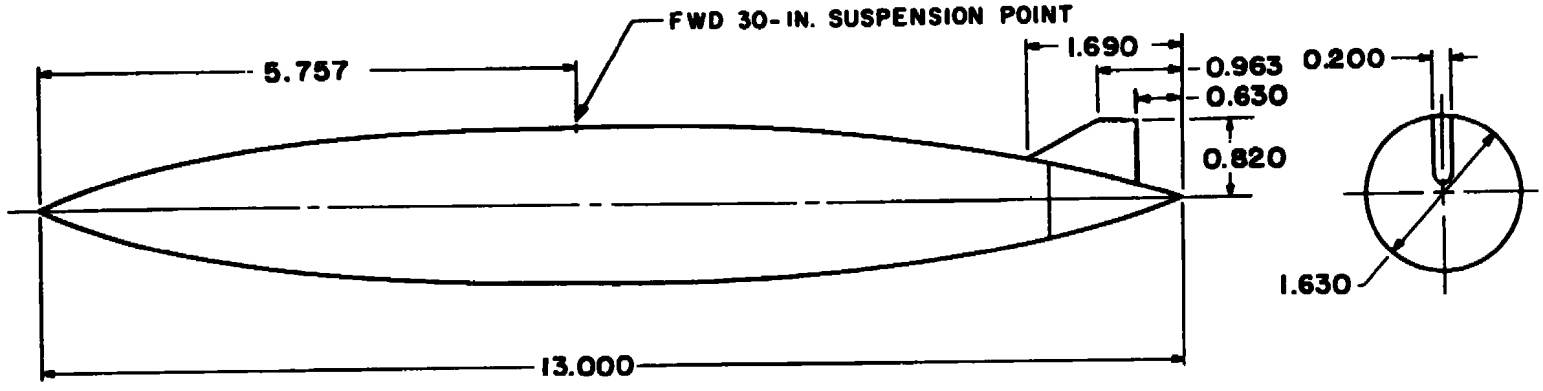

DIMENSIONS IN INCHES

c. F-15 600-gal fuel tank model
Figure 6. Continued.

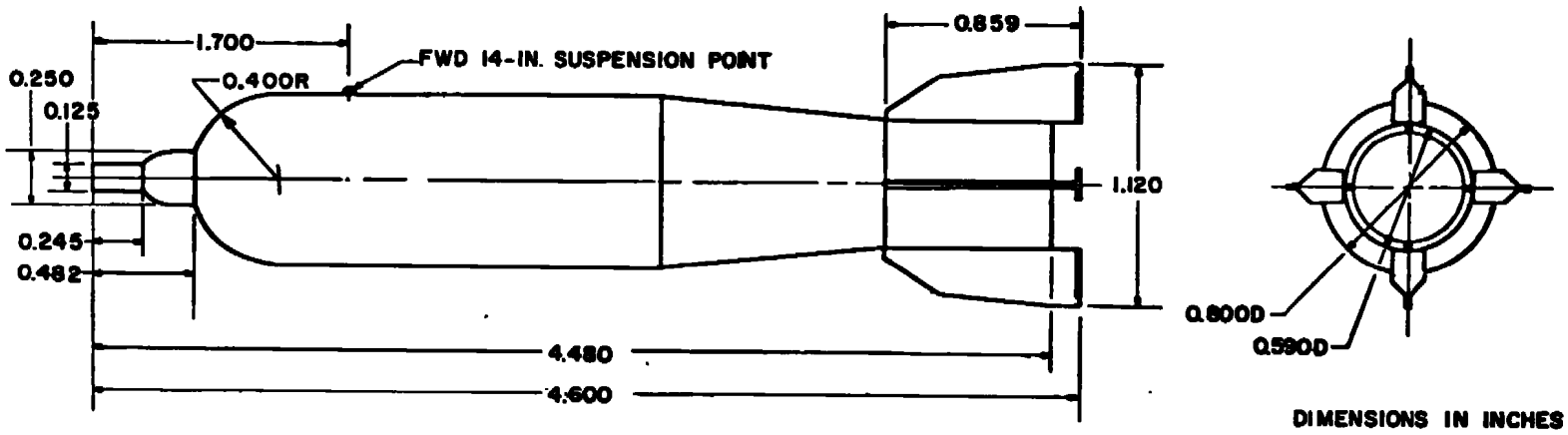

d. SUU-30H/B

Figure 6. Continued.

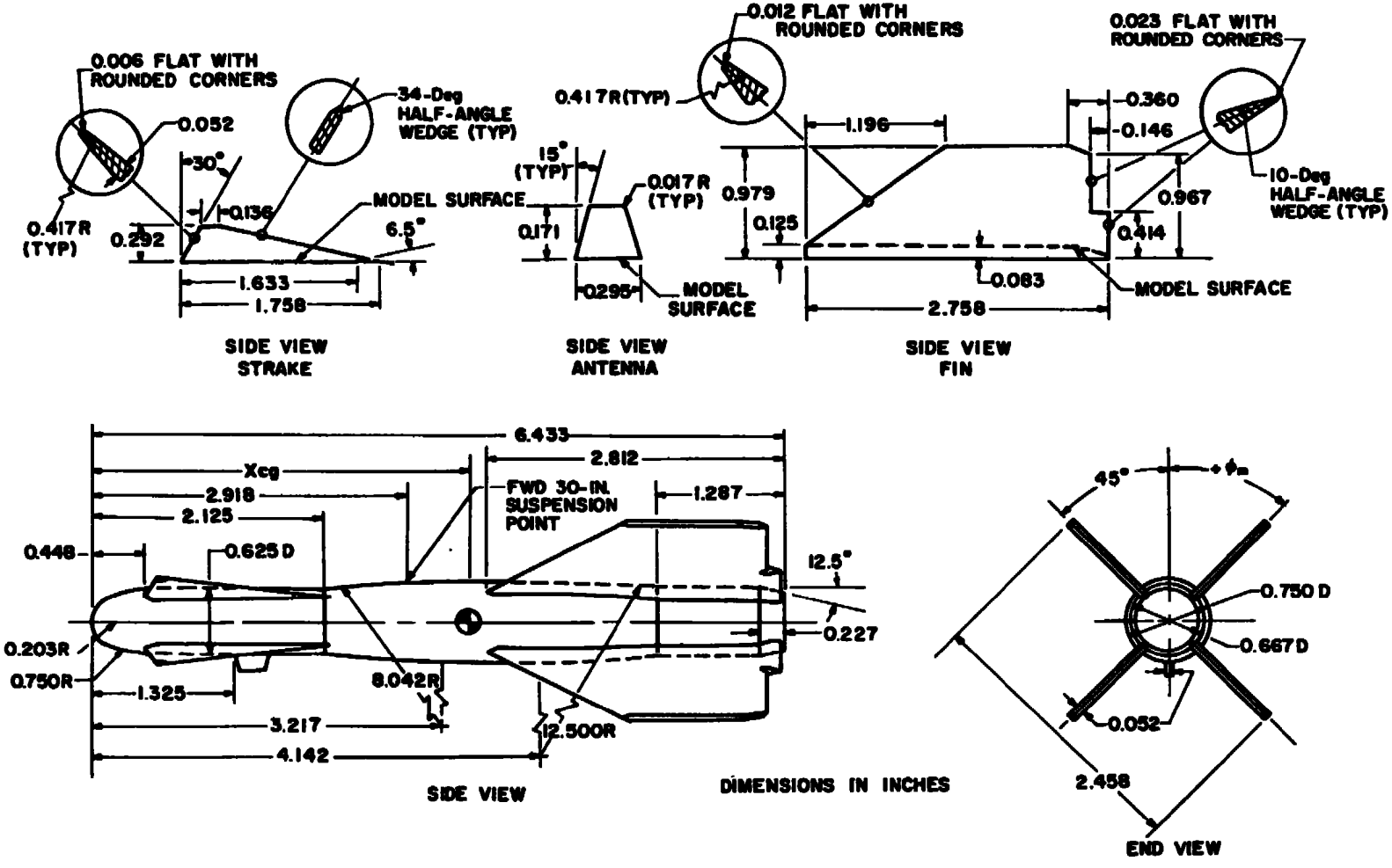

e. GBU-15 (cruciform wing)
Figure 6. Concluded.

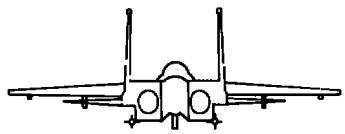

Config. No.	External Armament	Armament Profile	Armament Stations 1	2	F 3 A 4	5	F 6 A 7	8	9	[ΔC$_D$]
101 201	None		Clean	Clean	Clean	Clean	Clean	Clean	Clean	0.0027
202	TEWS		♁	Clean	Clean	Clean	Clean	Clean	♁	0.0011
203	TEWS 600-gal Fuel Tank		♁	Clean	Clean	♁	Clean	Clean	♁	0.0028
204	TEWS 330-gal Fuel Tank		♁	♁	Clean	♁	Clean	♁	♁	0.0061
205	AIM-7F 600-gal Fuel Tank		Clean	♁	✧ ✧	♁	✧ ✧	♁		0.0060
206	GBU-15 (CW) AIM-7F 600-gal Fuel Tank		Clean	⌑	✧ ✧	♁	✧ ✧	⌑	Clean	0.0074
207	GBU-15 (CW) AIM-7F		Clean	⌑	✧ ✧	Clean	✧ ✧	⌑	Clean	0.0057
208	SUU-30H/B AIM-7F		Clean	F A	✧ ✧	Clean	✧ ✧	F A	Clean	0.0134
209	SUU-30H/B AIM-7F 600-gal Fuel Tank		Clean	F A	✧ ✧	♁	✧ ✧	F A	Clean	0.0154
210	AIM-7F 600-gal Fuel Tank		Clean	Clean	✧ ✧	♁	✧ ✧	Clean	Clean	0.0090
211	AIM-7F		Clean	Clean	✧ ✧	Clean	✧ ✧	Clean	Clean	0.0012
212	ASRM AIM-7F		Clean	⌑	✧ ✧	Clean	✧ ✧	⌑	Clean	0.0033
213	ASRM AIM-7F		Clean	F A	✧ ✧	Clean	✧ ✧	F A	Clean	0.0043
214	TEWS GBU-15 (CW) AIM-7F		♁	⌑	✧ ✧	Clean	✧ ✧	⌑	♁	0.0076
215	600-gal Fuel Tank		Clean	Clean	Clean	♁	Clean	Clean	Clean	0.0034
216	600-gal Fuel Tank		Clean	♁	Clean	♁	Clean	♁	Clean	0.0049
217	TEWS GBU-15 (CW) AIM-7F 600-gal Fuel Tank		♁	⌑	✧ ✧	♁	✧ ✧	⌑	♁	0.0095
218	GBU-15 (CW) AIM-9 AIM-7F 600-gal Fuel Tank		Clean	⌑	✧ ✧	♁	✧ ✧	⌑	Clean	No Data
219	GBU-15 (CW)		Clean	⌑	Clean	Clean	Clean	⌑	Clean	0.0049

*Drag coefficient increment is referenced to configuration 201 at C_L = 0.3 and M_∞ = 0.6.

Figure 7. Configuration identification key.

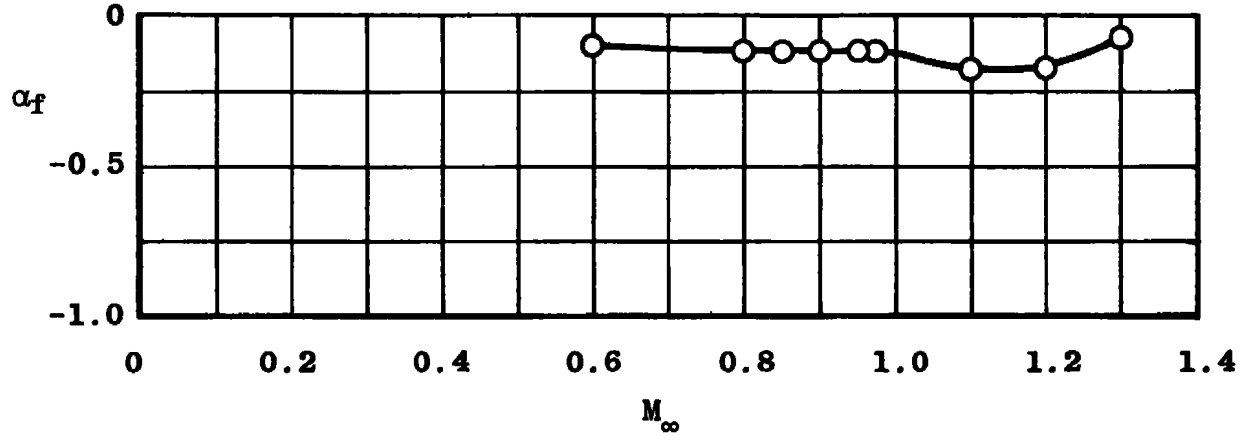

Figure 8. Tunnel flow angle as a function of Mach number.

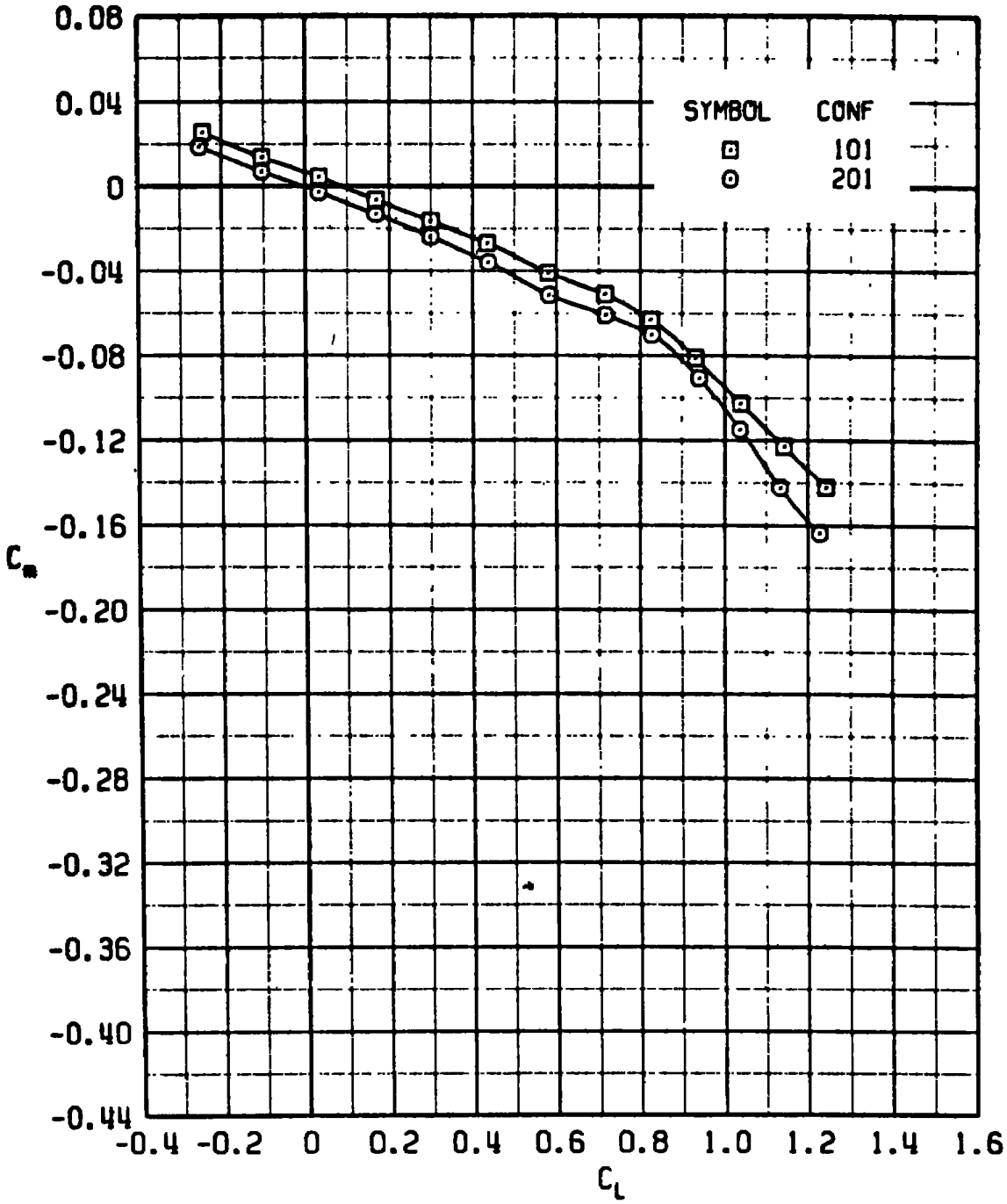

a. $M_\infty = 0.60$

Figure 9. Effect of inlet configuration on static longitudinal stability.

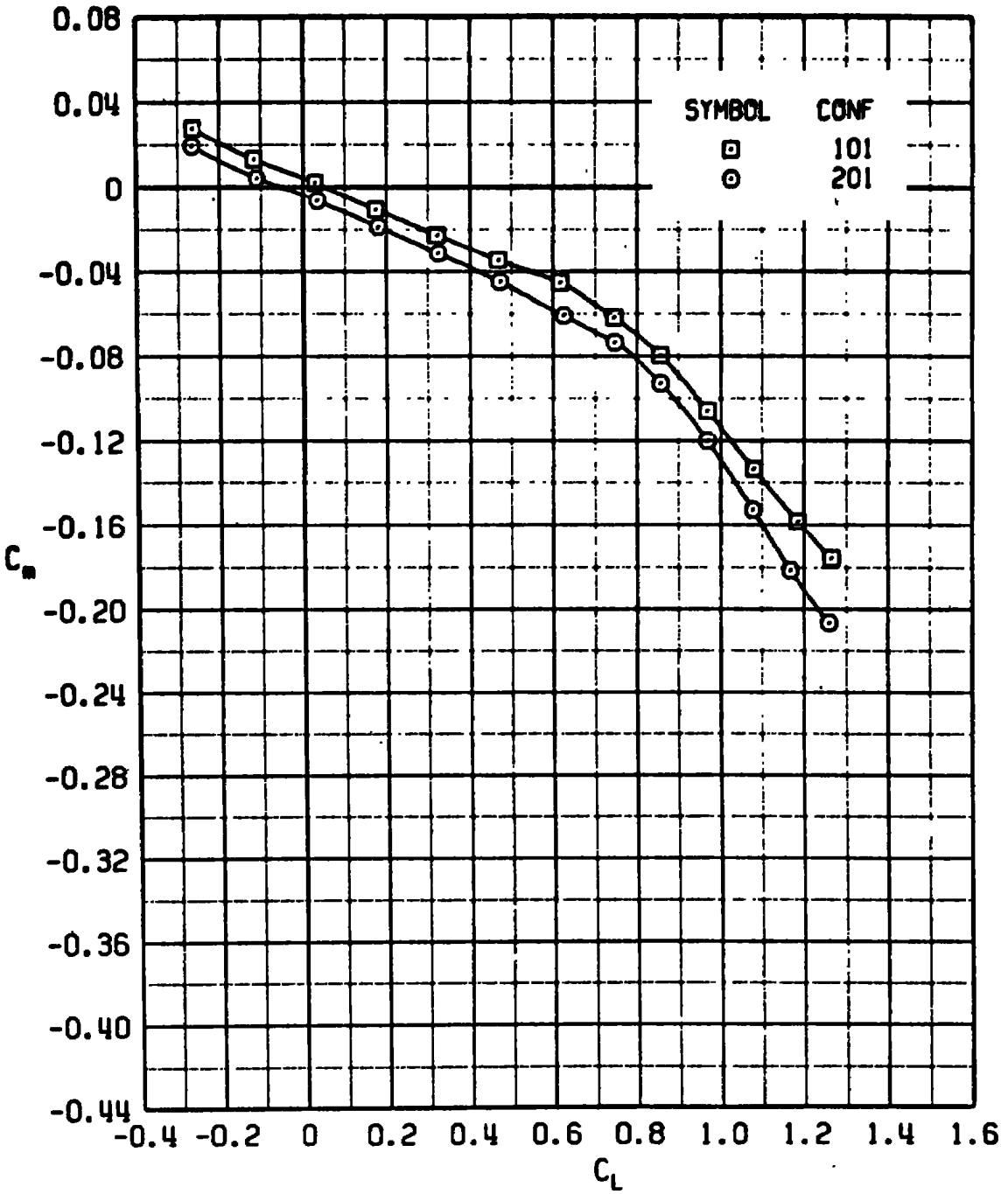

b. $M_\infty = 0.80$

Figure 9. Continued.

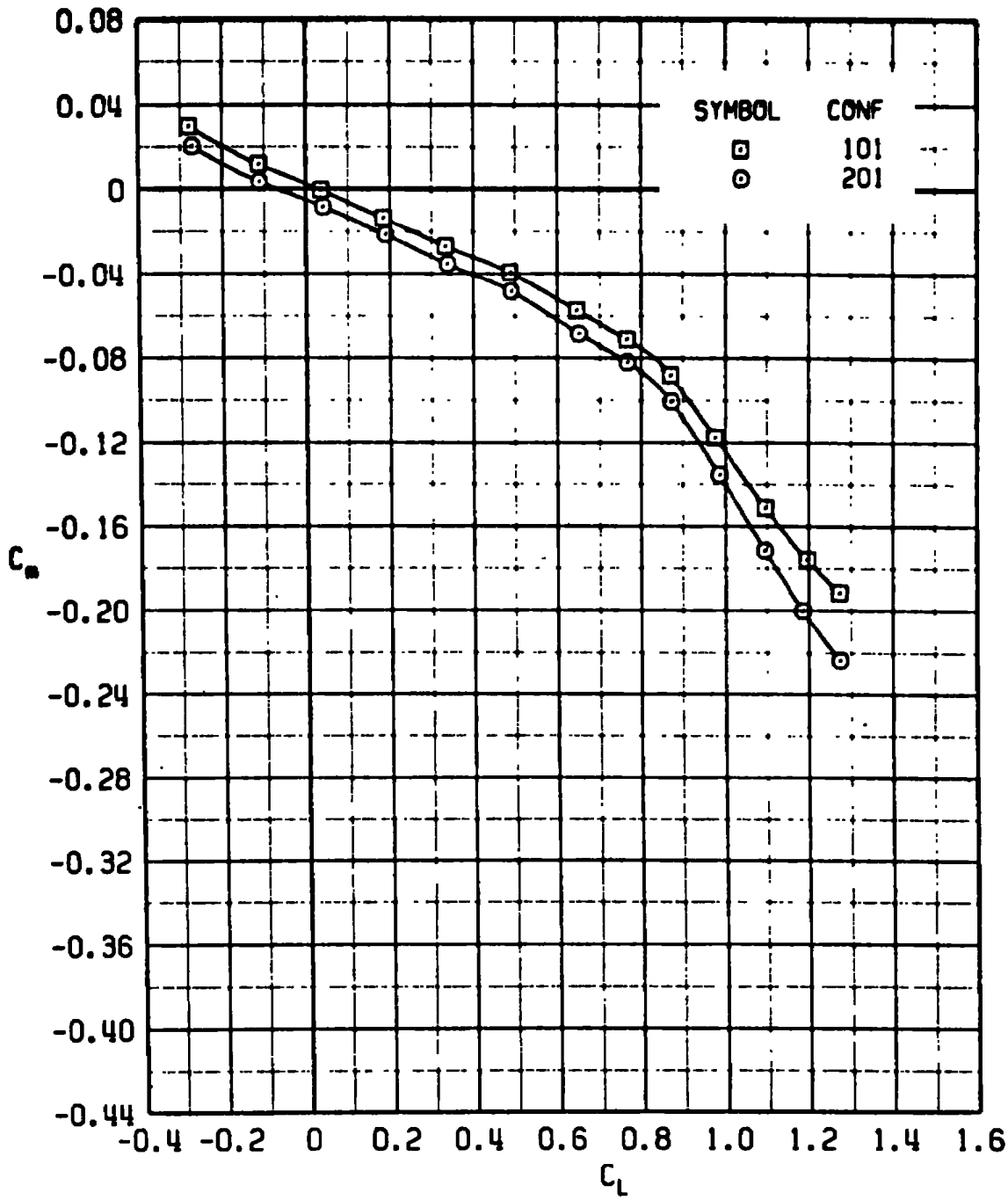

c. $M_\infty = 0.85$

Figure 9. Continued.

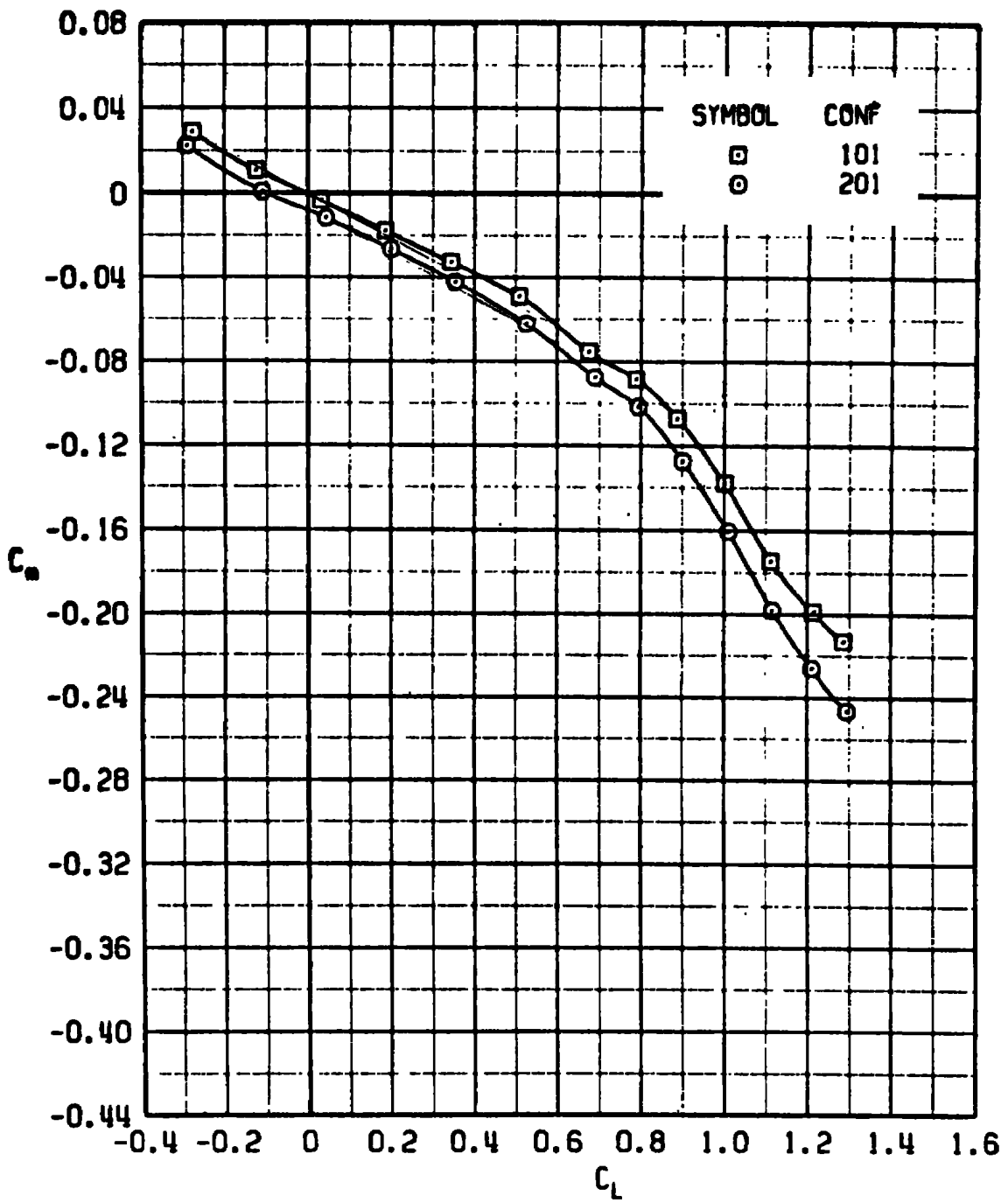

d. $M_\infty = 0.90$

Figure 9. Continued.

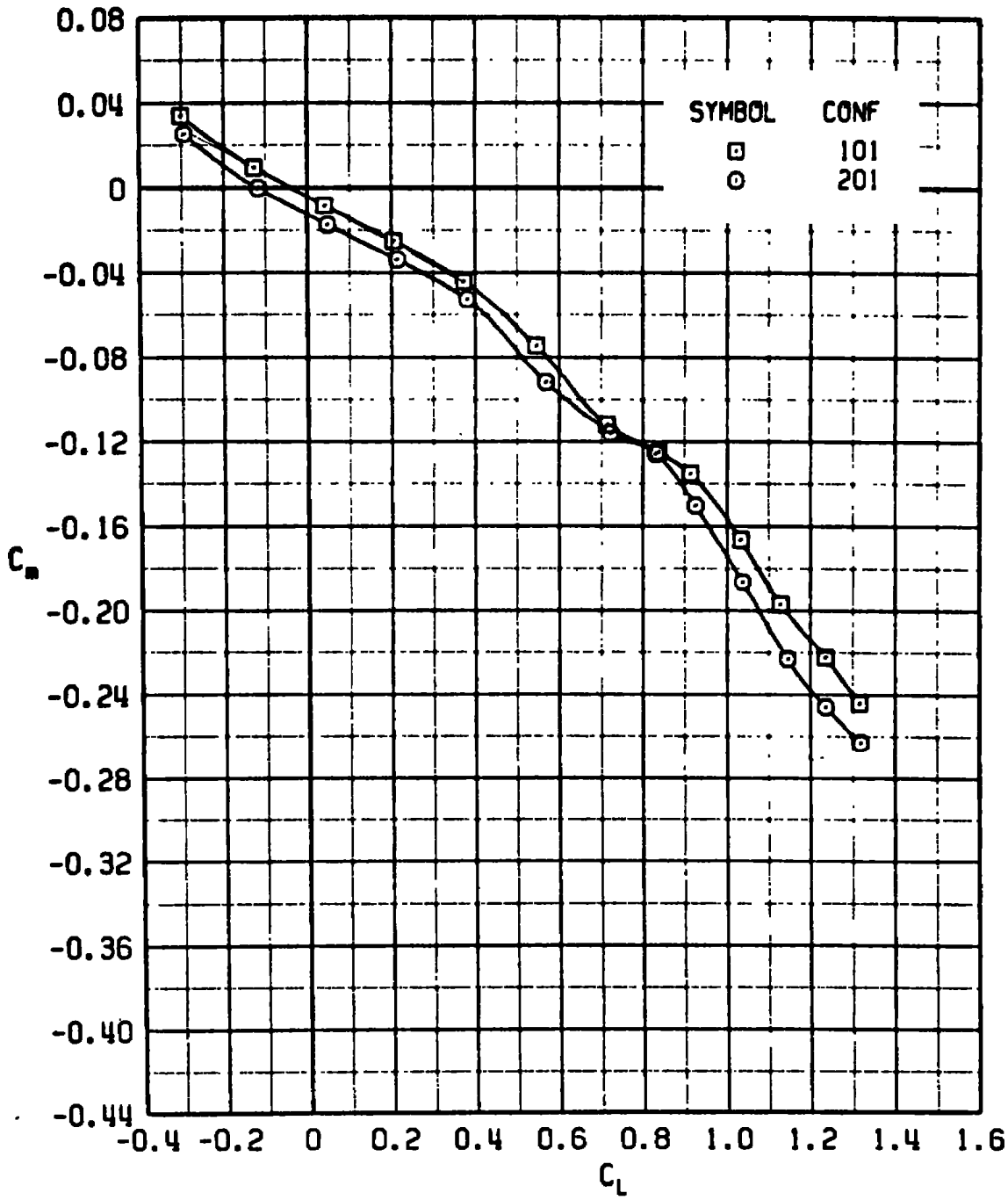

e. $M_\infty = 0.95$

Figure 9. Continued.

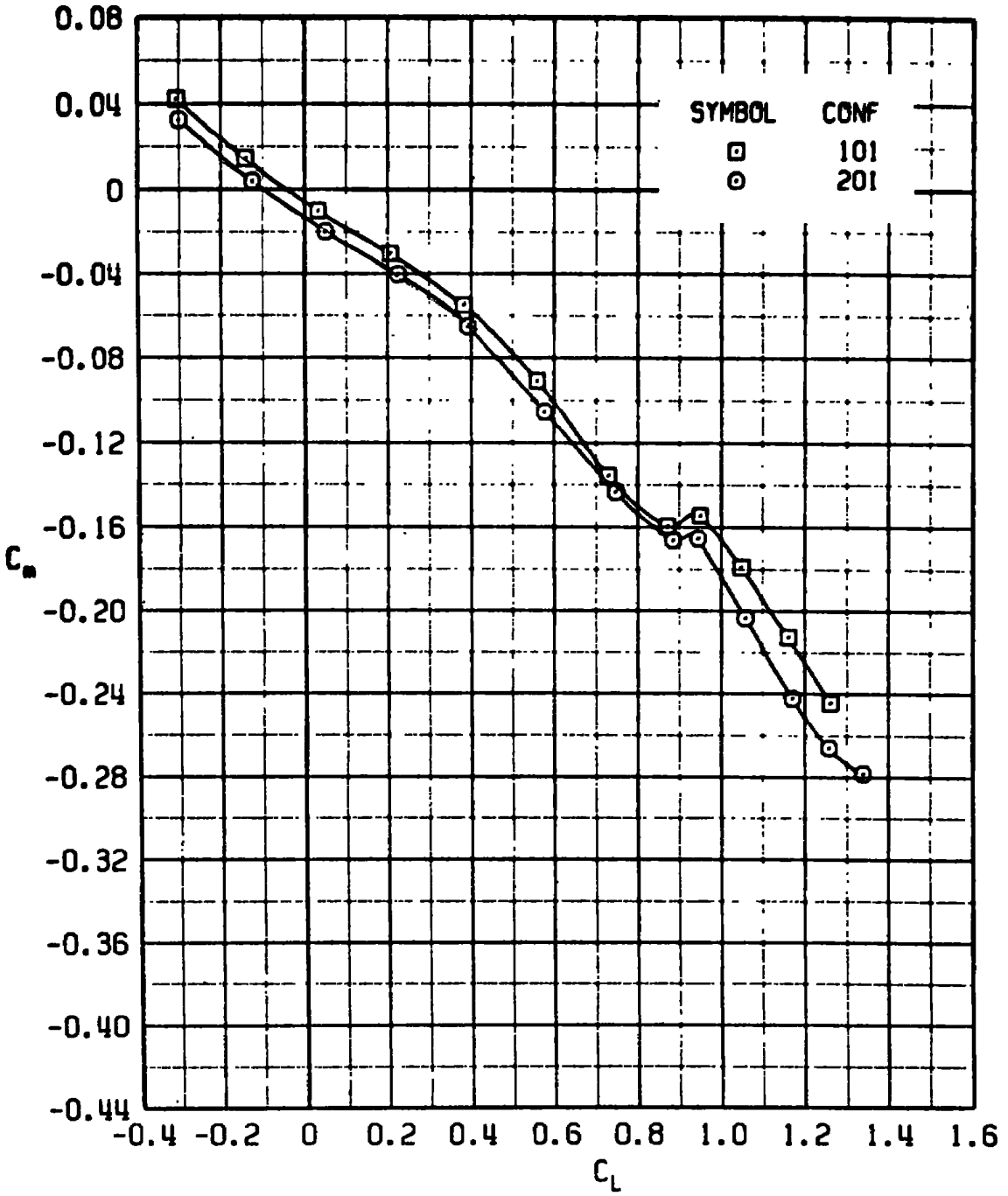

f. $M_\infty = 0.975$

Figure 9. Continued.

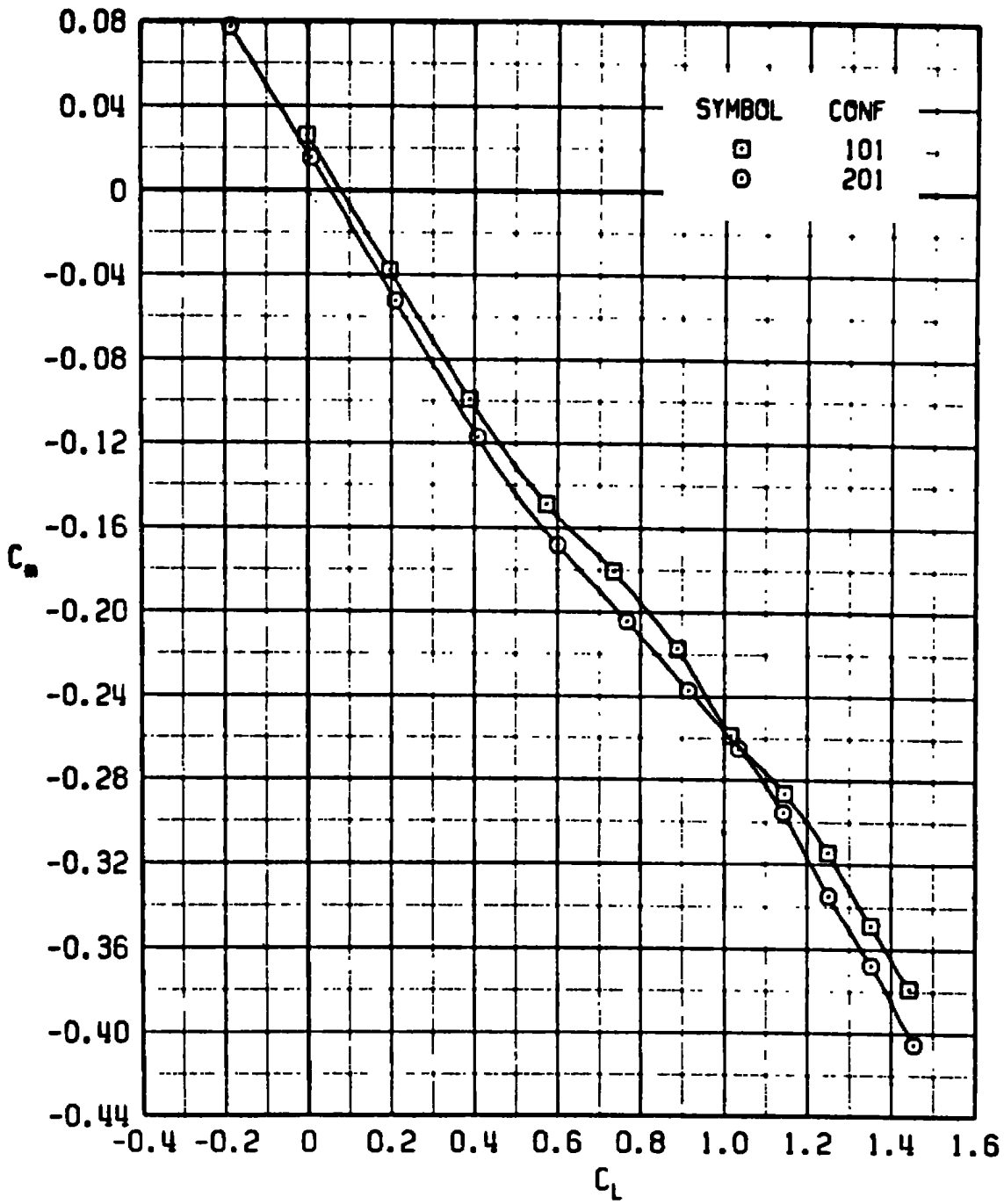

g. $M_\infty = 1.10$

Figure 9. Continued.

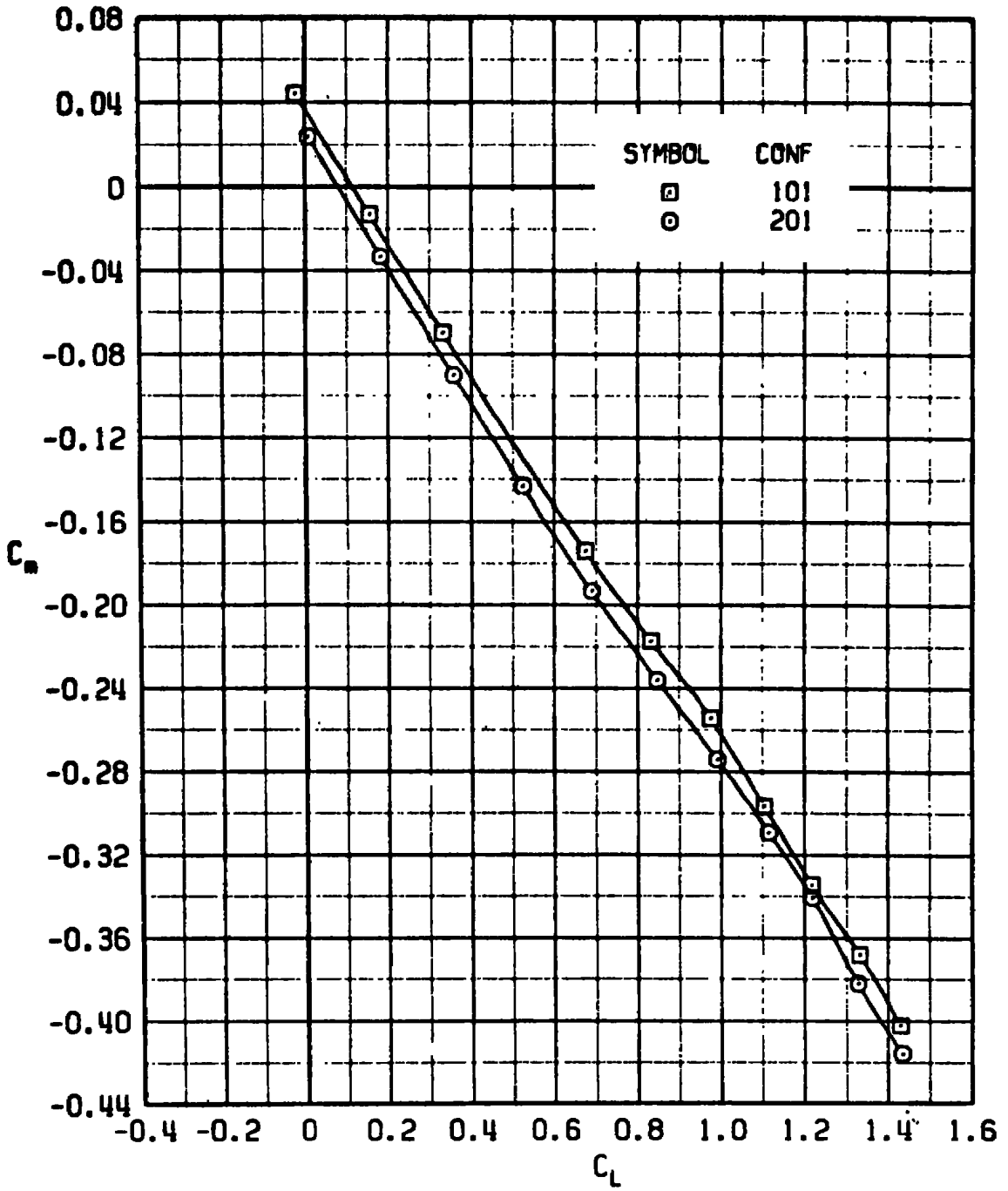

h. $M_\infty = 1.20$

Figure 9. Continued.

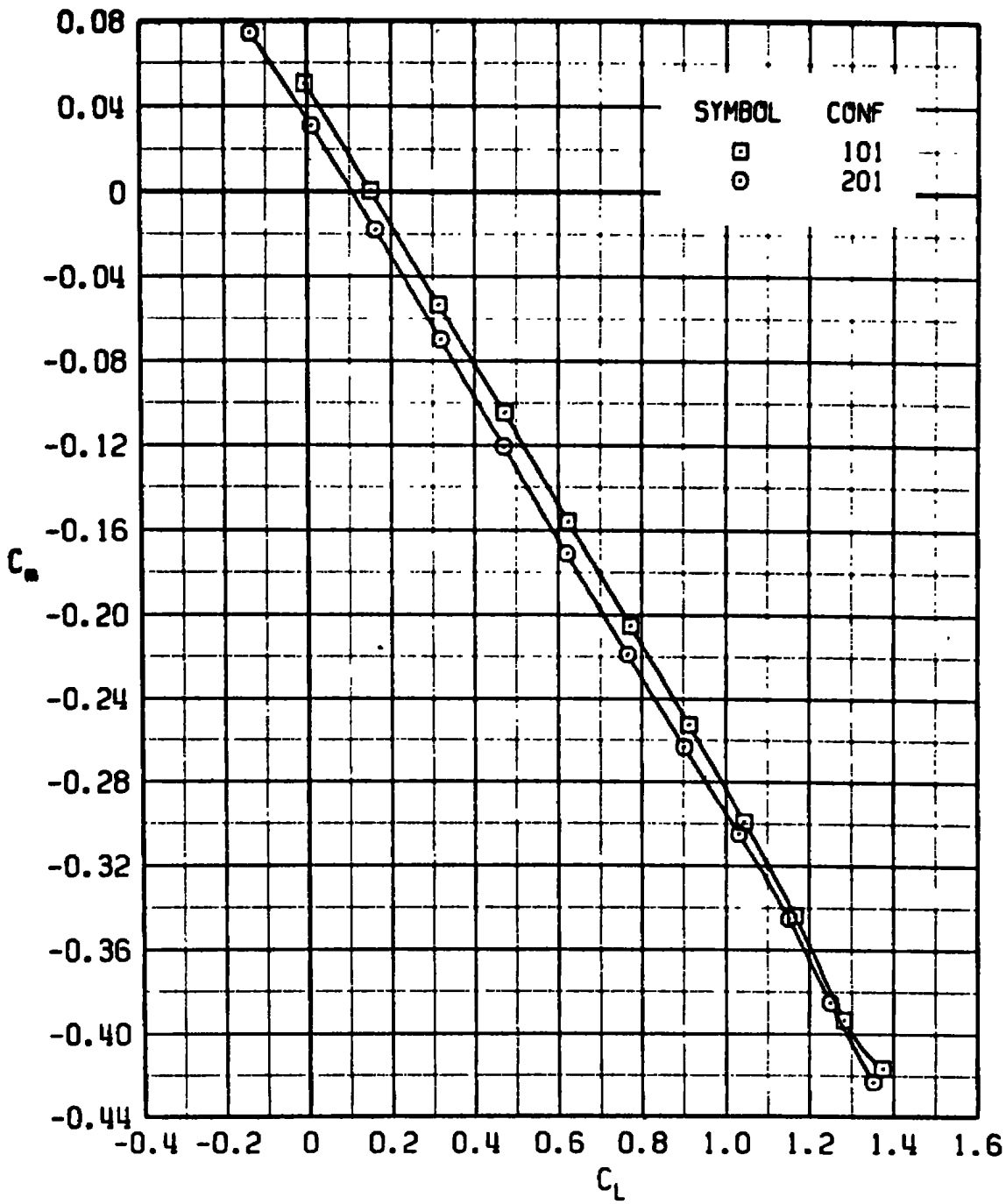

i. $M_\infty = 1.30$

Figure 9. Concluded.

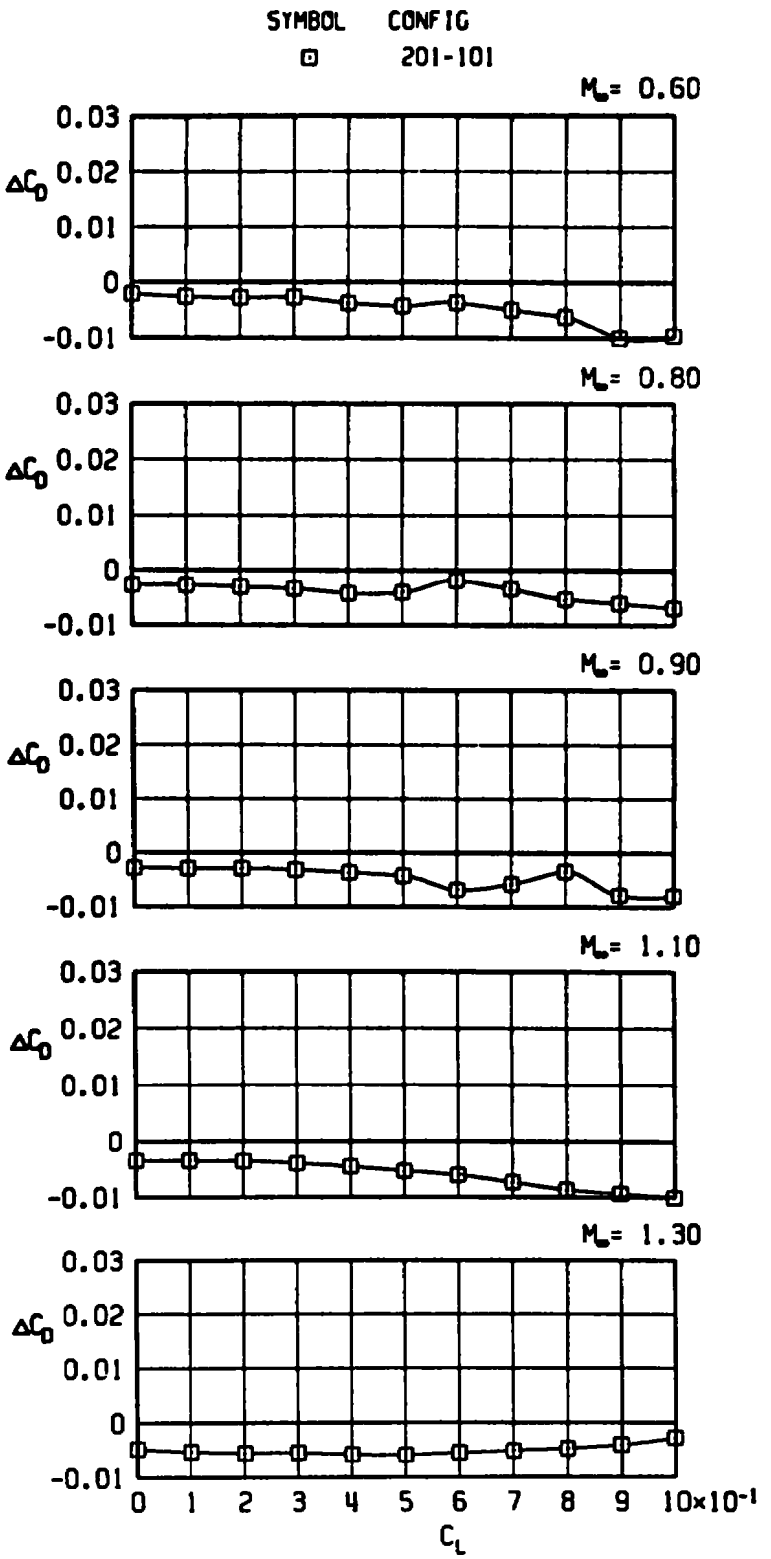

Figure 10. Drag difference between the high alpha and the low alpha inlet.

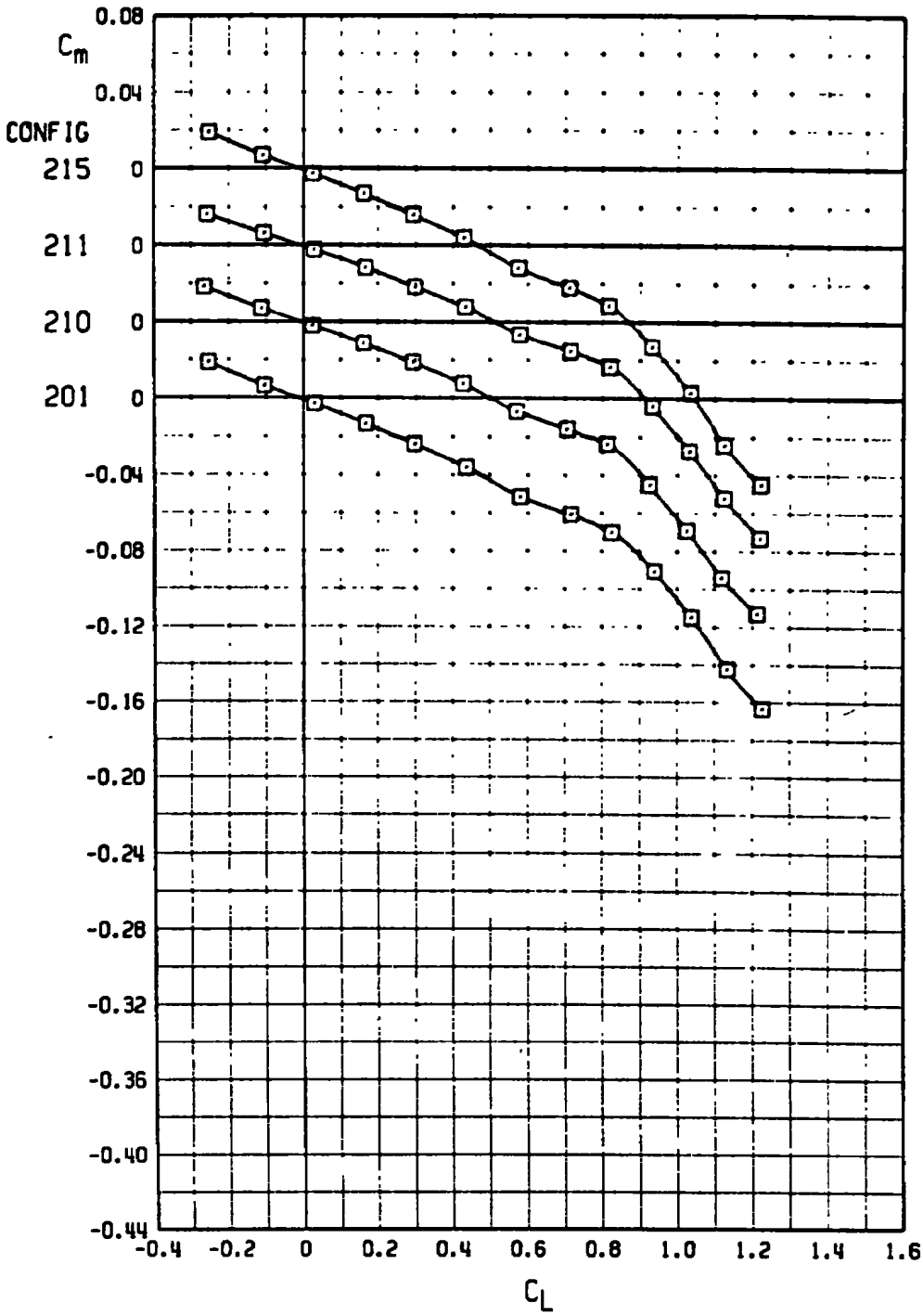

a. $M_\infty = 0.60$

Figure 11. Static longitudinal stability characteristics of the baseline store configurations.

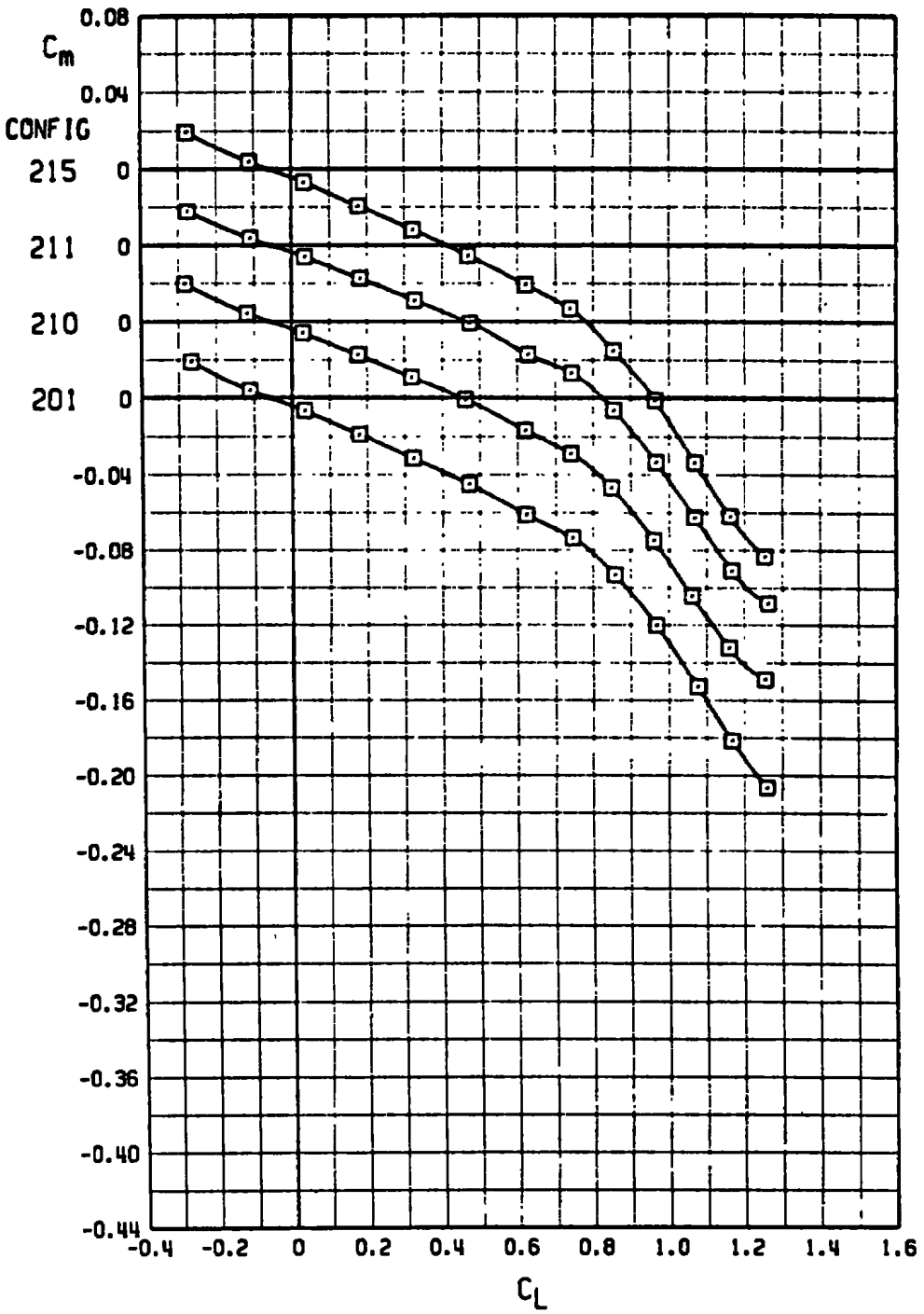

b. $M_\infty = 0.80$

Figure 11. Continued.

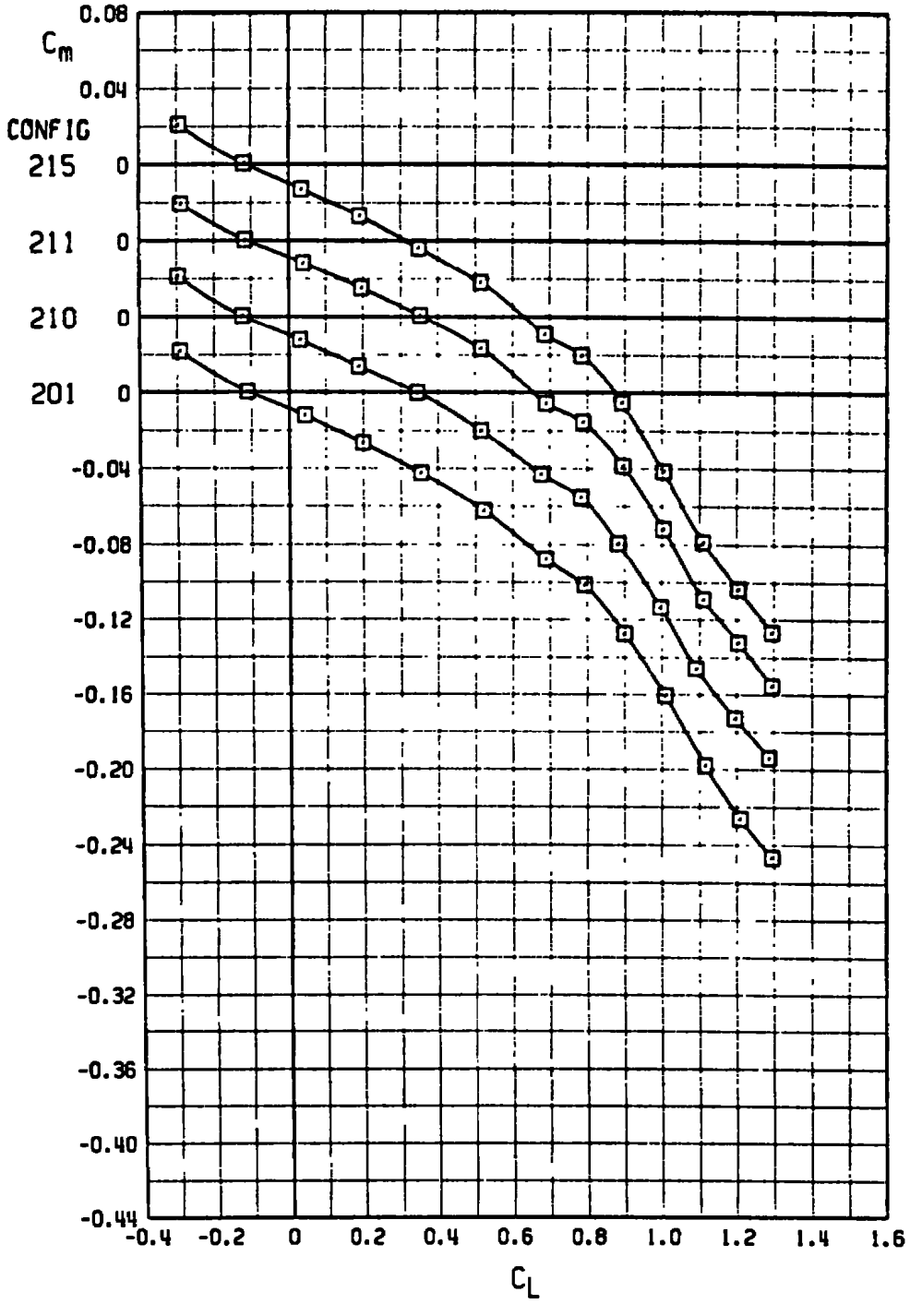

c. $M_\infty = 0.90$

Figure 11. Continued.

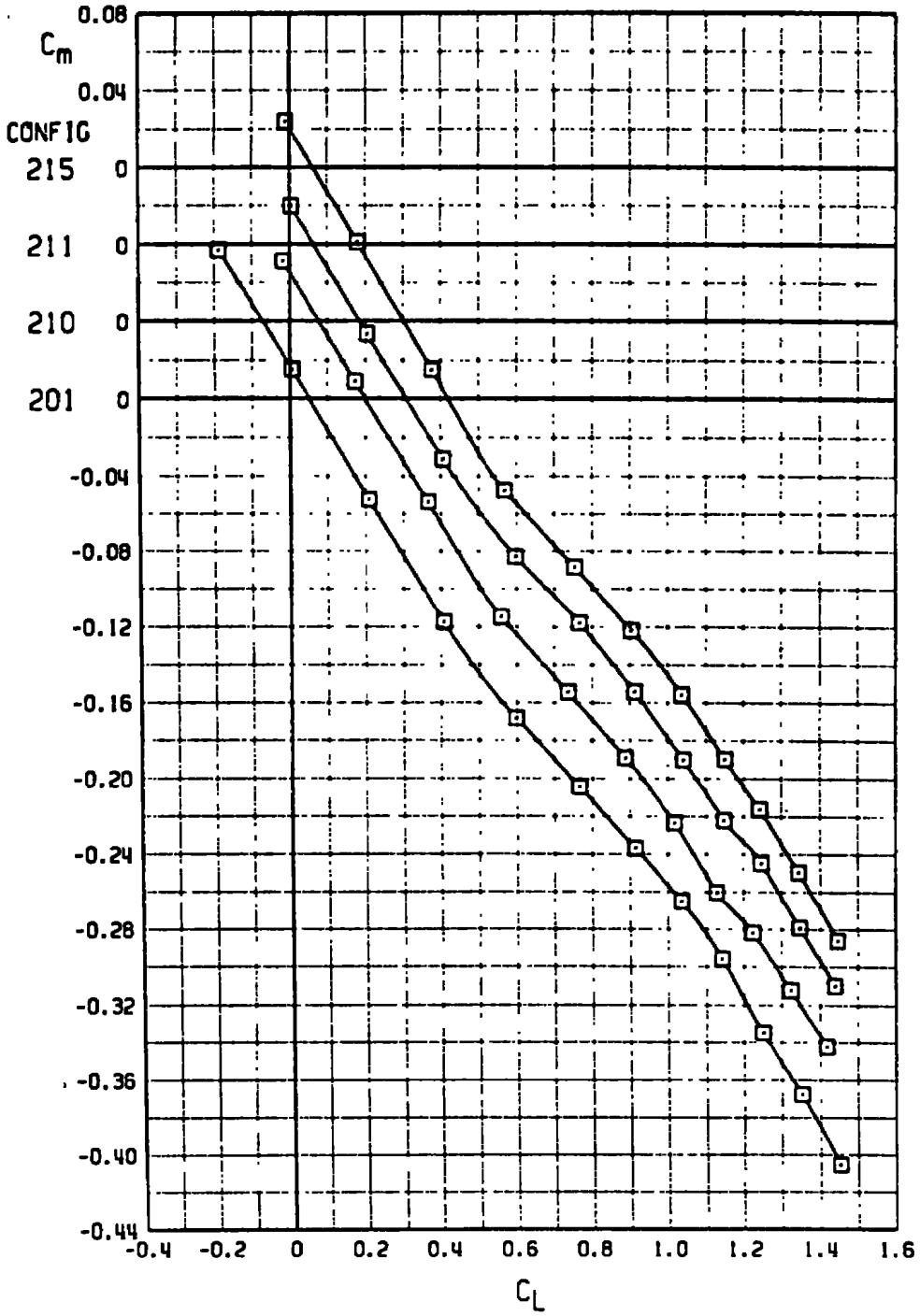

d. $M_\infty = 1.10$

Figure 11. Continued.

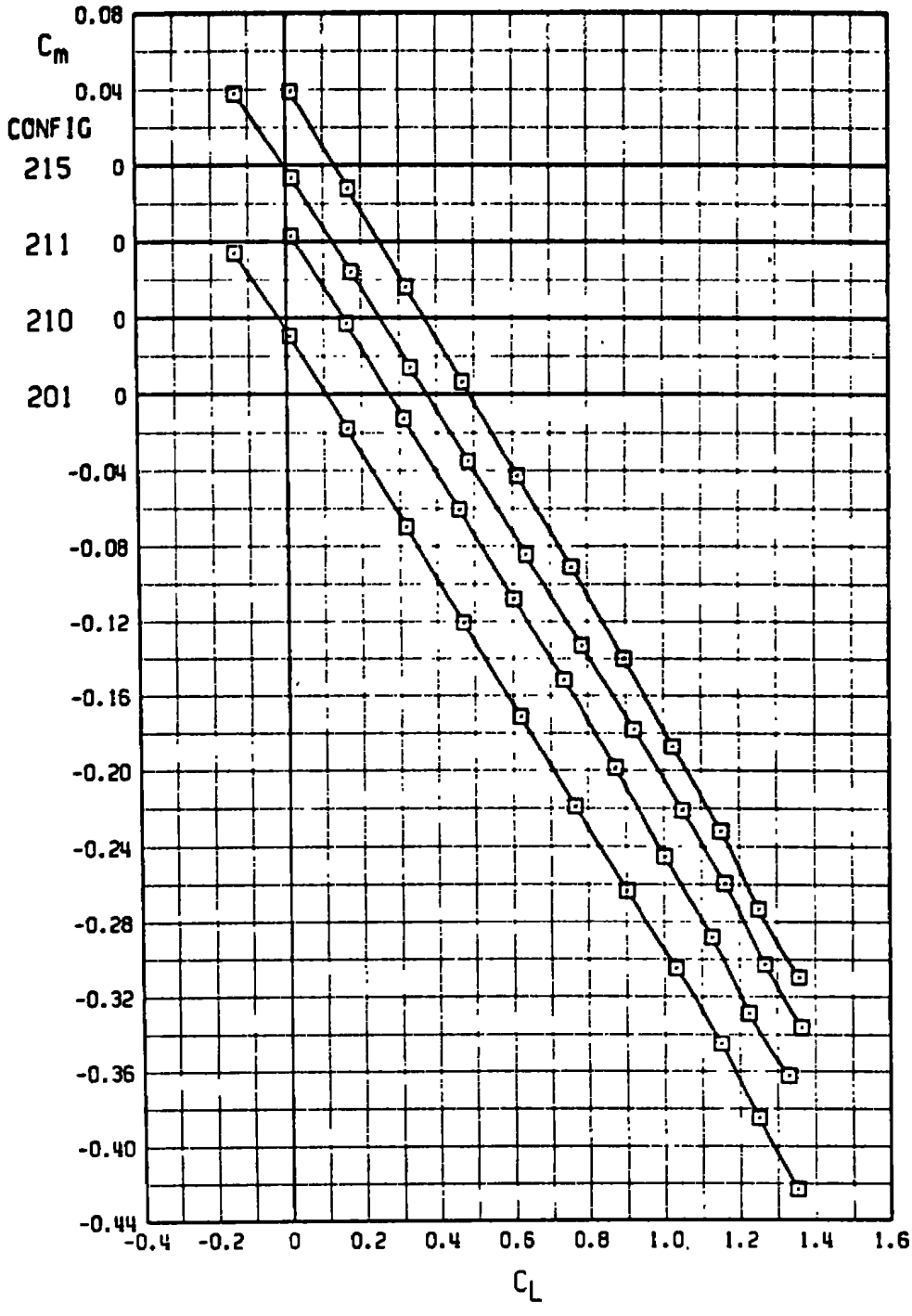

e. $M_\infty = 1.30$

Figure 11. Concluded.

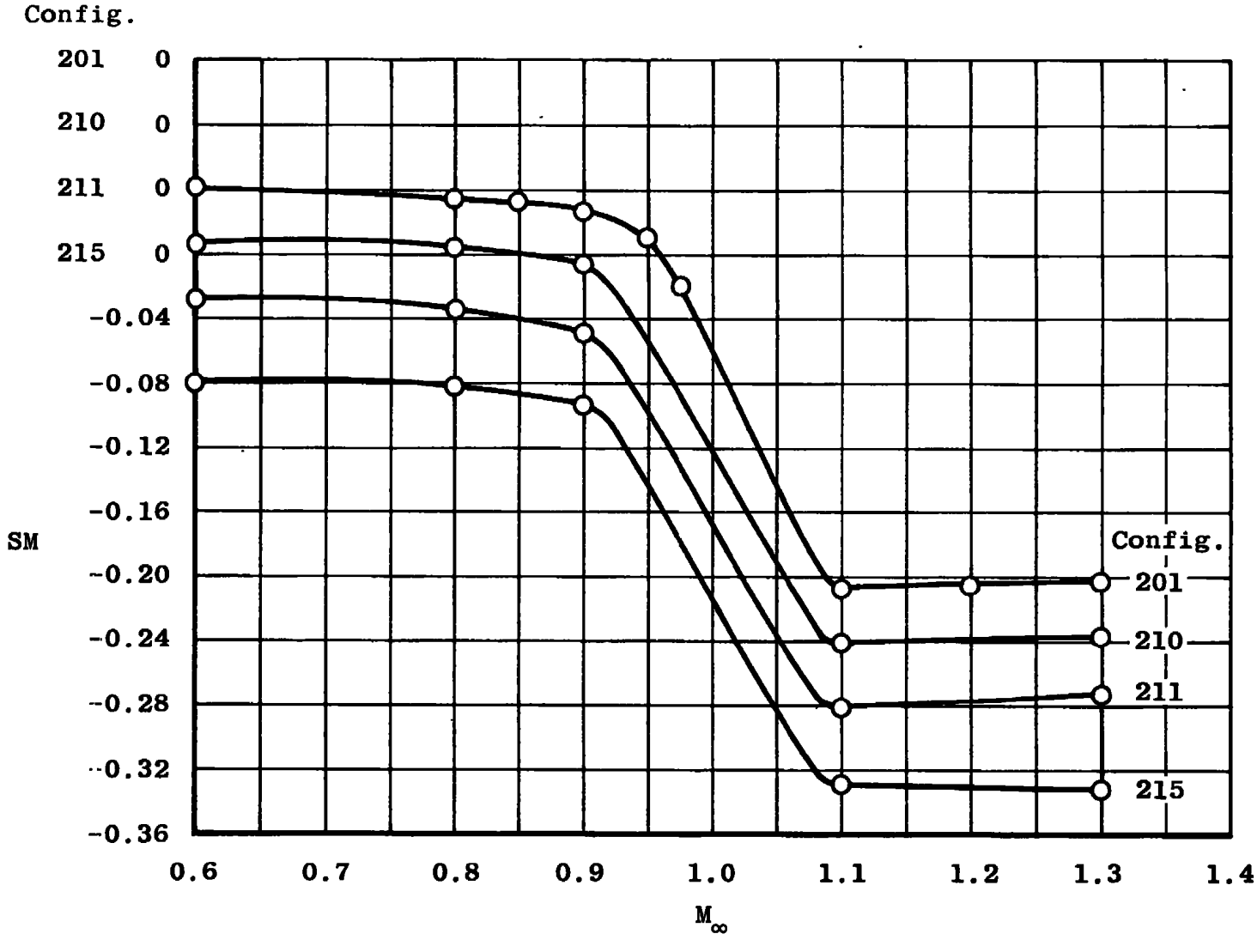

Figure 12. Static margin as a function of Mach number for the baseline store configurations.

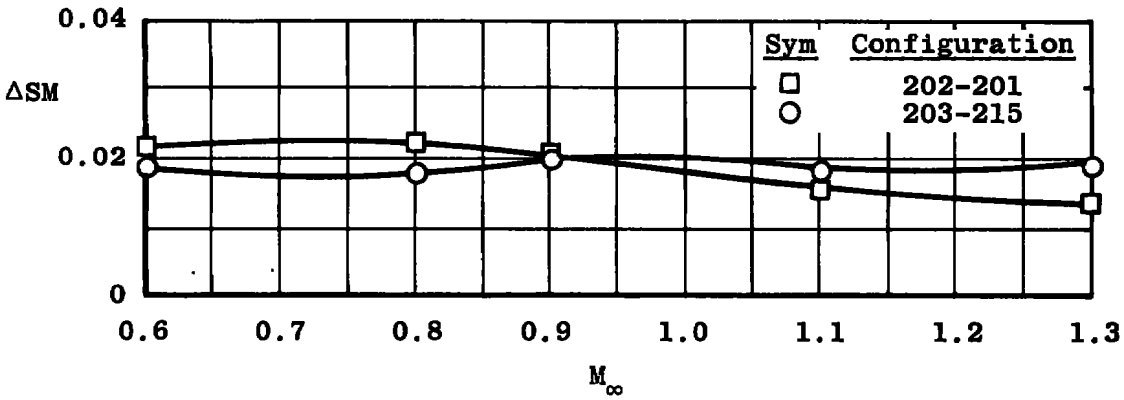

a. Centerline 600-gal tank

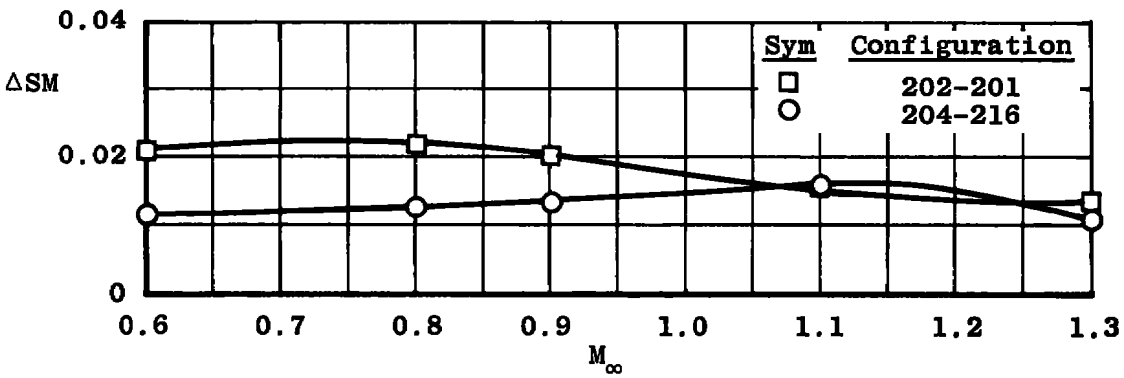

b. 600-gal tanks at stations 2, 5, and 8

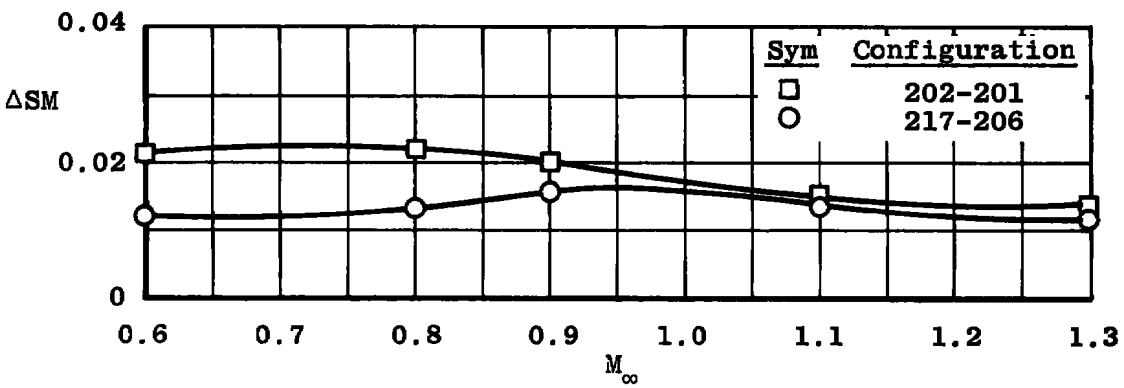

c. GBU-15 (CW) + AIM-7F + centerline 600-gal tank

Figure 13. Effect of various store loadings on the static margin change caused by adding the TEWS stores to armament stations 1 and 9.

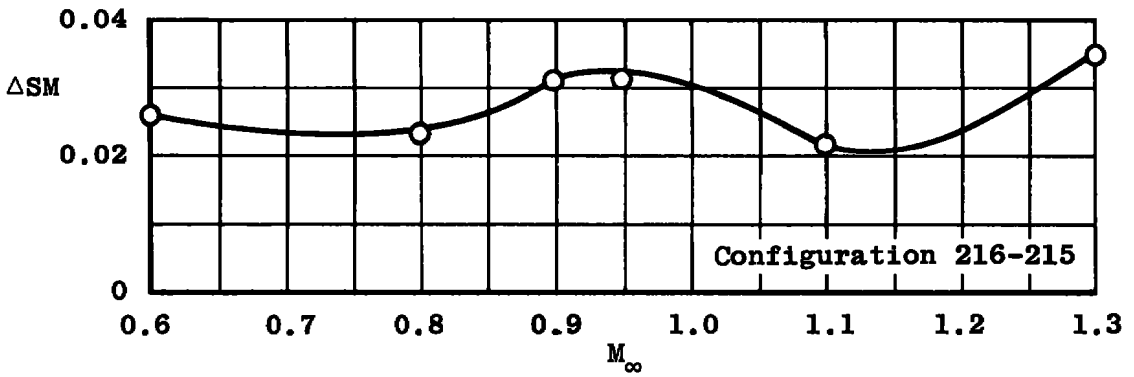

a. Centerline 600-gal tank

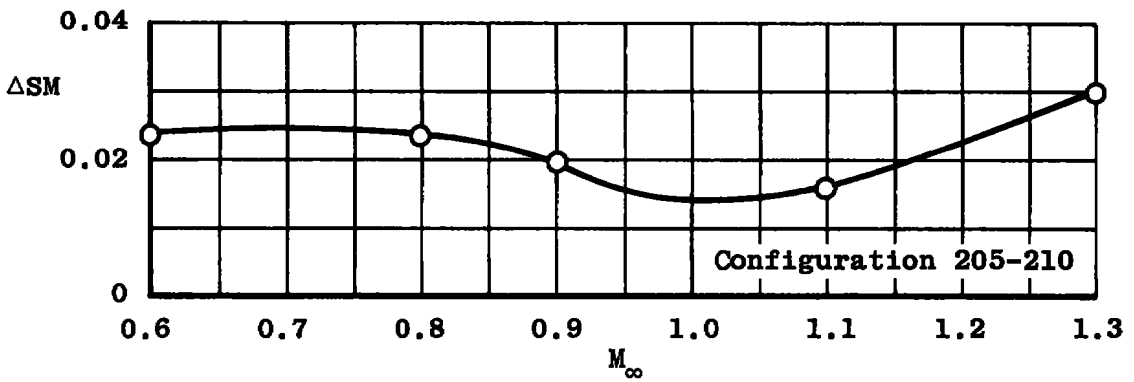

b. AIM-7F + centerline 600-gal tank

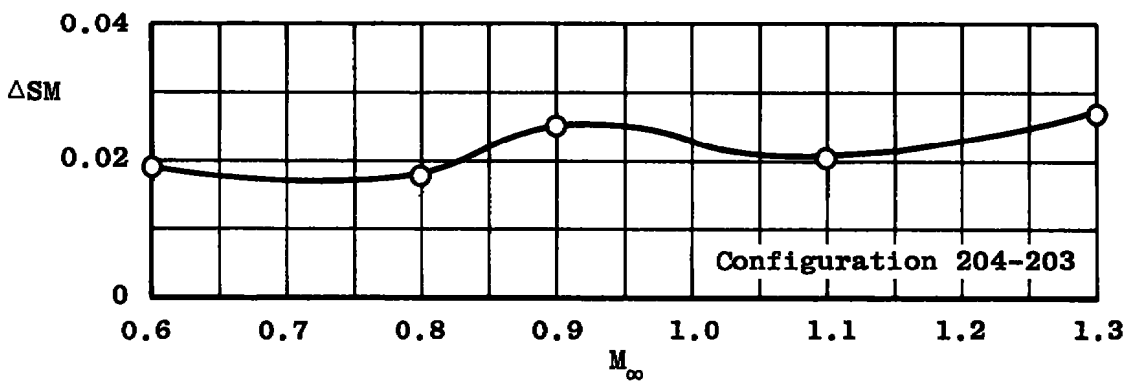

c. Centerline 600-gal fuel tank + TEWS

Figure 14. Effect of various store loadings on the static margin change caused by adding inboard 600-gal fuel tanks to armament stations 2 and 8.

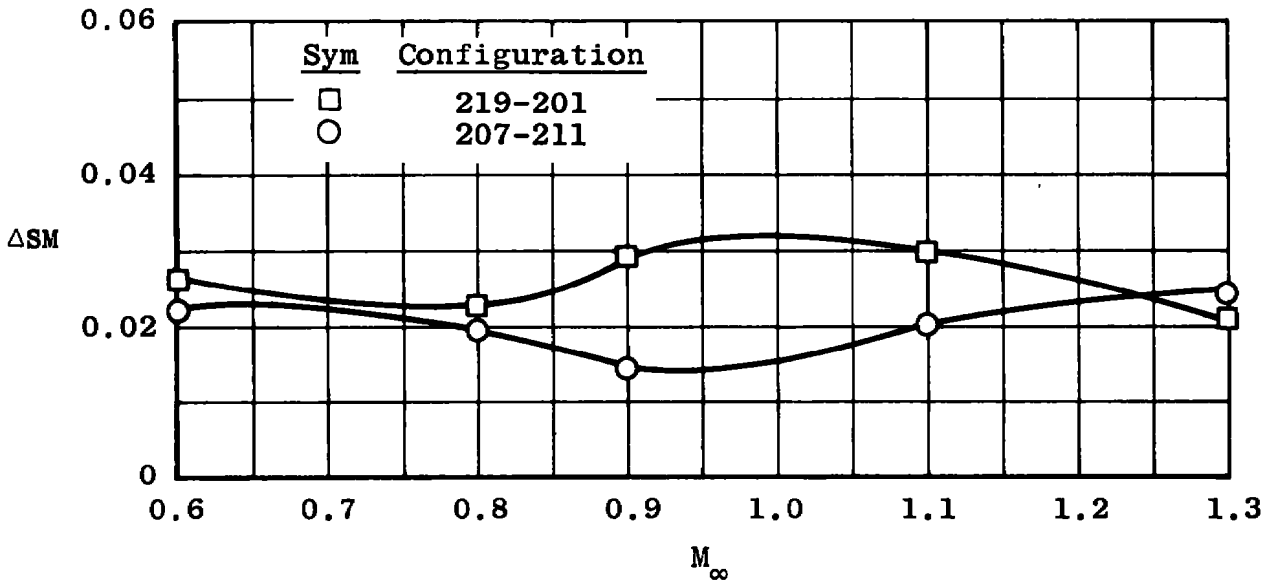

a. AIM-7F + centerline 60-gal tank

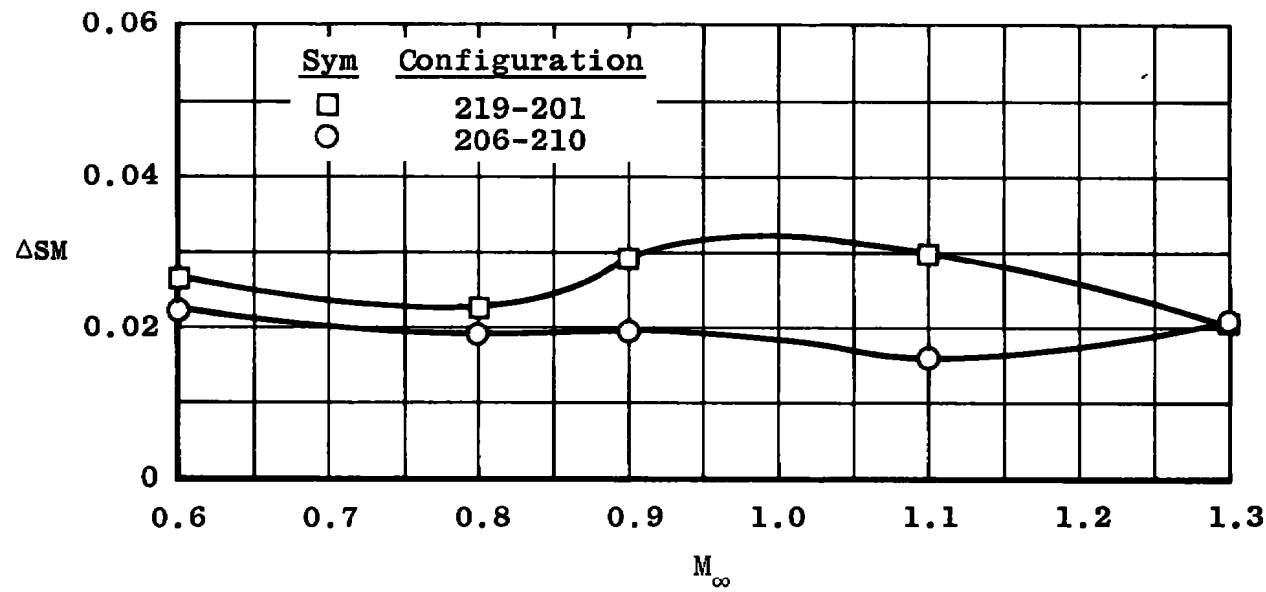

b. AIM-7F + centerline 600-gal tank

Figure 15. Effect of various store loadings on the static margin change caused by adding the GBU-15 (CW) store to armament stations 2 and 8.

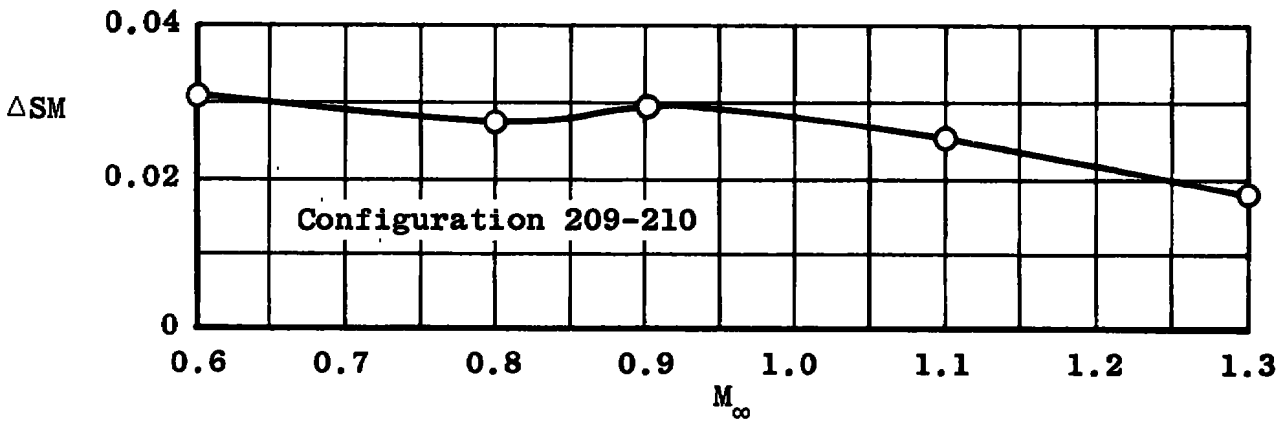

a. AIM-7F + centerline 60-gal tank

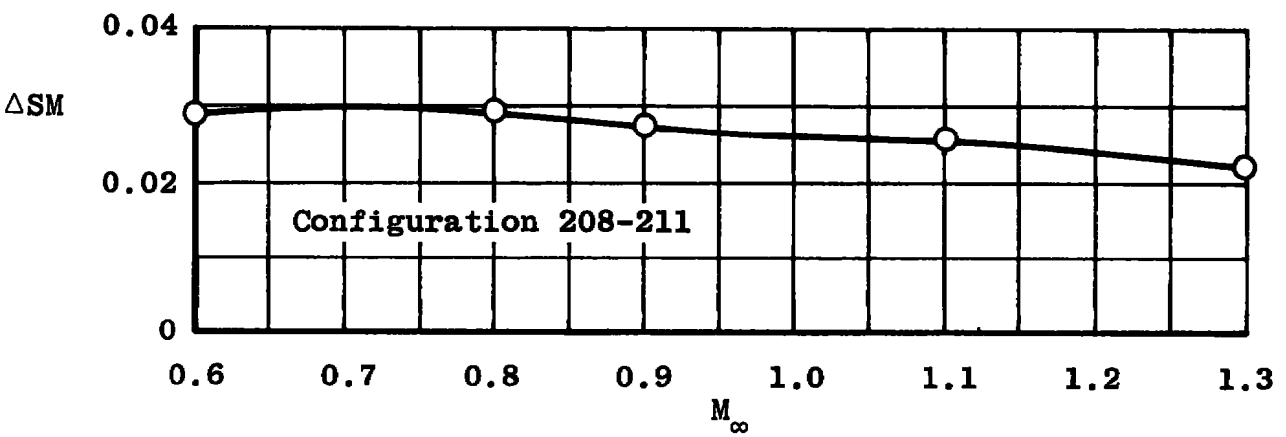

b. AIM-7F

Figure 16. Effect of various store loadings on the static margin change caused by adding 12 SUU-30H/B stores to armament stations 2 and 8.

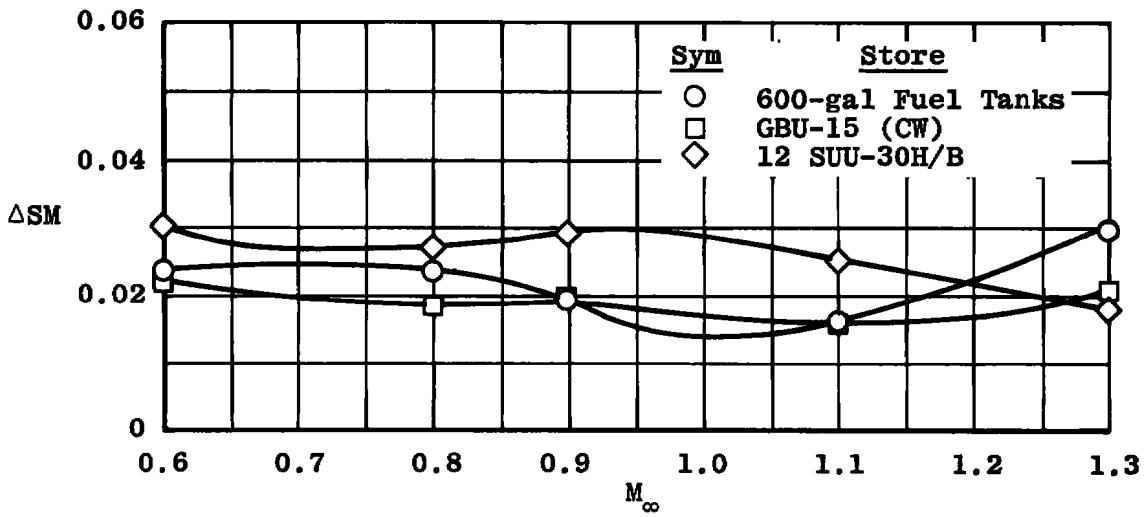

Figure 17. Comparison of static margin changes caused by various store configurations at armament stations 2 and 8 in the presence of the AIM-7F and centerline 600-gal fuel tank.

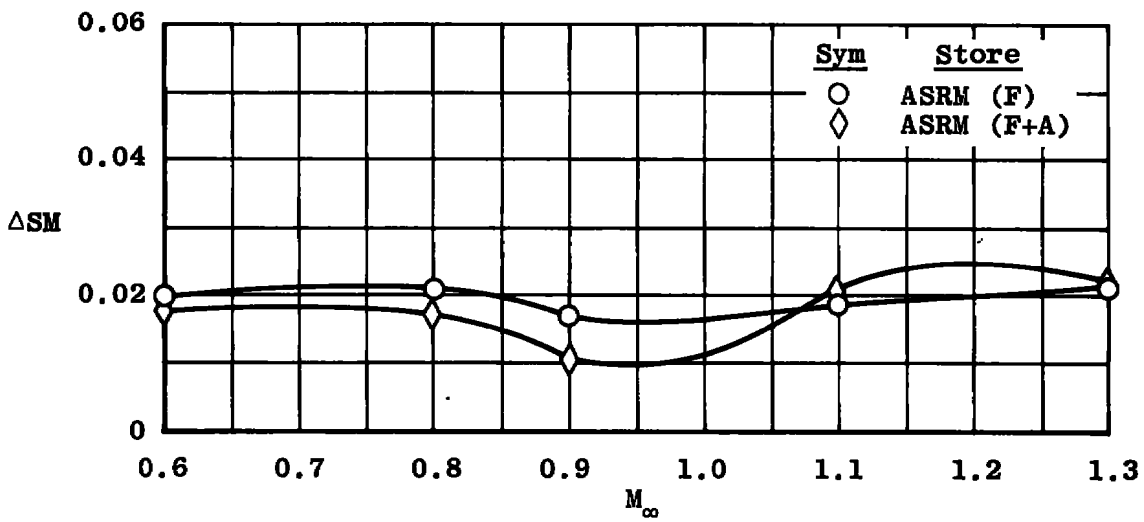

Figure 18. Comparison of the static margin change caused by adding one ASRM and two ASRM stores in tandem at armament stations 2 and 8.

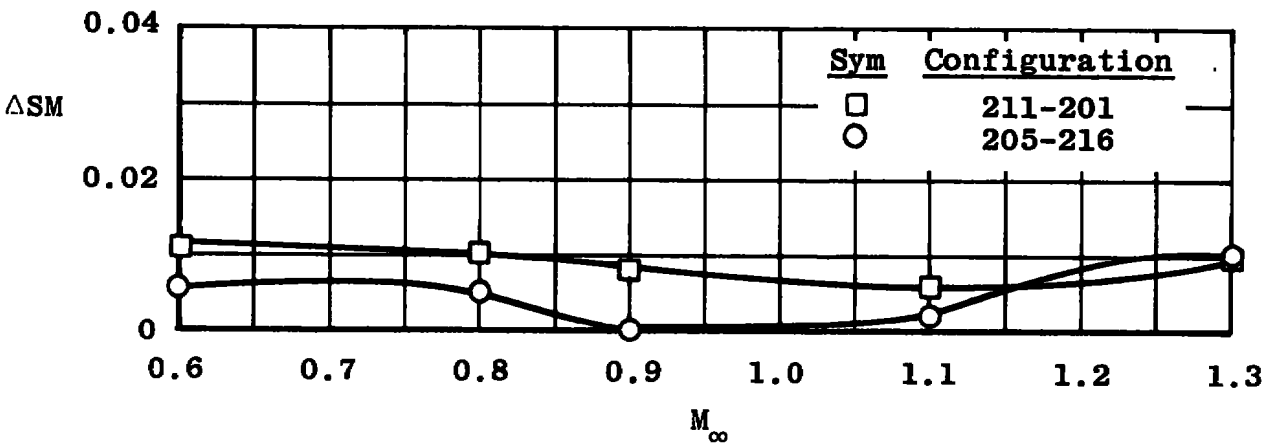

Figure 19. Effect of the 600-gal fuel tanks at armament stations 2, 5, and 8 on the static margin change caused by adding the AIM-7F stores to armament stations 3, 4, 6, and 7.

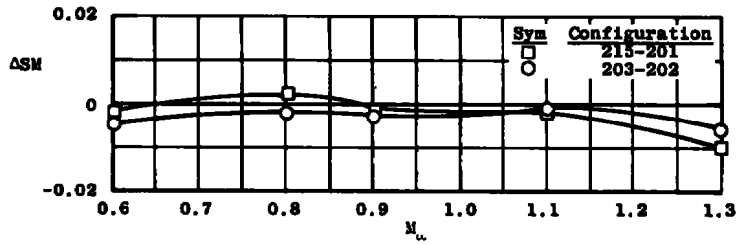

a. TEWS

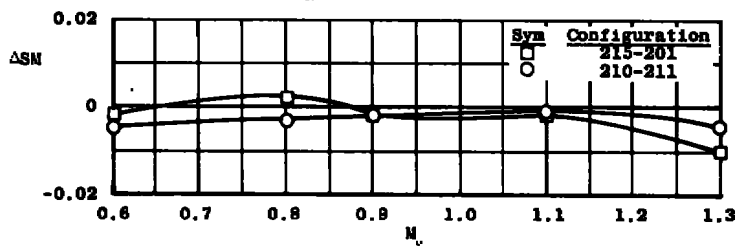

b. AIM-7F

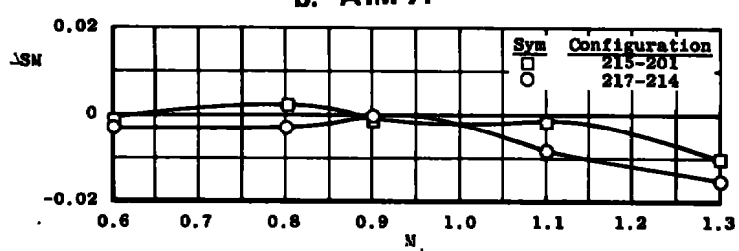

c. TEWS + AIM-7F + GBU-15 (CW)

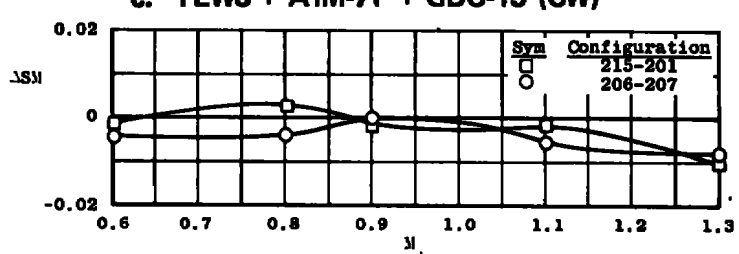

d. AIM-7F + GBU-15 (CW)

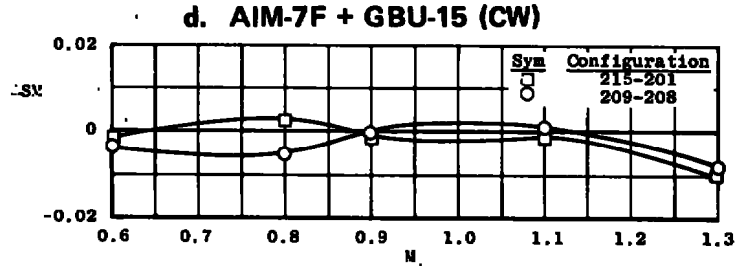

e. AIM-7F + SUU-30H/B

Figure 20. Effect of various store loadings on the static margin change caused by adding the centerline 600-gal fuel tank to the F-15 aircraft at armament station 5.

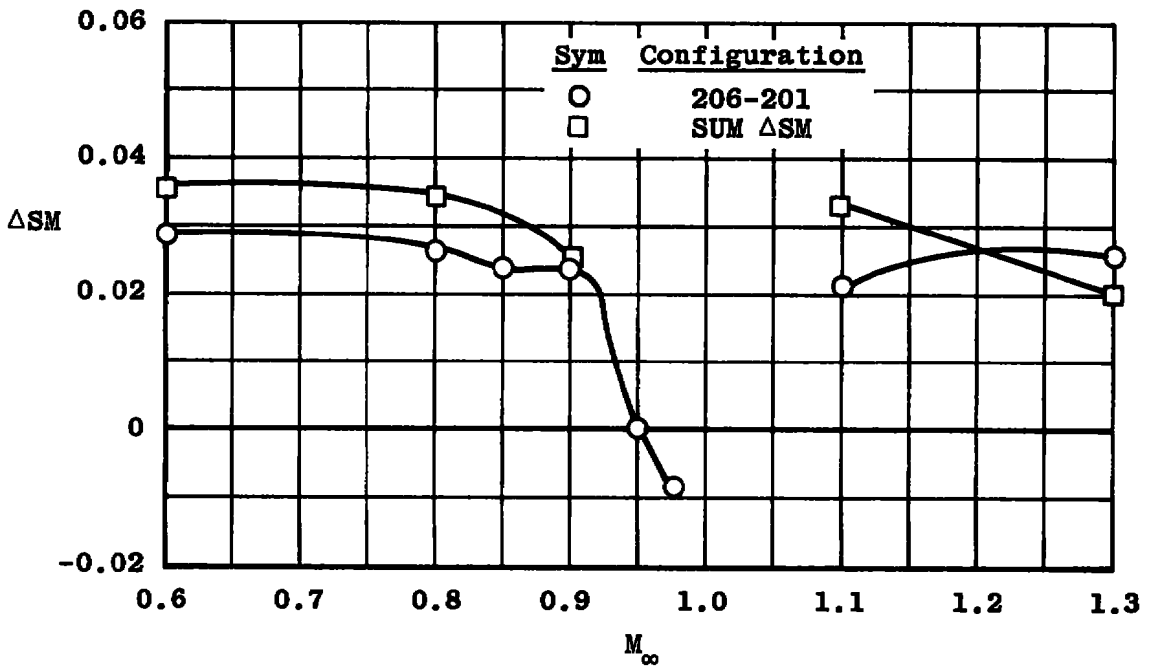

a. GBU-15 (CW) + AIM-7F + centerline 600-gal tank

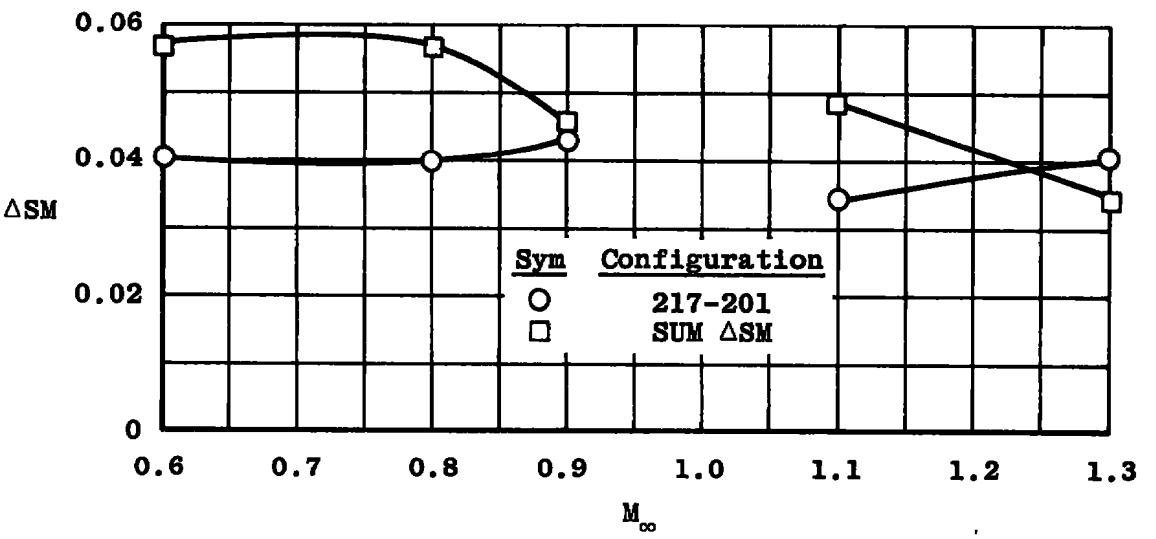

b. TEWS + GBU-15 (CW) + AIM-7F + centerline 600-gal tank

Figure 21. Static margin change obtained by summing individual components compared to the total change measured.

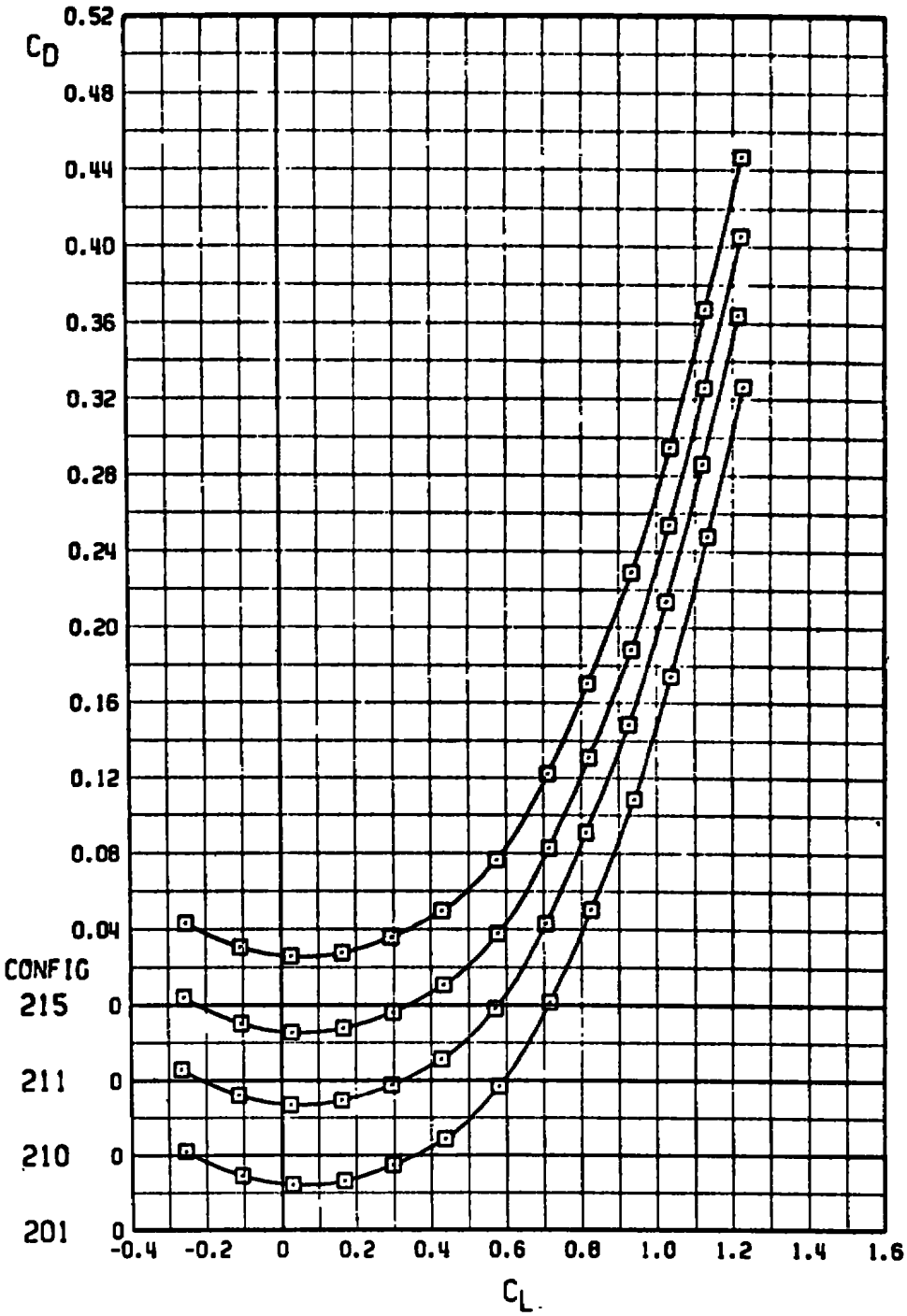

a. $M_\infty = 0.60$

Figure 22. Drag polars of the baseline configurations.

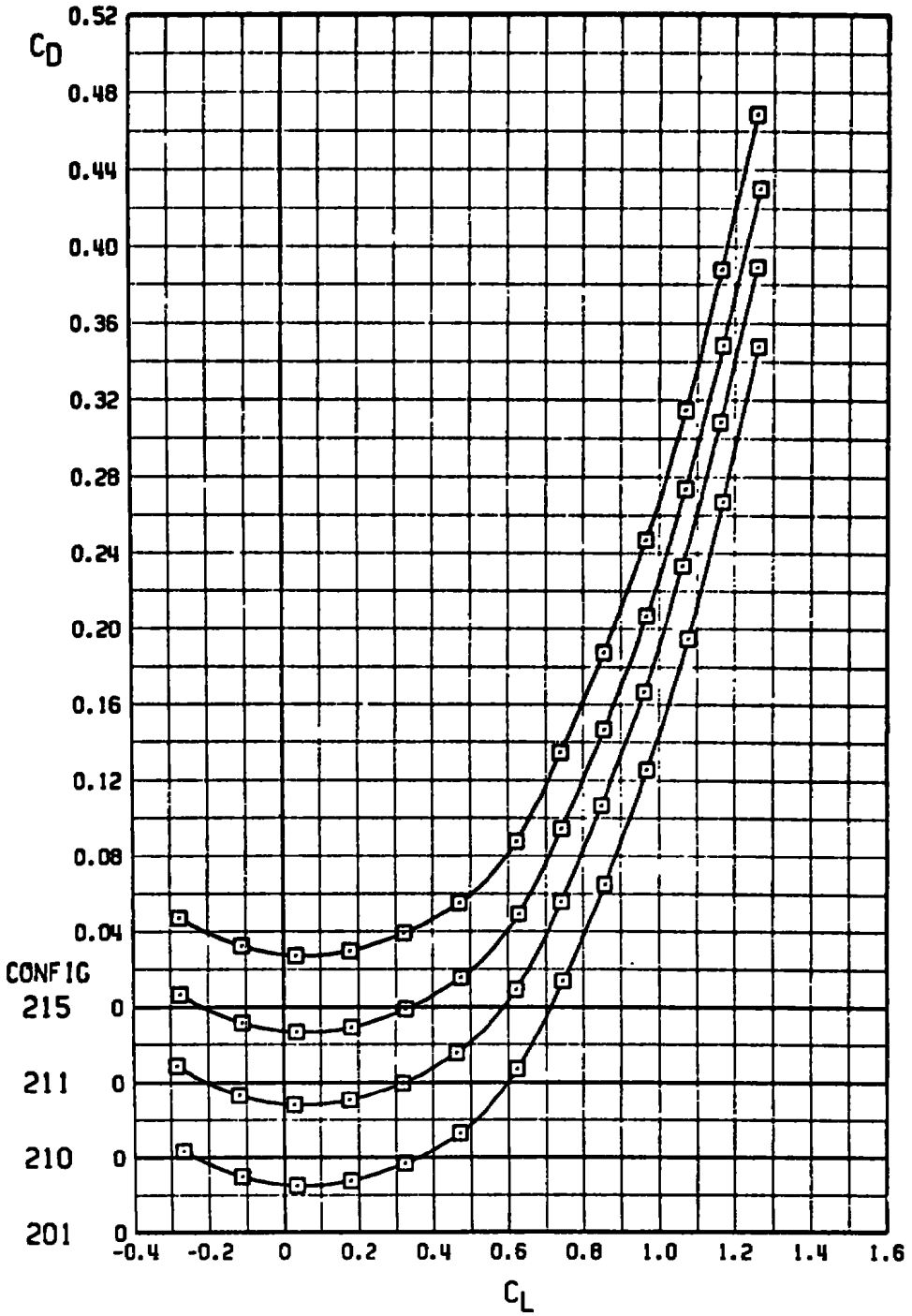

b. $M_\infty = 0.80$

Figure 22. Continued.

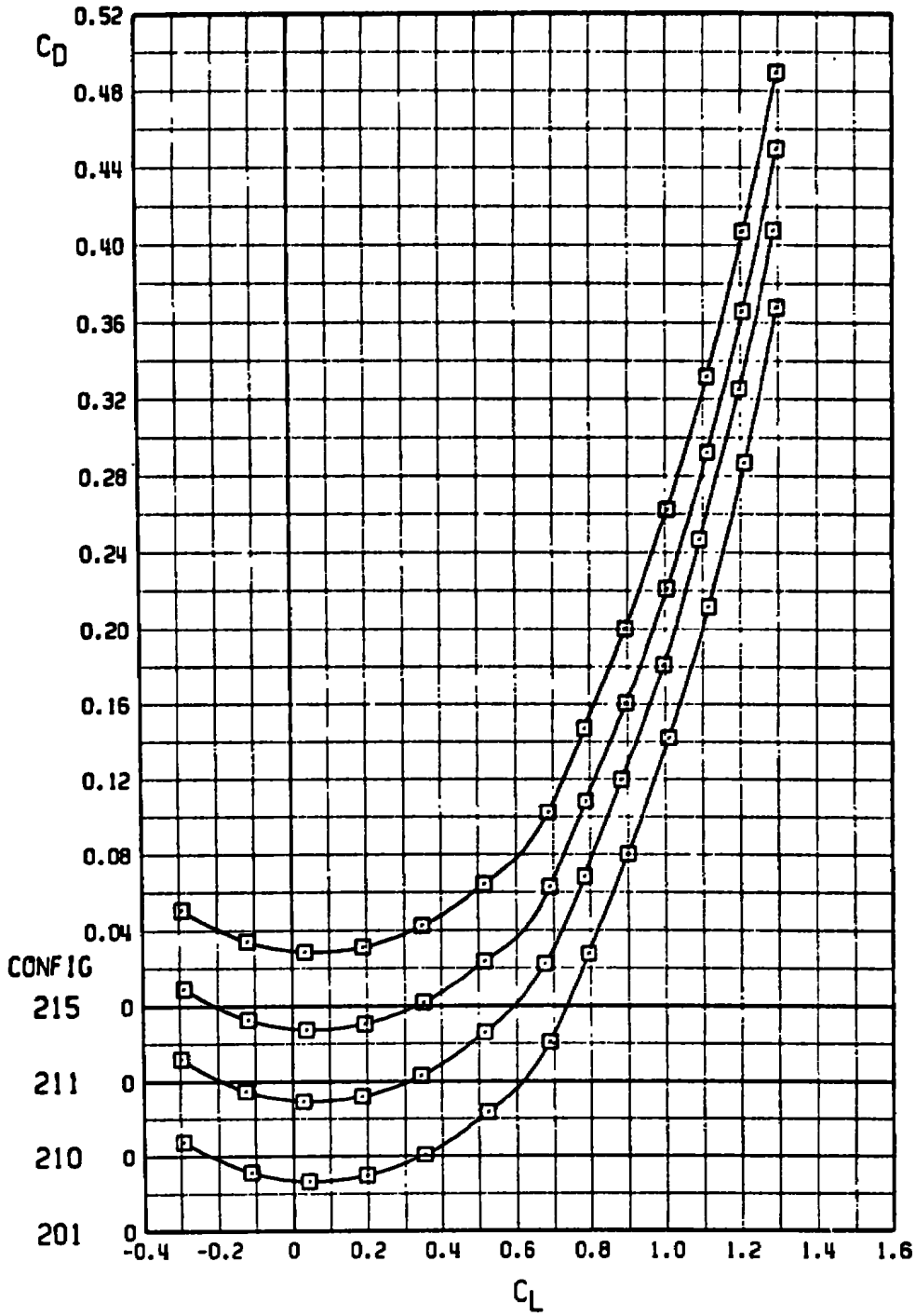

c. $M_\infty = 0.90$

Figure 22. Continued.

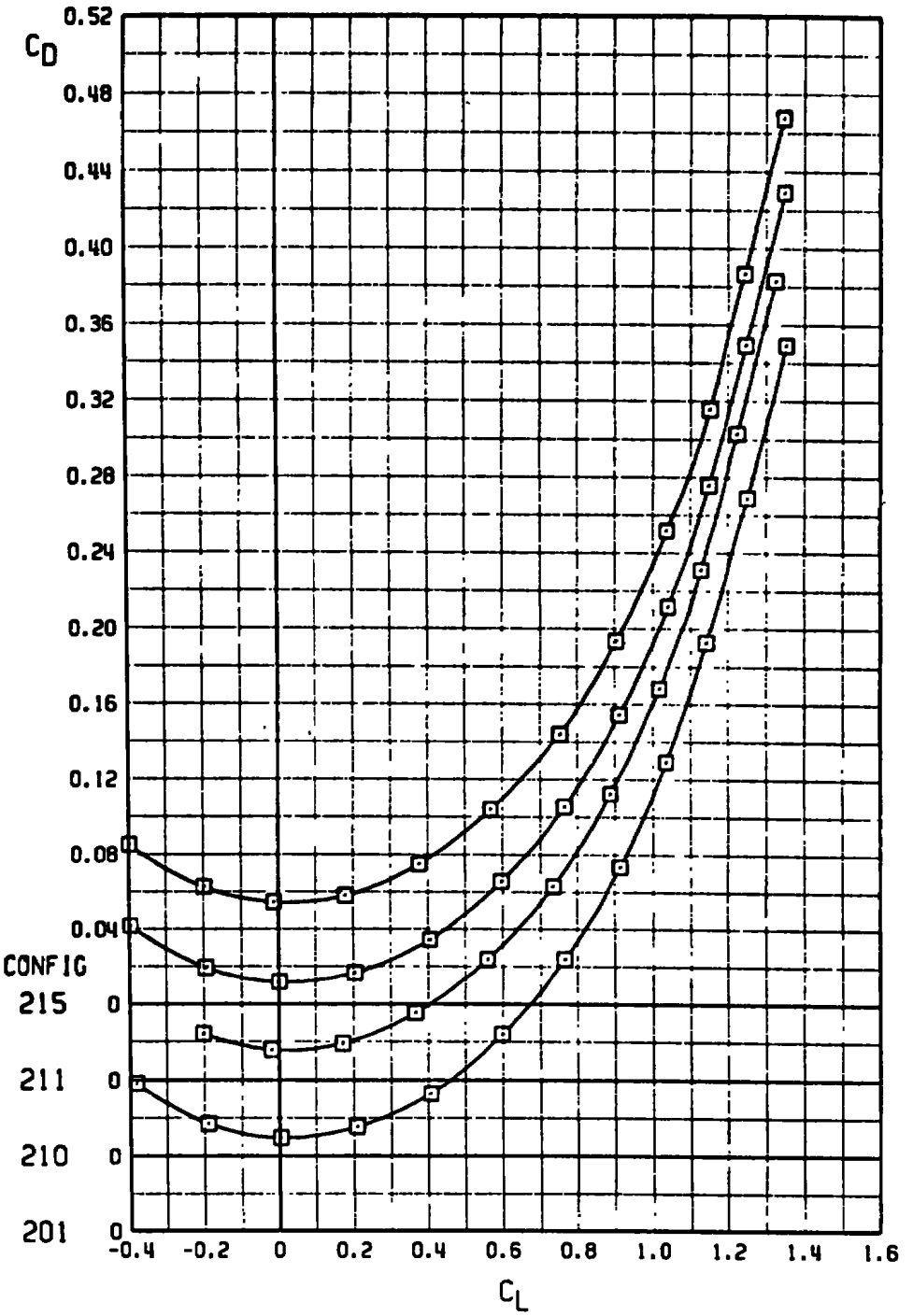

d. $M_\infty = 1.10$

Figure 22. Continued.

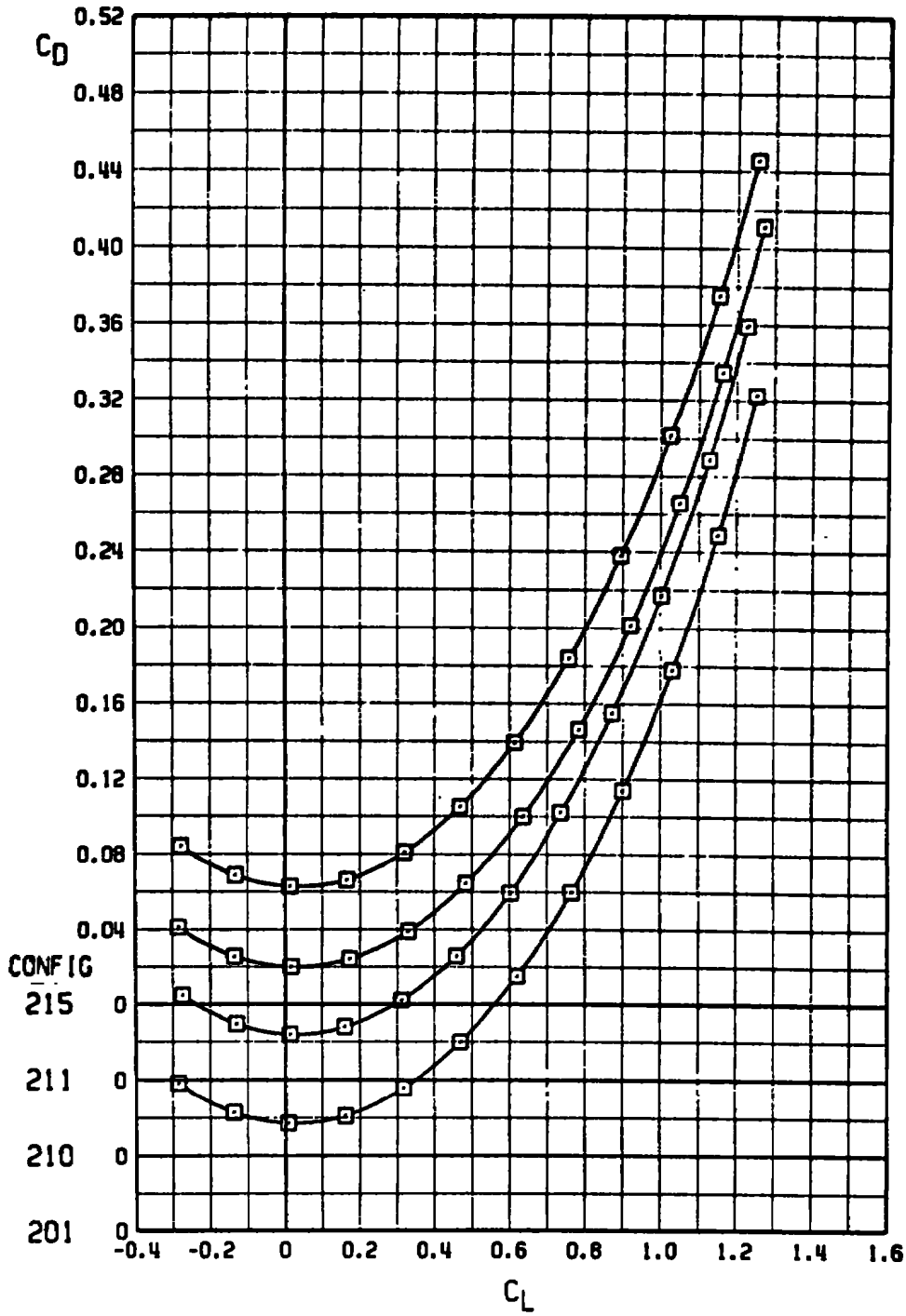

e. $M_\infty = 1.30$

Figure 22. Concluded.

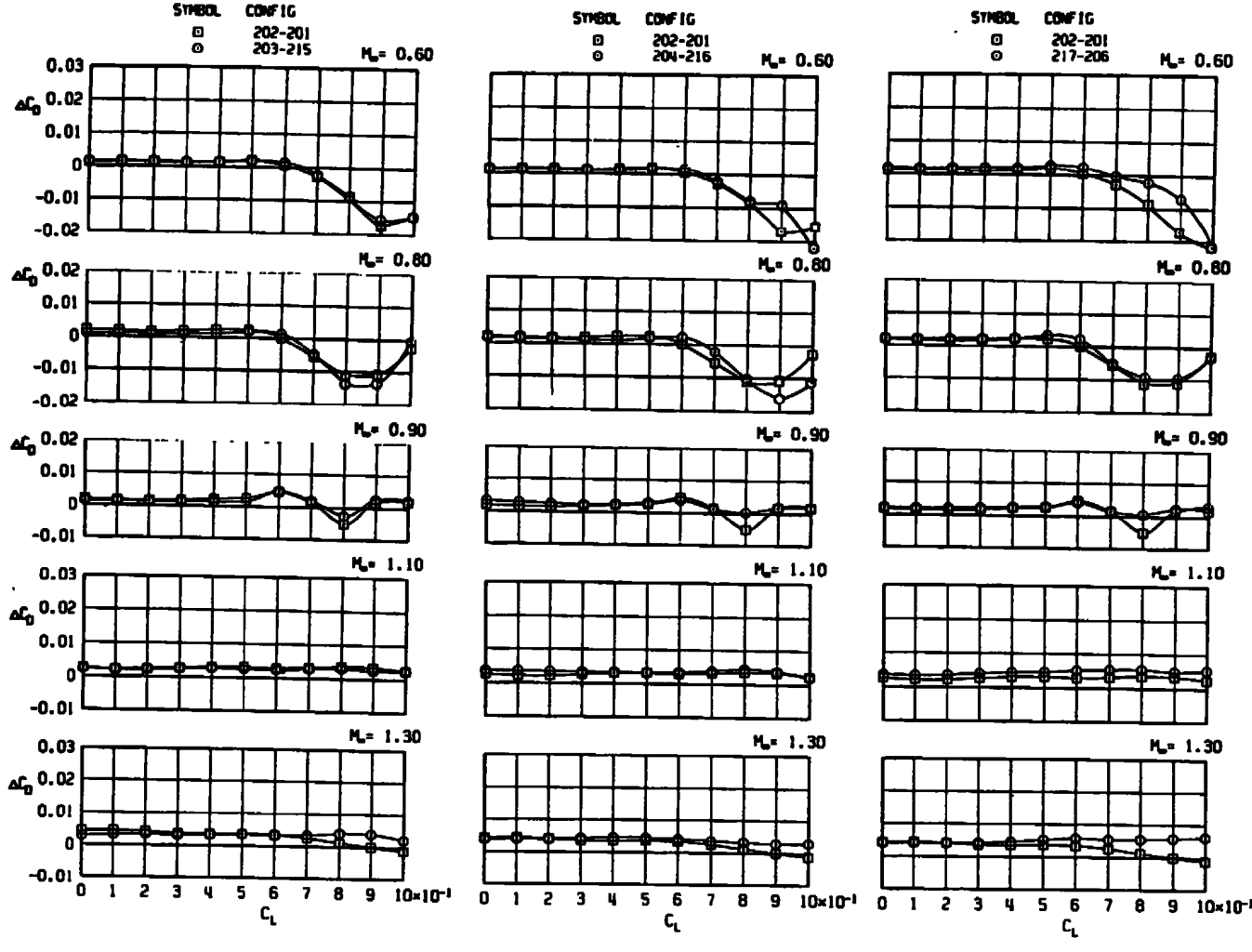

a. Centerline 600-gal tank

b. I.B. + centerline 600-gal tanks

c. GBU-15 (CW) + AIM-7F + centerline 600-gal tanks

Figure 23. Effect of various store loadings on the drag increment caused by adding the TEWS stores at armament stations 1 and 9.

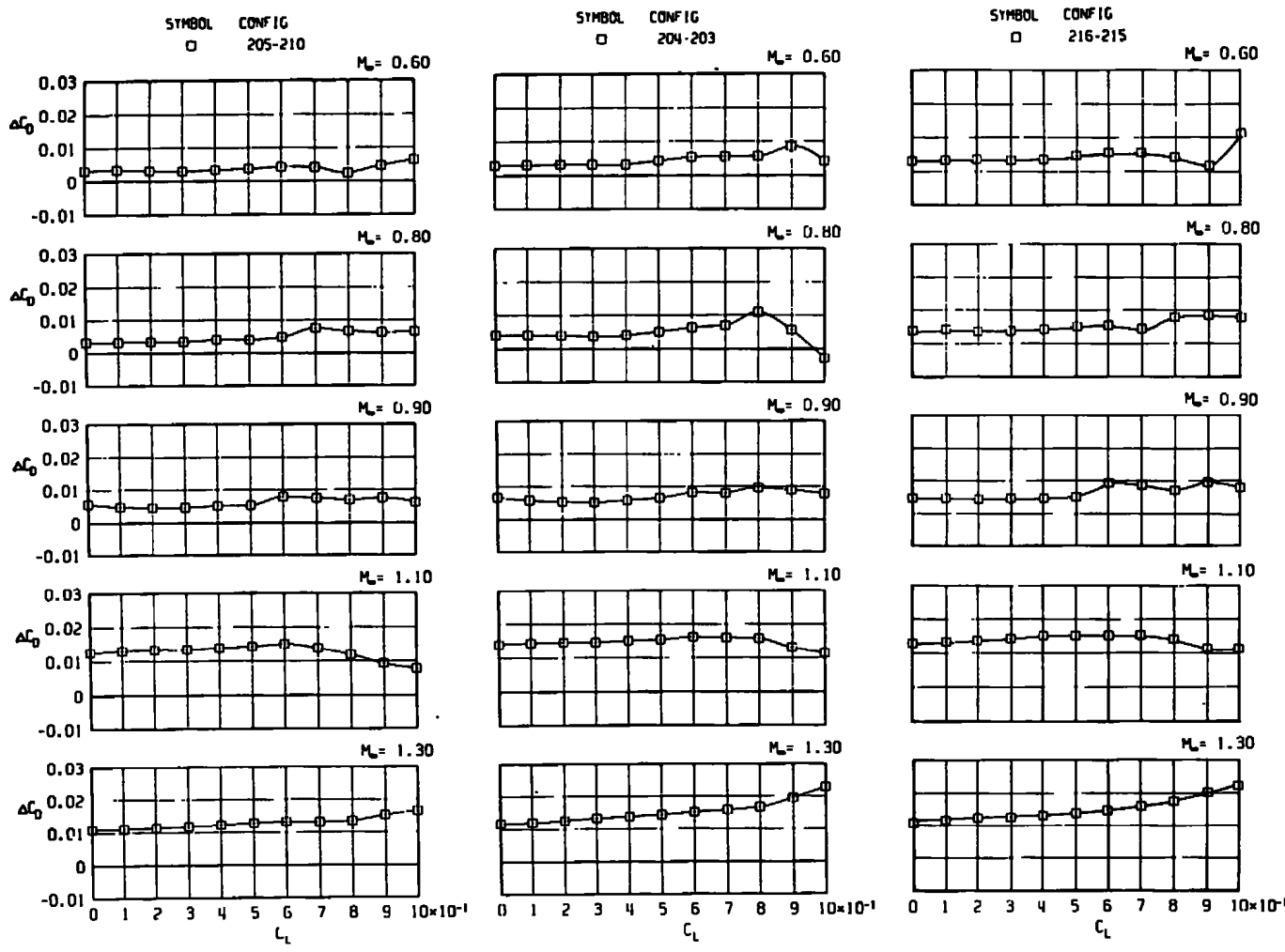

a. AIM-7F + centerline 600-gal tank

b. TEWS + centerline 600-gal tank

c. Centerline 600-gal tank

Figure 24. Effect of various store loadings on the drag increment caused by adding the 600-gal fuel tanks to armament stations 2 and 8.

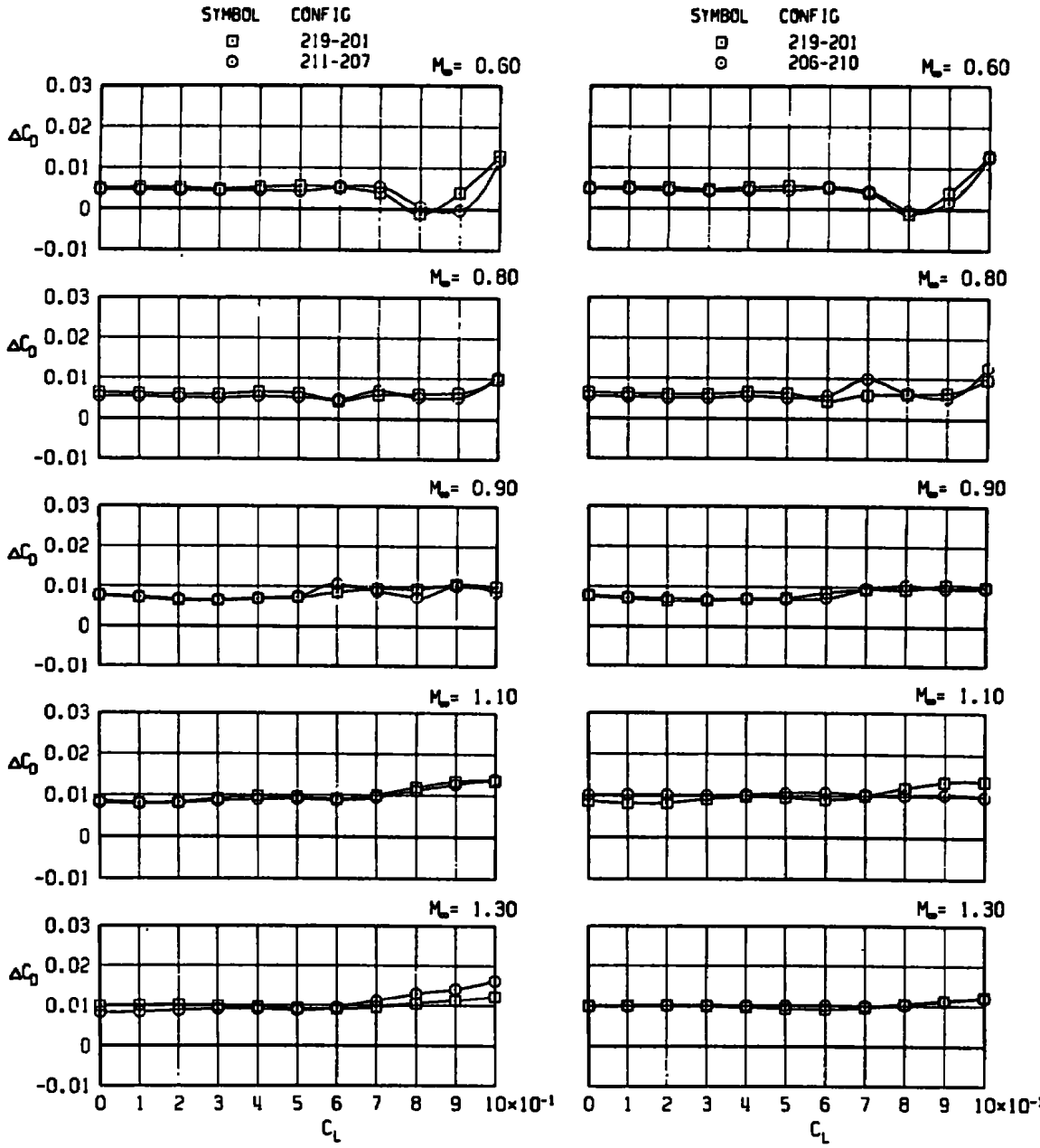

a. AIM-7F

b. AIM-7F + centerline 600-gal tank

Figure 25. Effect of various store loadings on the drag increment caused by adding the GBU-15 (CW) stores at armament stations 2 and 8.

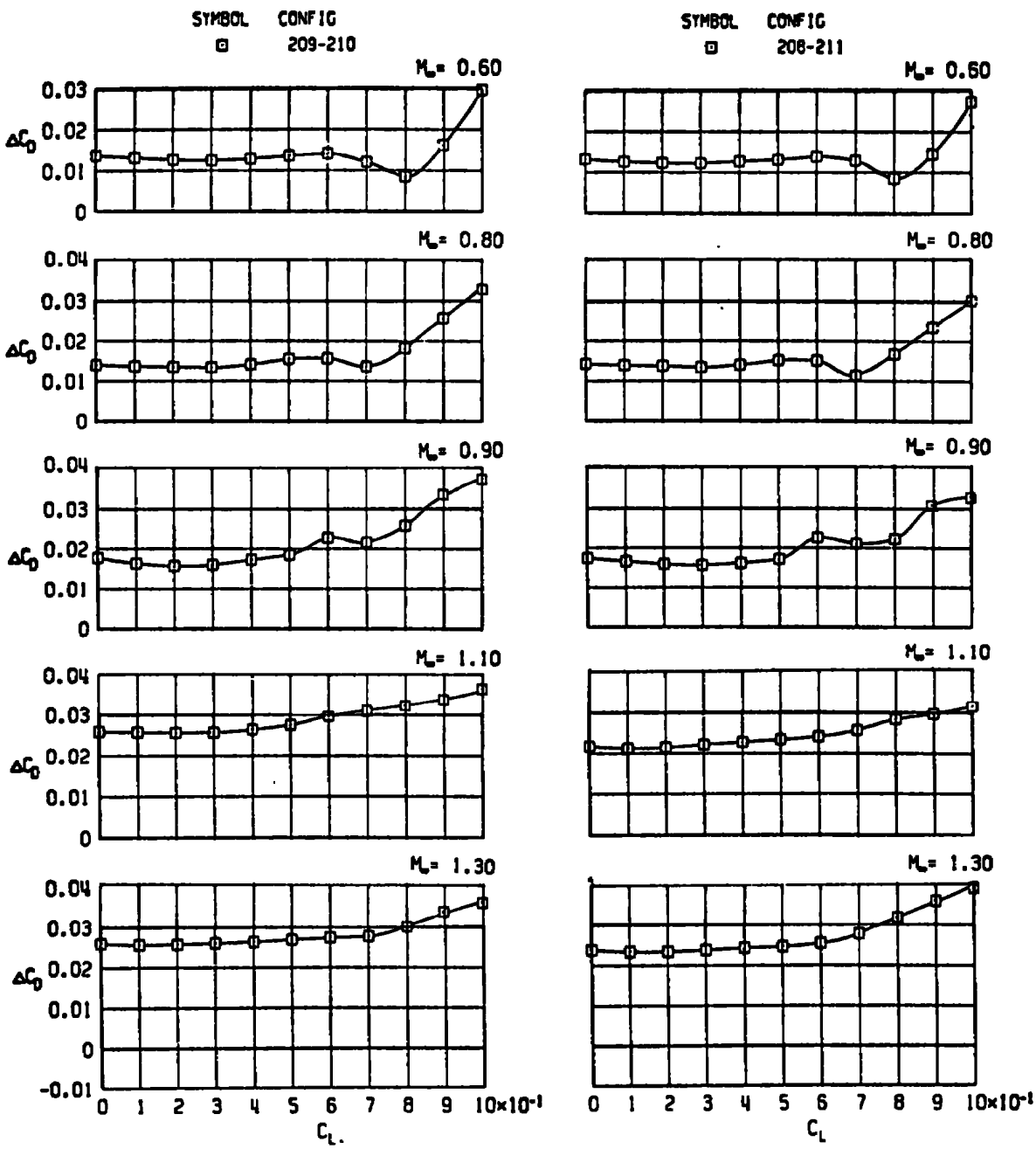

a. AIM-7F + centerline 600-gal tank

b. AIM-7F

Figure 26. Effect of various store loadings on the drag increment caused by adding 12 SUU-30H/B stores at armament stations 2 and 8.

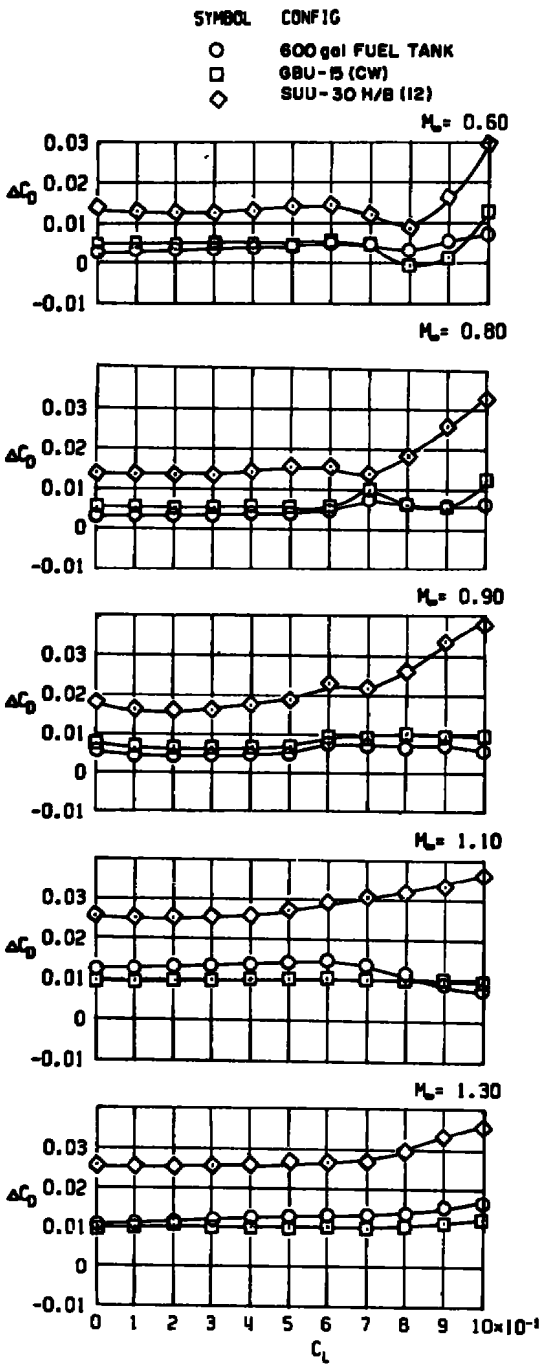

Figure 27. Comparison of drag increment caused by adding various stores at armament stations 2 and 8 in the presence of the AIM-7F stores and the centerline 600-gal fuel tank.

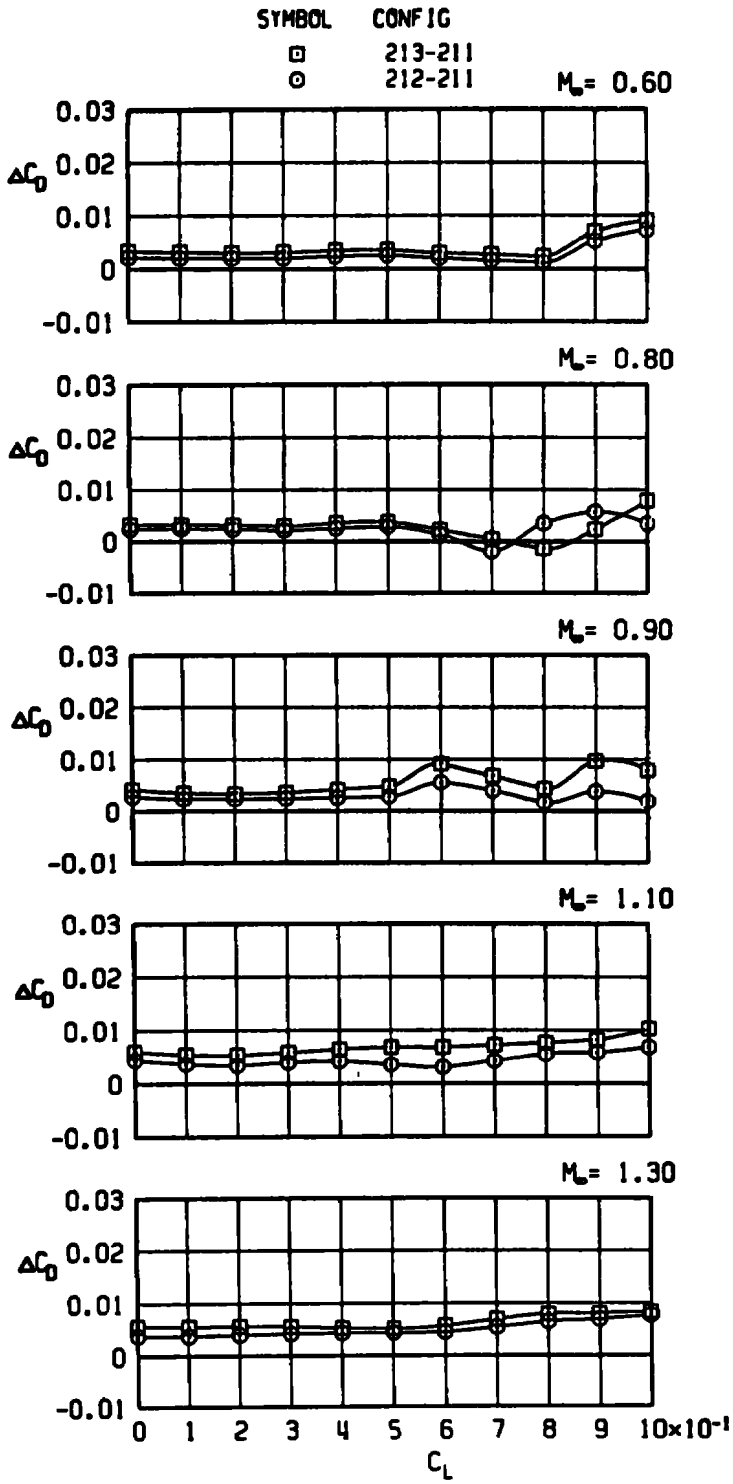

Figure 28. Comparison of the drag increment produced by adding one ASRM and two ASRM stores in tandem at armament stations 2 and 8.

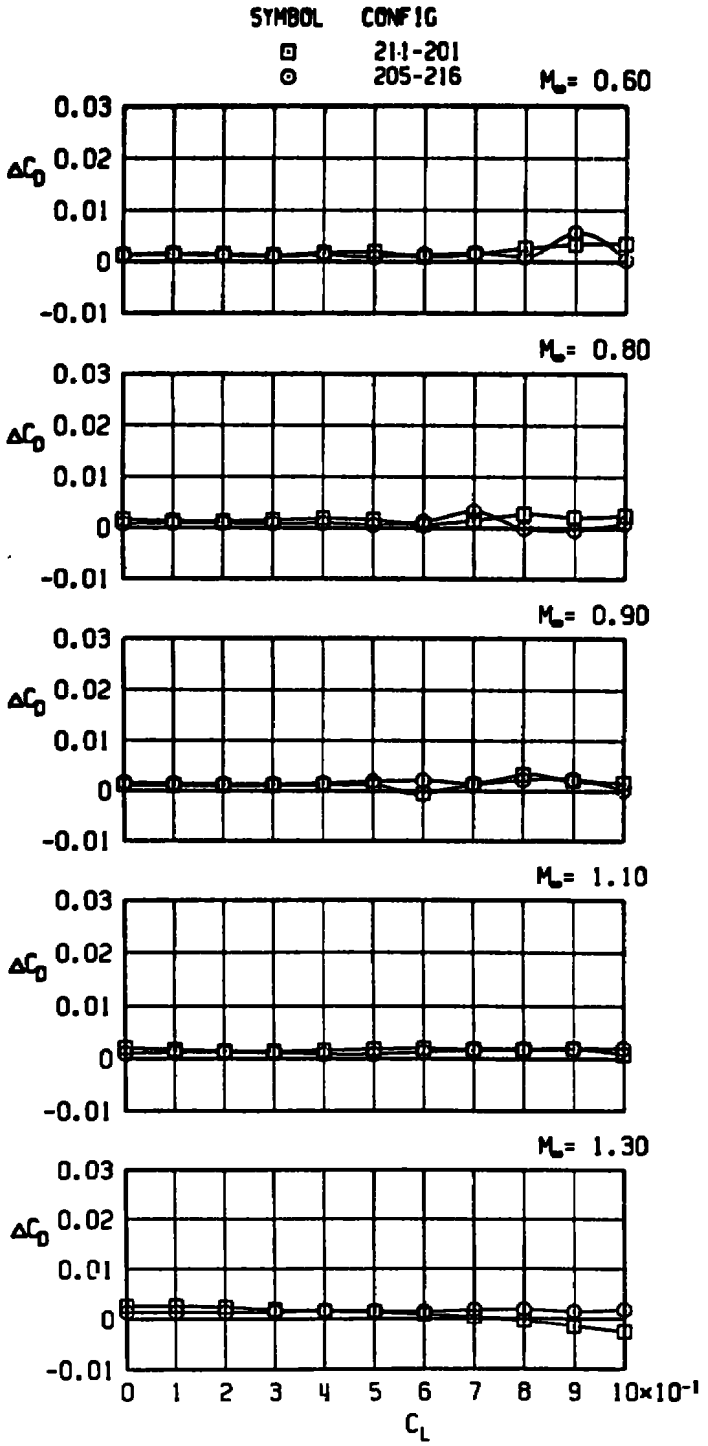

Figure 29. Effect of the 600-gal fuel tanks at armament stations 2, 5, and 8 on the drag increment caused by adding the AIM-7F stores at armament stations 3, 4, 6, and 7.

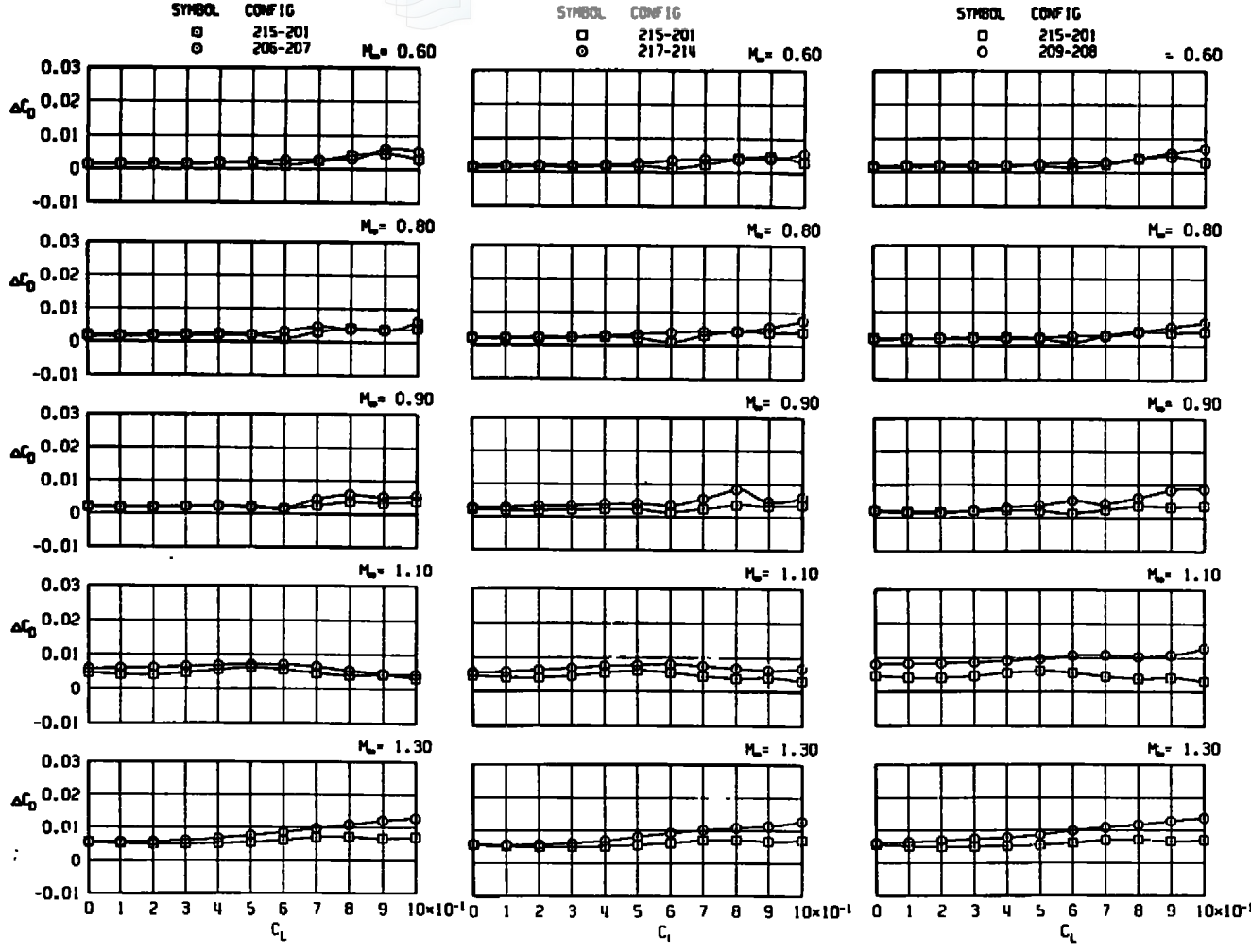

a. GBU-15 + AIM-7F b. TEWS + GBU-15 + AIM-7F c. SUU-30H/B + AIM-7F

Figure 30. Effect of various store loadings on the drag increment caused by adding the 600-gal fuel tank at armament station 5.

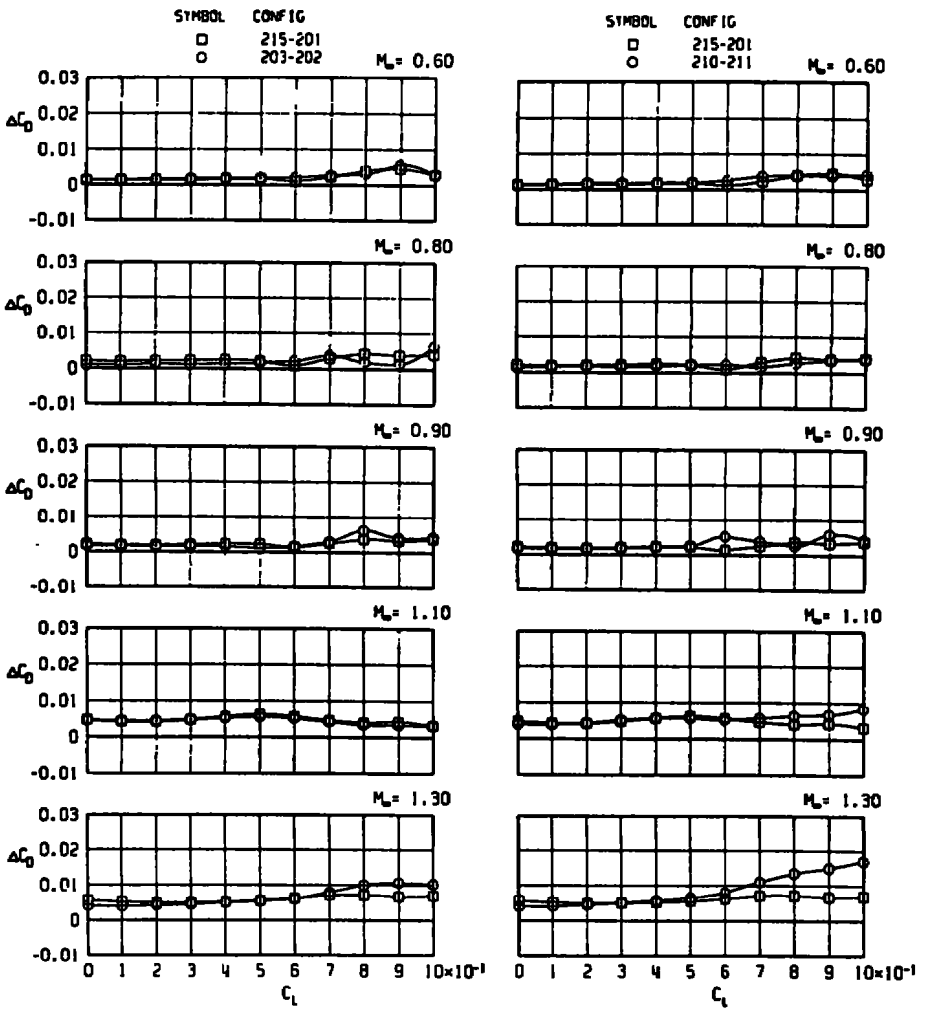

d. TEWS

e. AIM-7F

Figure 30. Concluded.

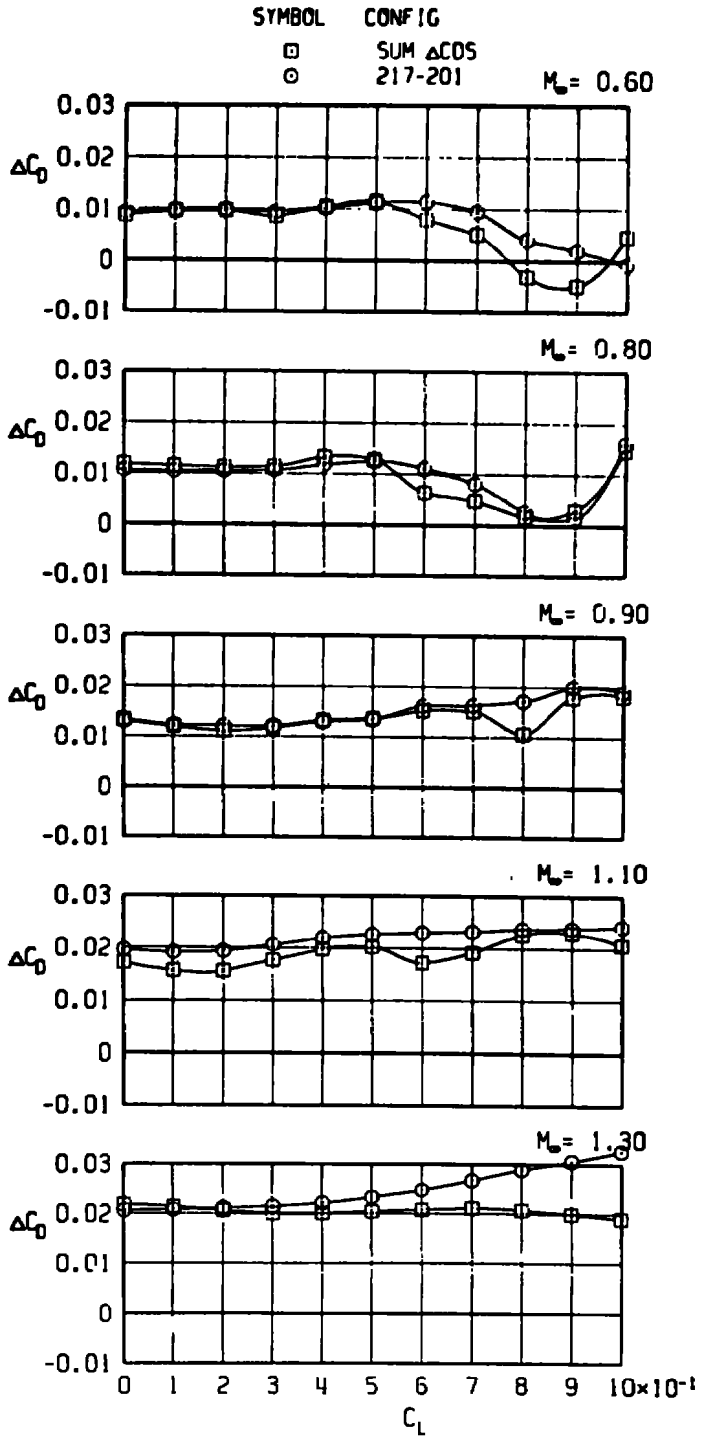

a. TEWS + GBU-15 (CW) + AIM-7F + centerline 600-gal tank

Figure 31. Drag increment obtained by summing individual components compared to measured value.

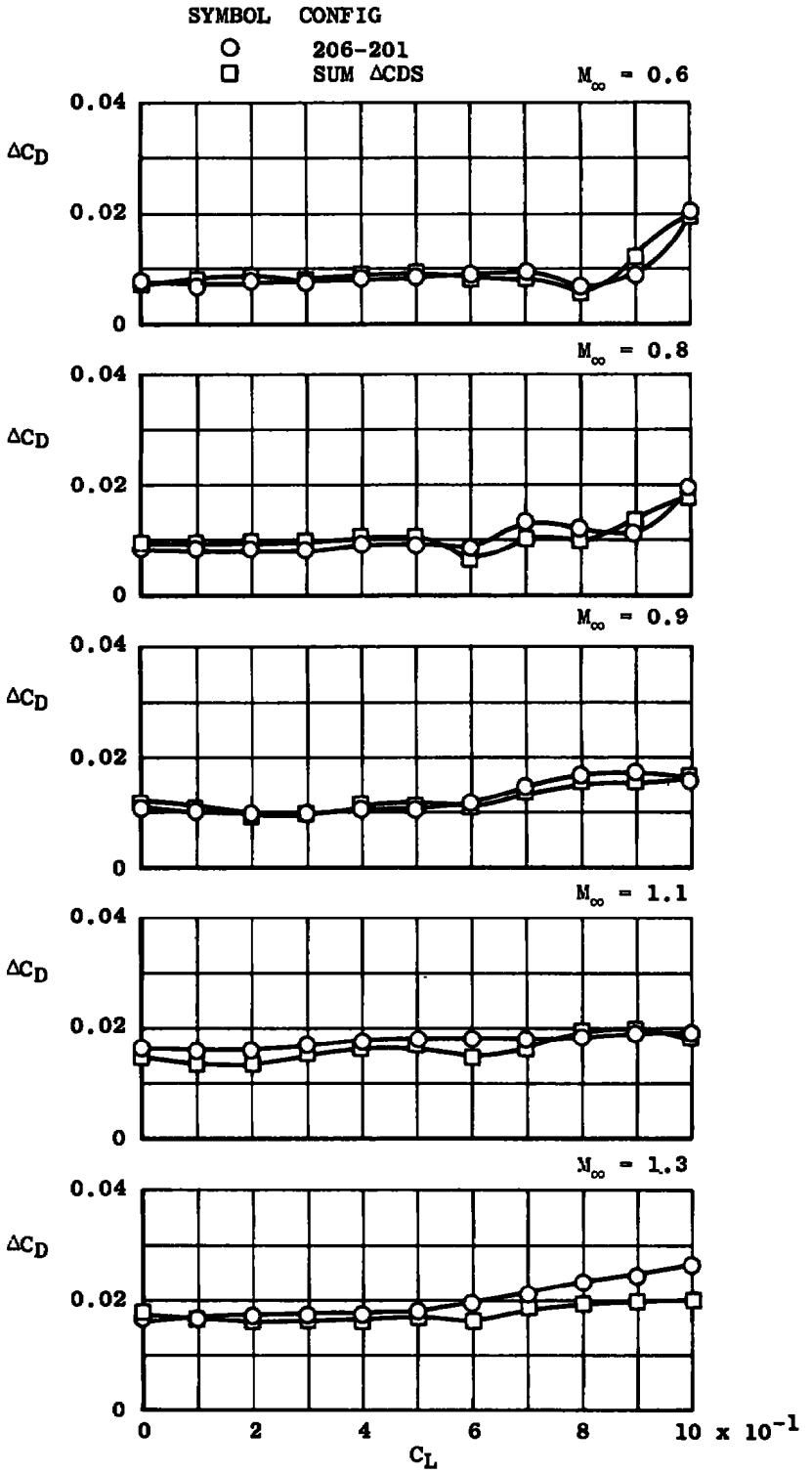

b. GBU-15 (CW) + AIM-7F + centerline 600-gal tank
Figure 31. Concluded.

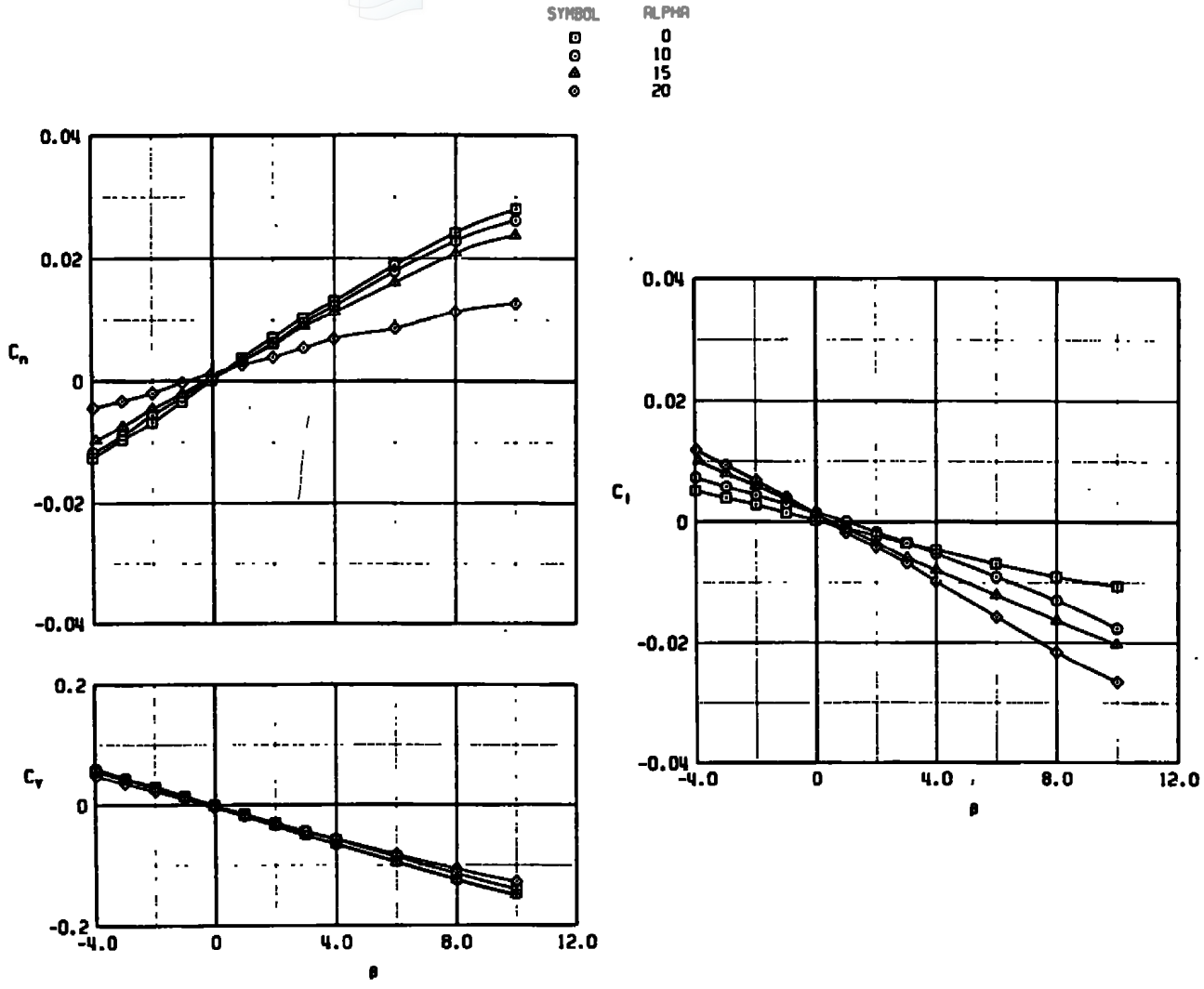

a. $M_\infty = 0.6$

Figure 32. Lateral-directional aerodynamic characteristics of configuration 201.

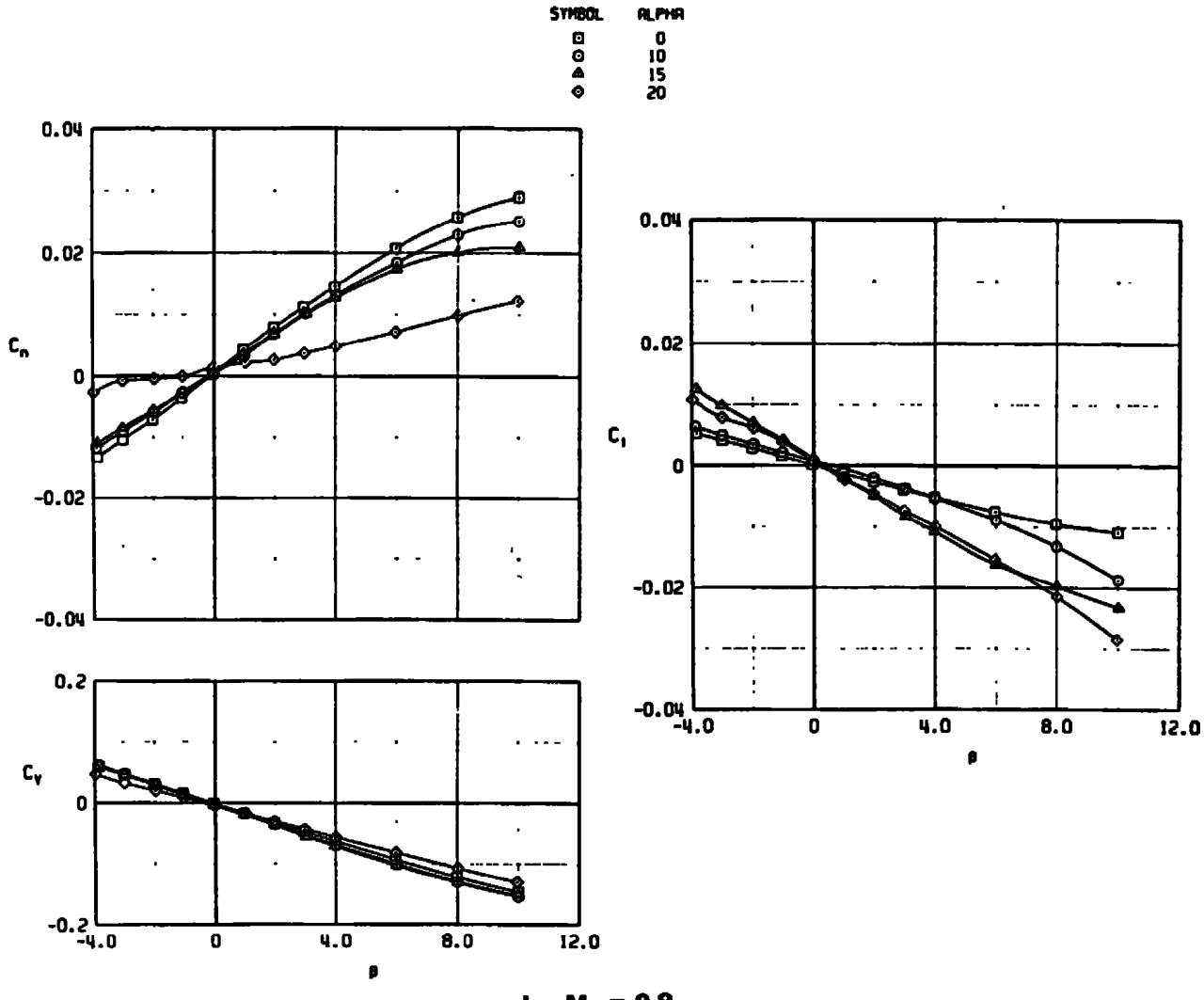

b. $M_\infty = 0.8$

Figure 32. Continued.

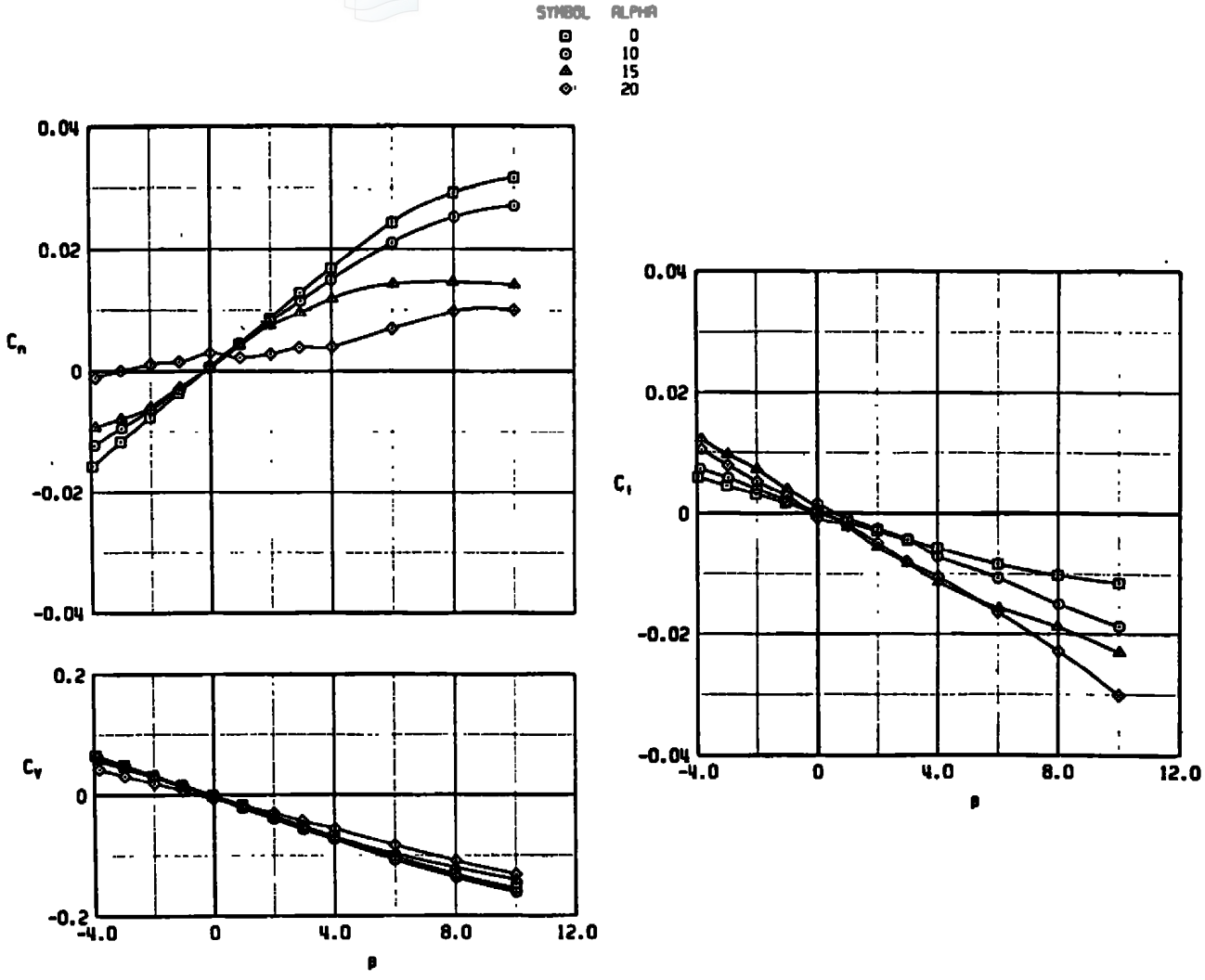

c. $M_\infty = 0.9$

Figure 32. Continued.

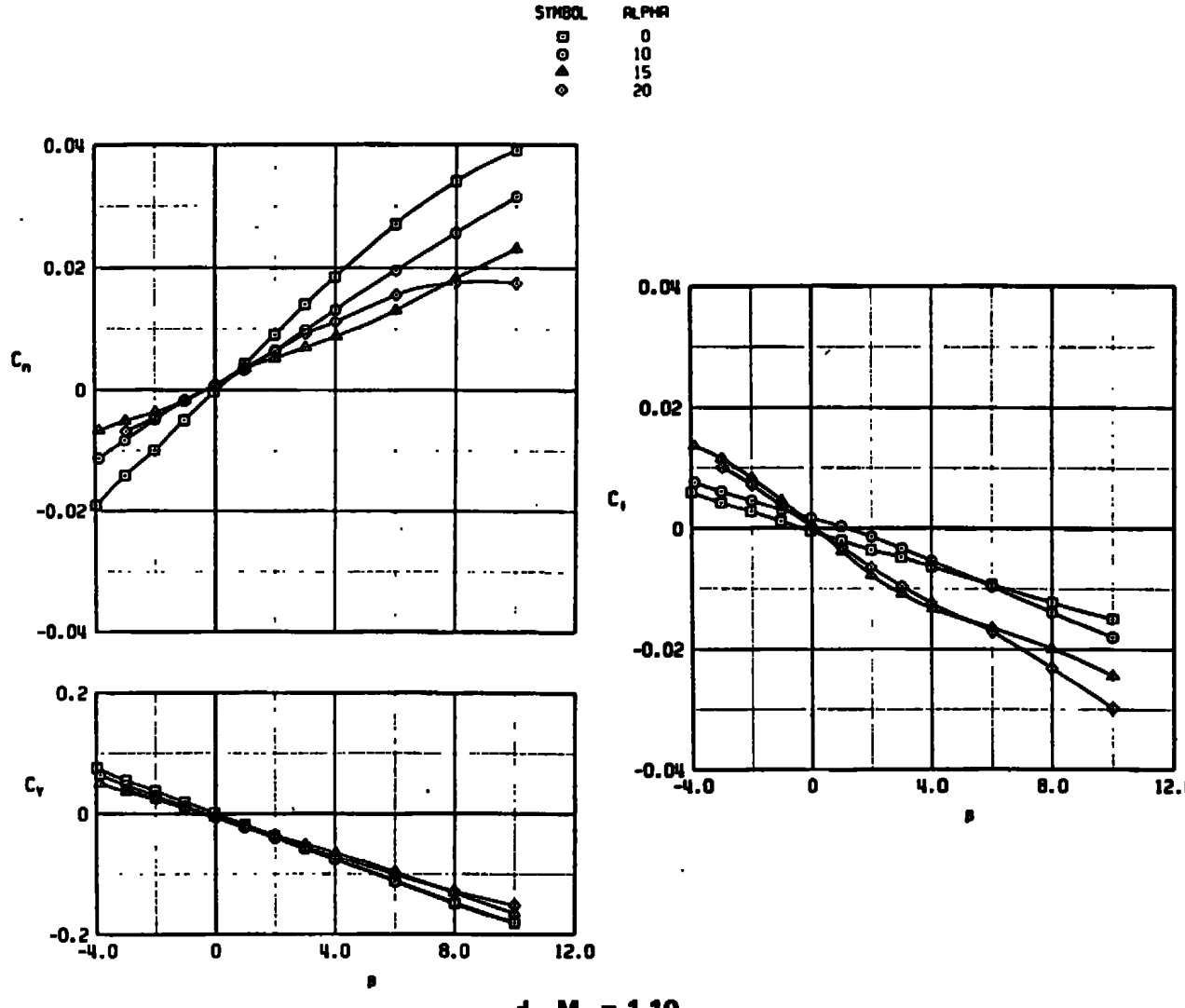

d. $M_\infty = 1.10$

Figure 32. Continued.

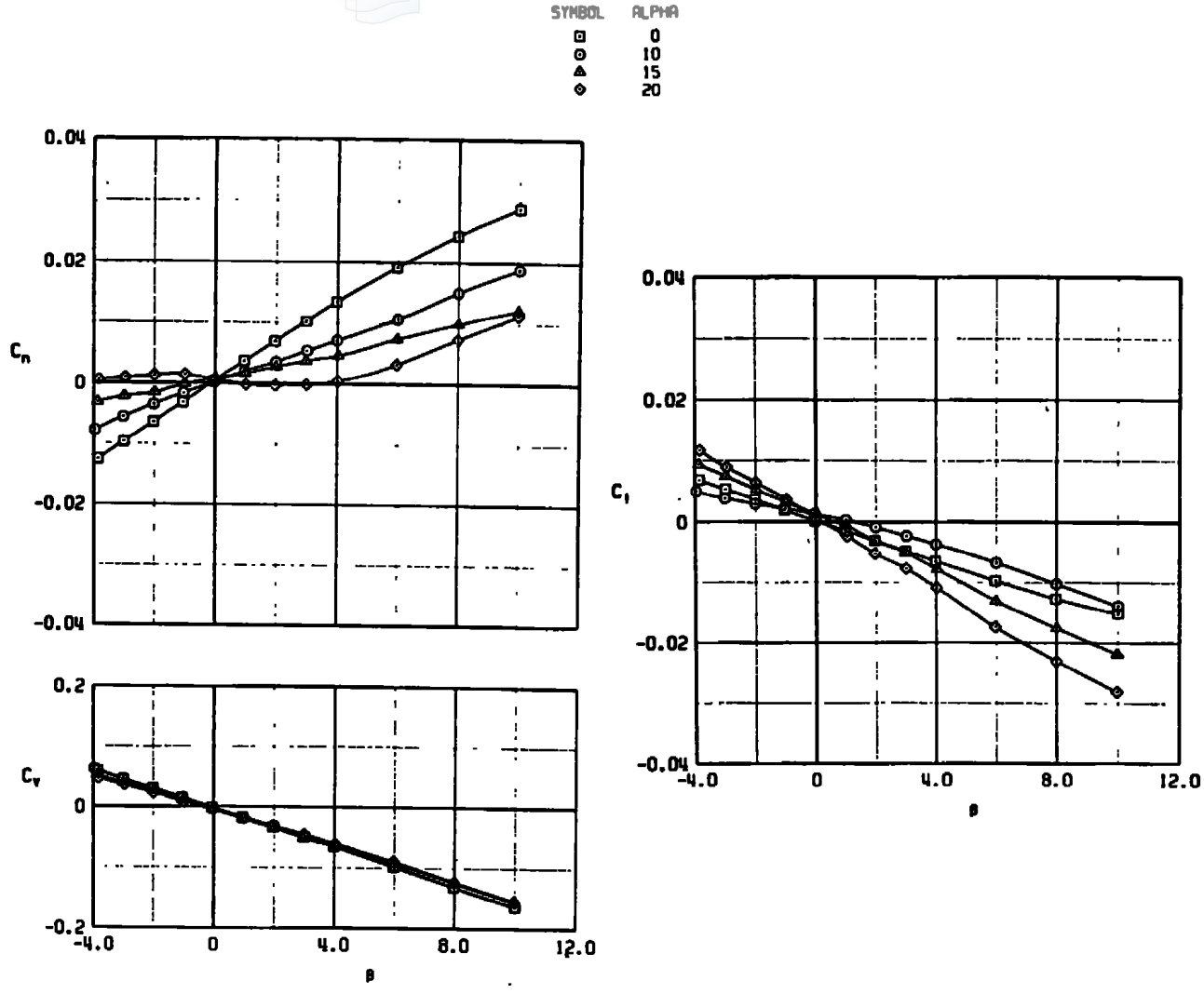

e. $M_\infty = 1.3$

Figure 32. Concluded.

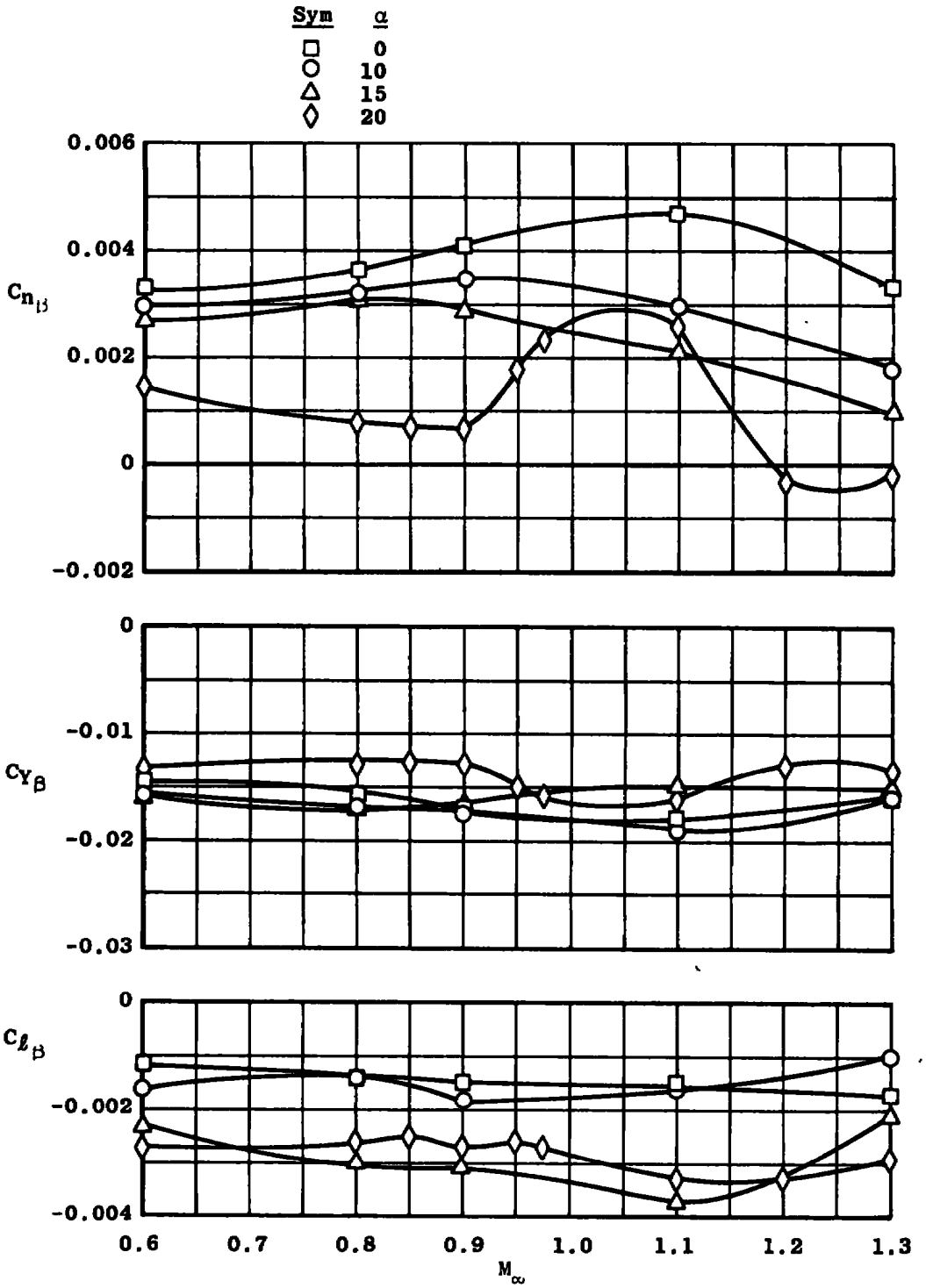

Figure 33. Effect of angle of attack on the lateral-directional stability derivatives of configuration 201.

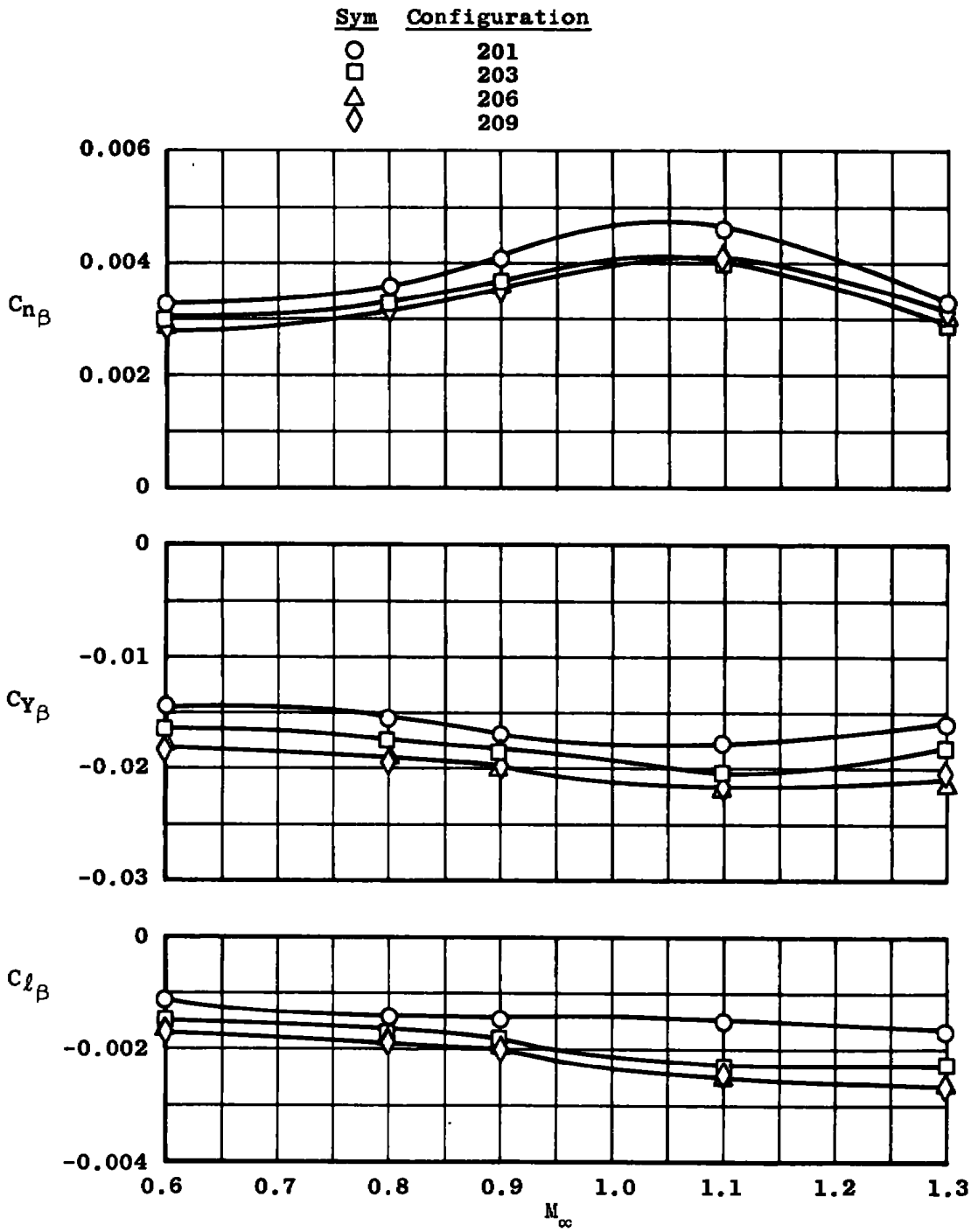

a. $\alpha = 0$

Figure 34. Effect of various external store configurations on the lateral-directional stability derivatives.

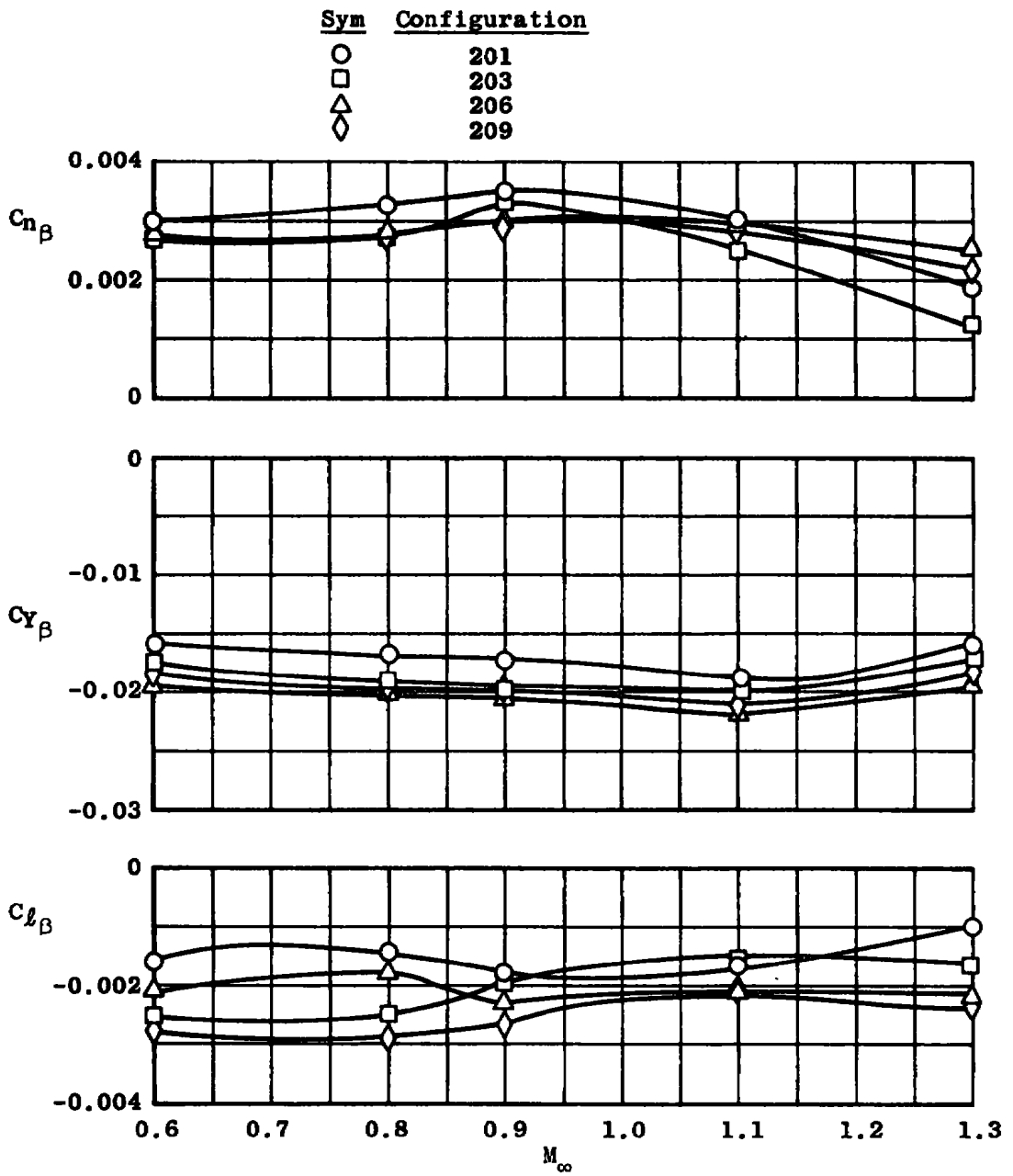

b. α = 10 deg

Figure 34. Continued.

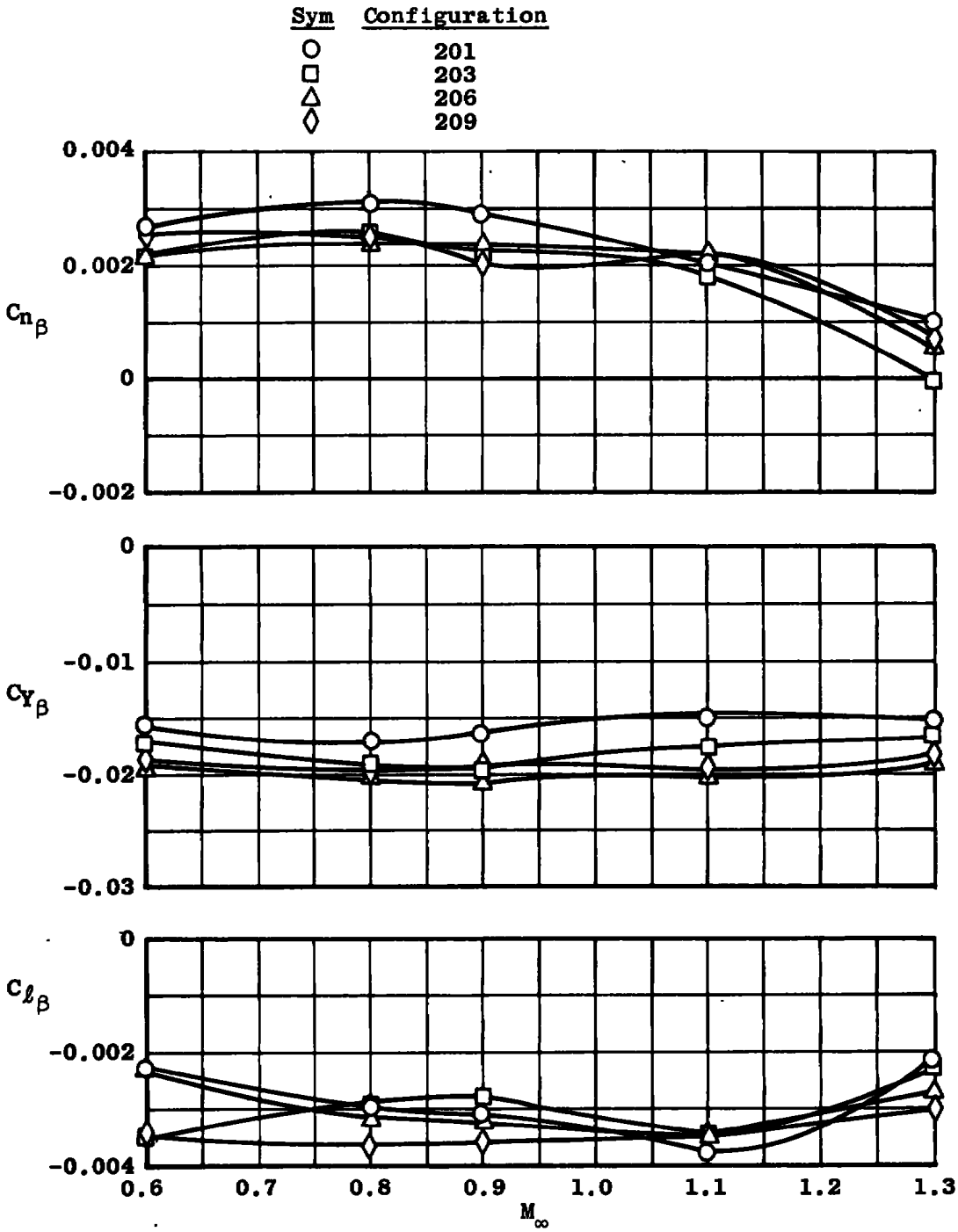

c. α = 15 deg

Figure 34. Continued.

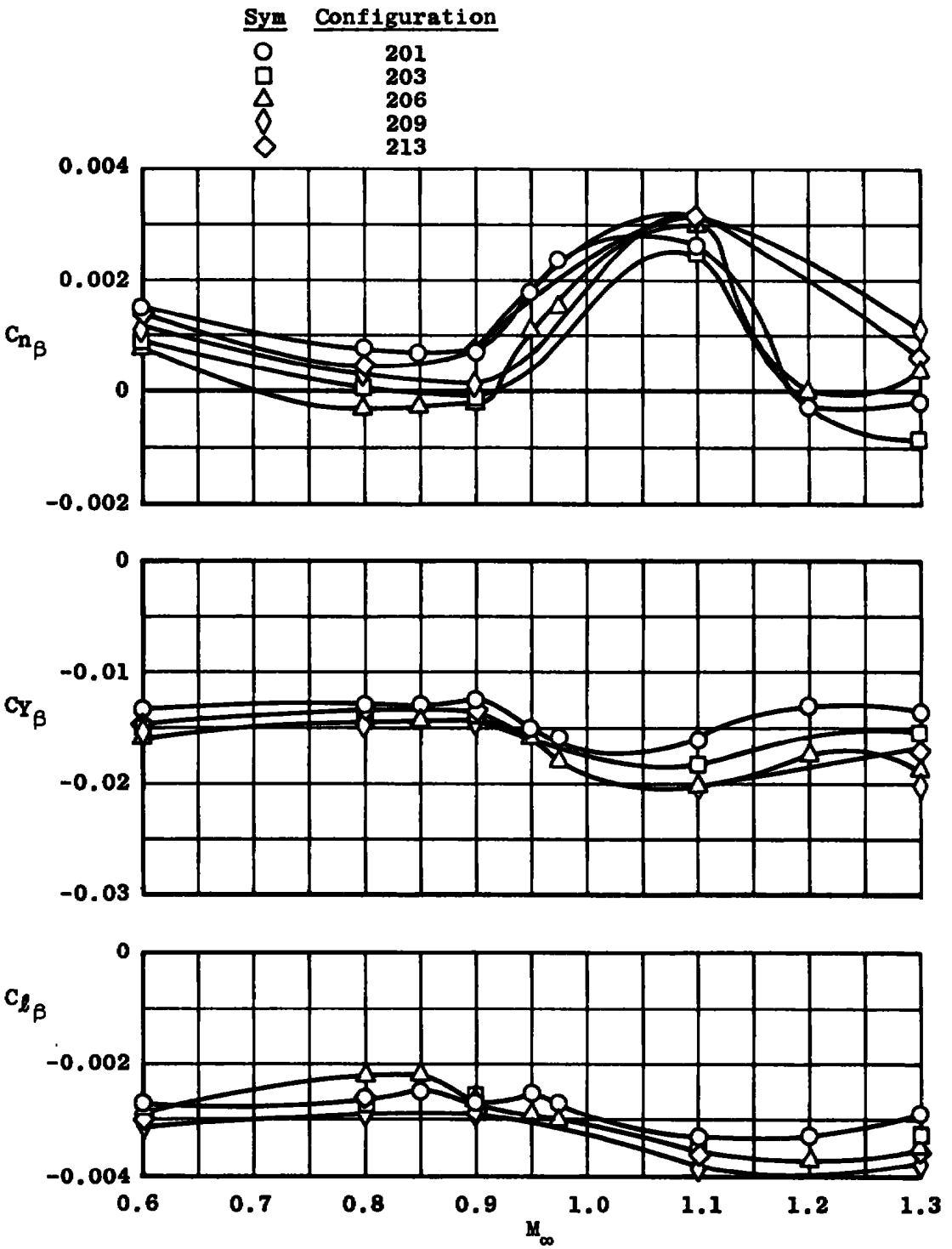

d. α = 20 deg

Figure 34. Concluded.

Table 1. Part Number Summary Log

Config	α	β	Mach Number 0.60	0.80	0.85	0.90	0.95	0.975	1.10	1.20	1.30	Remarks
101	Var	0	6,7,8	—	—	—	—	—	—	—	—	Reynolds No. Var.
101	↓	↓	8,9	11,10	12,13	15,14	16,17	19,18	20,22	27,26	28,29,31*	*α = 0, β Sweep
201	↓	↓	35	68	63	36	55	51,53	48	44	37	Flow Angularity Runs
↓	0	Var	70	69		62			50		38	All Configuration
	10	↓	71	67		61			47		40	Numbers in 200's
	15		72	66		58			46		41	
↓	20	↓	73	65	64	57	56	54,52	45	43	42	Indicate High α Inlet.
202	Var	0	77	78		79			80		81	100's Indicate
203	Var	0	85	94		97			106		107	Low α Inlet
↓	0	Var	96	93		98			105		108	
	10	↓	87	92		99			104		109	
	15		88	91		100			103		110	
↓	20	↓	89	90		101			102		111	
204	Var	0	115	116		117			118		119	
205	Var	0	123	124		125			126		127	
206	Var	0	131	141	142	150	151	154	155	161	162	
206	0	Var	132	140		149			156		163	
↓	10	↓	133	139		146			157		164	
	15		134	138		145			158		165	
↓	20	↓	135	137	143	144	152	153	159	160	166	
207	Var	0	170	171		172			173		174	
208	↓	↓	178	179		180			181		182	
209	↓	↓	188	197		199			209		210	
↓	0	Var	189	196		200			208		211	
	10	↓	190	195		201			207		212	
	15		191	194		202			206		213	
↓	20	↓	192	193		203			205		215	204 = β Run, α = 18 deg
210	Var	0	220	221		222			223		224	
211	Var	0	230	231		232			233		234	
213	Var	0	239	242		243			247		248	
213	20	Var	240	241		244			245		249	
212	Var	0	253	254		255			256		257	
214	↓	↓	261	262		263			264		265	
215			293	294		295			296		297	
216			285	286		287			288		289	
217			269	270		271			272		273	
218			Did Not Fit – Fin Interference									
219	↓	↓	277	278		279			280		281	

Table 2. Aerodynamic Coefficient Uncertainties

M_∞	q_∞, psf	$\pm\delta C_L$	$\pm\delta C_m$	$\pm\delta C_n$	$\pm\delta C_Y$	$\pm\delta C_D$	$\pm\delta C_\ell$
0.60	240	0.0201	0.0048	0.0009	0.0062	0.0067	0.0008
0.80	350	0.0119	0.0033	0.0006	0.0041	0.0044	0.0005
0.85	375	0.0108	0.0031	0.0006	0.0038	0.0042	0.0004
0.90	400	0.0100	0.0029	0.0005	0.0035	0.0039	0.0004
0.95	425	0.0092	0.0028	0.0005	0.0033	0.0037	0.0004
0.975	430	0.0092	0.0028	0.0005	0.0032	0.0037	0.0004
1.10	475	0.0087	0.0028	0.0004	0.0029	0.0036	0.0003
1.20	500	0.0082	0.0027	0.0004	0.0028	0.0035	0.0003
1.30	515	0.0023	0.0026	0.0004	0.0029	0.0033	0.0003

NOMENCLATURE

BL	Model butt line, in.
b	Model reference span, 25.62 in.
C_D	Drag coefficient. drag/$q_\infty S$
ΔC_D	Incremental changes in drag coefficient caused by adding external stores, positive values indicate a drag increase (Values presented in Fig. 7 are referenced to configuration 201 at a C_L of 0.3 and M_∞ = 0.6.)
C_L	Lift coefficient, lift/$q_\infty S$
℄	Centerline
C_ℓ	Rolling-moment coefficient referenced to WL 5.81 BL 0, rolling moment/$q_\infty Sb$
C_{ℓ_β}	Effective dihedral, slope of a least-squares curve fit of the rolling-moment coefficient versus sideslip angle curve from $-4 \leqslant \beta \leqslant 4$ deg, per degree
C_m	Pitching-moment coefficient referenced to FS 27.86 (25.65-percent MAC), WL 5.81, BL 0, pitching moment/$q_\infty S\bar{c}$
C_n	Yawing-moment coefficient referenced to FS 27.86 (25.65-percent MAC), WL 5.81, BL 0, yawing moment/$q_\infty Sb$
C_{n_β}	Static directional stability derivative, slope of a least-squares curve fit of the yawing-moment coefficient versus sideslip angle curve from $-4 \leqslant \beta \leqslant 4$ deg, per degree
C_Y	Side-force coefficient, side force/$q_\infty S$
C_{Y_β}	Side-force derivative, slope of a least-squares curve fit of the side-force coefficient versus angle of sideslip curve from $-4 \leqslant \beta \leqslant 4$ deg, per degree
$\bar{c}$, MAC	Theoretical mean aerodynamic chord (Fig. 3), 9.564 in.
cg	Center of gravity, MS 27.86 (25.65-percent MAC), WL 5.81, BL 0
FS	Model fuselage station, in.
M_∞	Free-stream Mach number

p_t	Free-stream total pressure, psfa
q_∞	Free-stream dynamic pressure, psf
S	Model reference area, wing area, 1.52 ft^2
SM	Static margin, slope of a least-square curve fit of the pitching-moment coefficient versus lift coefficient curve from $-2 \leqslant \alpha \leqslant 6$ deg, fraction of $\bar{c}$, negative when aft of cg
ΔSM	Incremental change in static margin caused by adding external stores, positive values indicate a destabilizing effect
WL	Model waterline from reference horizontal plane, in.
α	Wing chord (and model waterline) angle of attack, deg
α_f	Tunnel-flow and model-balance misalignment angle, deg, positive for flow upwash
β	Angle of sideslip, deg